CHAPTER 1

INTRODUCTION

1.1 Background

As a mechanical system, crane system is designed for repeat motions such as hoisting, transporting which includes longitudinal, transverse motion, and lowering heavy payload, as well as combination of each motion. The ability to transport the heavy payload in repetitive way leads to their wide spread use in ports, factories, construction sites and other places. Moreover, the increase in productivity and the capability of transporting heavy payload which are impossible, difficult or dangerous to humans are other motives for enhancing the use of crane syste ms. In its specific application, there are different types of crane such as overhead crane, gantry crane, tower crane and various special purpose cranes.

Gantry crane system, a non-slewing-luffing crane system is most widely used in several work places. The schematic of the gantry crane system is shown in Figure 1.1. In practice, the trolley is equipped with wheels and houses drive mechanism for trolley and hoist. The trolley will underslung on the top if the top beam of crane framework is single member, while rides on top when the top beam is made of more than one member. During crane operations, the trolley traverses along the top beam of the crane framework. The hoist houses cable drum, drive transmission and hoist motor. The function of cable drum is to wind up or unwind the cable, raises or lowers the payload attached to the hook. The trolley and hoist work simultaneously to perform the task of gantry crane. In general, the task performed by a gantry crane is to pick the payload, raise it, move it to target position and lower it down on the crane framework.

In the perspective of a structural system, this gantry crane system has crane supporting structure called crane framework. Some crane frameworks are equipped with wheels which allow the crane framework to travel on a parallel pair of rails and the others are fixed to the ground. The structure that spans between the two supporting columns is called top beam of crane framework. It is usually designed with single rolled section, a large welded wide flange steel girder, truss or a pair of box girders.

The structural parts of gantry crane system are manufactured from different types of material and designed in various form. If the structural parts of gantry crane system are designed to remain stiff for crane operations, the crane is considered as rigid gantry crane. Currently in many places, almost all the used gantry cranes are rigid with strict deflection requirements as reported by N. Zrnić *et al*. [2], so that their flexibility is neglected in many control system applications. However, the lifting capacities are heavier and the sizes of crane have increased continuously due to the increase of productivity and capacity. Such a condition makes the rigid gantry cranes are heavy and massive.

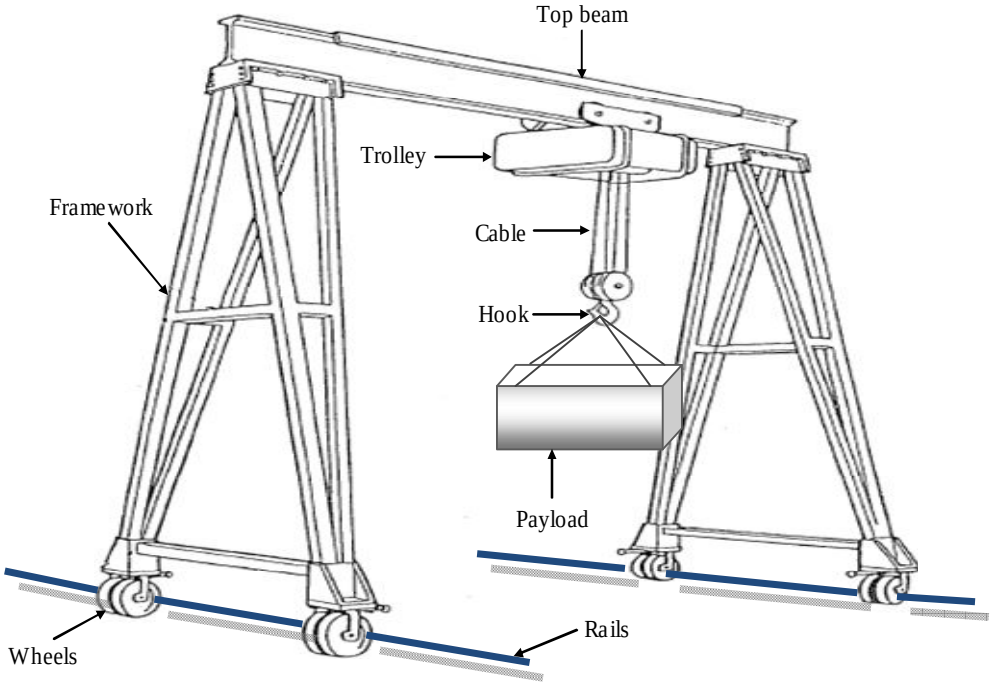

Figure 1.1: Gantry crane system [1]

The heavier lifting capacities and the greater size of gantry crane, the vibrational motion become more significant during crane operations and it must be considered. This condition is getting serious when the increase of stiffness has not kept pace with the increase of structural mass as mentioned in [3]. The increase in mass and smaller increase in stiffness creates longer natural periods and larger magnitudes swing angle as further discussed in the next chapters.

In view of loading condition, there is a number of loading cases that gantry crane system experience either the crane framework or gantry crane itself during crane operations. Dead load of individual members of framework and stationary gantry crane components are static loads. Earthquake is dynamic load from environment, together with wind gust or snow fall if it is located on a yard. With respect to the gantry crane, traversing or hoisting the payload at any place under the crane framework is significant dynamic load which exists at any point on the crane framework. This dynamic load moves at any position along the span of the top beam of crane framework. It makes the magnitude and position of the load vary in both time and space.

The other types of dynamic load are unevenness on the surface of the flange of the top beam and imperfect wheel alignment. They may cause the gantry crane traversing along the top beam to vibrate and to excite the crane framework. In the point of view of trolley motion, starting and stopping the trolley changes the velocity of the gantry crane and generates acceleration and deceleration effect. The changes in trolley velocity cause the crane framework are to experience significant inertial forces, the payload attached to the hook to swing freely and the increase of condition tension of hoist cable as further discussed in the next chapters. As demonstrated in [4], the swinging motion of payload is an important cause of the dynamic forces on the crane framework.

1.2 Problem Statement

Moving load as a total weight of trolley, lift system and lifted load according to Bhimani [3] which is accompanied by swing effects, moves along the top beam causing dynamic effects on the gantry crane and crane framework.

It can produce larger responses than those produced by the same load if it were stationary on the top beam. The fact that the motion of gantry crane is taking place at higher speed due to the increase of productivity leads to the possibility of payload to swing erratically. Because of low damping in the system dynamics, gantry crane system can vibrate with large amplitudes which may vanish for many seconds or minutes.

If the gantry crane is taken as a moving subsystem, then this moving subsystem will induce the crane framework motion and conversely. They will create bidirectional dynamic interaction as mentioned in [5], [6] and constitute nonlinear coupling terms between the gantry crane and crane framework. The motion of gantry crane system will be affected. These dynamic characteristics cannot be described by classical model of pendulum system with moving pivot point. In classical model of a pendulum system, the support structure of pendulum system is assumed to be rigid, so that the pendulum swings in a static pivot point. Regarding to the crane framework construction, the actual motion a pendulum-like swinging motion will be different. In order to lift heavy payloads, crane frameworks usually have very strong structures and big dimension, they are still large flexible mechanical structures and weakly damped according to Rahman *et al.* [7].

Under heavy payload, the crane framework construction will deform under the total weight of gantry crane. The elastic deformation of all elements of gantry crane system cannot be neglected anymore, particularly for bigger and longer crane framework as shown by References [2], [3], [8]. The pivot point of the swinging payload will not remain static because of deformed construction. The hoist cable that suspends the payload will undergo deformation as well. It reflects that the actual condition of gantry crane motion differs from the pendulum system theory. It is also known that the presence of elastic deformability will induce the unwanted vibration when it is subjected to dynamic loads. It causes issues related with safety of gantry crane system, operators and surrounding environment.

Mostly the crane frameworks are complex structures. Numerical method is the best approach to approximate the solutions, while further advances in computational

technology allow the finite element to handle structural response induced by moving load.

Commercial software such as ANSYS and other software packages can handle most cases like dynamic analysis under moving load, but they are not usually set up easily as mentioned in [9]. They need extended subroutine to run such a case. This is going to be more complicated for coupled dynamic system like interaction between crane system and its framework.

Besides the modeling, simulation and dynamic analysis of cranes system, in perspective of vibration control, active vibration control has not been widely investigated in the area of flexible crane system. Mostly, it is implemented with rigid body assumption either in simulation or real time experiment. Most published work with the consideration of the aforementioned condition is quite rare. There seems to be a limited number of works dealing with this class of problem. For those reasons, this thesis is addressed.

1.3 Objective

The goal of this research is to increase the understanding of dynamic behaviors of flexible gantry crane system during normal crane operation. This will further pave the ground of the possibilities in providing dynamic model for control purposes by introducing the structural flexibility of gantry crane into industrial implementation. This thesis is focused on deriving physics-based model to simulate the dynamic behavior of gantry crane during traverse motion. Because of the model-based nature of the study, the dynamic model of flexible gantry crane must be derived first to underlie numerical solution and to develop active controllers. Based on that, the objectives of this research fall into the three main categories:

1. To propose the dynamical model of three dimensional gantry crane system by introducing the flexibility of crane framework and hoist cable into the model.
2. To develop computational technique to solve the first objective, and conduct the parametric studies to investigate its dynamic behavior numerically.
3. To design active vibration controller by applying the dynamical model as a plant in control algorithm with purpose of transferring the payload into a target

position as fast as possible, while minimizing the swing angles of payload during the crane maneuver.

For these objectives, computer codes have been developed using Matlab® language and some subroutines codes in ANSYS are generated.

1.4 Scope and Thesis Contribution

For simplicity, several simplifications in dynamic model are made as further described in the next chapters. For verification purposes, the dynamic responses obtained in this study are partially compared with the results obtained by ANSYS, state-space, ODE 45 and the well-known 3-DoF model of pendulum (rigid model of gantry crane system).

The contribution of this work is an effort to extend the application of moving load concept on gantry crane system by including the modeling of dynamics of gantry crane on flexible crane framework. Parts of this thesis are the development of some previous researches in [5]-[6], [9]-[12], additions to the present work are as follows:

1. Update dynamic model of three dimensional flexible gantry cranes by introducing the flexibility of crane framework and hoist cable onto the dynamic of gantry crane system. Combination between finite element method in conjunction with moving finite element method and the Lagrange's equations are proposed in order to analyze bidirectional coupling between the dynamics of gantry crane and crane framework. The analysis is in time domain together with Fast Fourier Transformation (FFT) to estimate the frequency content. Updated dynamic model covers 3D swinging motion of payload, inertial terms and kinematic nonlinearities of gantry crane on the flexible crane framework.
2. Provide numerical solver to predict dynamic responses of the gantry crane system. The tools apply two numerical integration methods, namely, Newmark-β and fourth-order Runge-Kutta technique simultaneously.
3. The application of control methods to suppress the vibration caused by the coupling between gantry crane system and crane framework in the presence of structural flexibility in plant dynamic model.

1.5 Thesis Organization

The chapters of this thesis have been arranged in order to cover the objectives explained above. The summaries of each chapter are as follows.

Chapter 1 presents an introduction to the gantry crane system to be studied within this thesis. Statements of problem are presented in addition to objective to be met; also contribution of this study is mentioned.

Chapter 2 contains literature review and background theory. Literature review provides state of the art in researches related with the title of this thesis. Background theory includes the basic of finite element method, the moving finite element for space frame and its application to moving load case. The utilization of numerical integration methods and control methods are described in the last subsection.

Next, deriving of the equations of motion of flexible gantry crane system is presented in Chapter 3. This dynamic model covers three cases of loading on flexible gantry crane system, namely: swinging motion of payload (case I), moving load (case II) and moving trolley carrying a swinging payload (case III). Numerical approach to solve the system equations are formulated step by step.

Chapter 4 deals with the evaluation of the work contained in Chapter 3. This chapter simulates the dynamics of crane framework and gantry crane under case I, the dynamics of skeletal structures under case II and finally, dynamics of crane framework and gantry crane under case III. The parametric studies are conducted to investigate the dynamic responses of gantry crane system.

The work contained in Chapter 3 and Chapter 4 is then used as basis to design active vibration control methods and presented in Chapter 5. Control methods are Zero Vibration Derivative-Derivative (ZVDD), Proportional Integral Derivative (PID) and Fuzzy Logic Controller (FLC). The performances of each controller are demonstrated in controlling the gantry crane.

Finally, conclusions concerning the overall work are presented in Chapter 6 and areas of future work on this research are recommended.

CHAPTER 2

LITERATURE REVIEW AND THEORY

2.1 Introduction

The current state of the art is assessed by reviewing the available literatures and the findings are discussed within this chapter. This subsection includes research on dynamics of crane system carrying moving load, structural systems carrying moving load and control of flexible structural systems. The selected theory related with this thesis covers the modeling of space frame structure traversed by a point force and mass by presenting the concept of equivalent nodal forces. The concept of moving finite element are described in order to consider the inertial effects and kinematic nonlinearities of the moving load on the overall matrices property of space frame. Numerical integration methods is used to solve the dynamic model related with the title of this thesis are presented as well. Finally, the methods of active vibration controllers are discussed, respectively in the last subsection.

2.2 Literature Review

2.2.1 Researches on Crane System

Literatures dealing with the dynamics of crane system are relatively scarce. Some of the researchers focus on the modeling, simulation and analysis, while the others deal with the control strategies and techniques for vibration suppression. In most studies dealing with the dynamics of the crane, the dynamic load is modeled as moving force or moving mass model. Researches on the dynamic of crane system carrying moving loads that have been reported are summarized in Table 2.1.

Table 2.1: Reports on the Dynamic of Crane Systems Carrying Moving Load

No.	Crane Type	Dynamic Load Type	Analysis Method	Remarks	Ref.
1.	Container crane	Interaction between trolley and supporting structure caused by a moving mass, including influence of moving mass inertia, influence of Coriolis and centripetal force and deceleration of moving mass.	Container crane was represented as single girder using 1-D beam element. This girder is supported by two linearized springs with additional lumped mass for each spring. Differential equations of motion were obtained from Lagrange's approach by using Assumed Modes Method (AMM). The differential equations were solved numerically by using the fifth-order Runge-Kutta.	Deflections, bending moments, Dynamic Amplification Factor (DAF), and acceleration of moving mass in vertical direction were investigated. They concluded that DAF of deflection was 1.137 with respect of static deflection, lower than recommended value by design standard codes.	[2]
2.	Slewing crane	Electrical motor as driving force	Payload was modeled as spherical pendulum. The nonlinear nature of the swinging motion for large angles and the nonlinearity of the power transmission were considered. The structure's elasticity and damping, the friction in the main bearing, and the air resistance were also taken into account. Lagrange equations were used to derive the equations of motion. The equations were solved numerically using the Runge-Kutta method.	The mathematical model was checked by means of measurement on the physical model. The results were much closer in time and frequency domain.	[4]

Table 2.1: Continued

3.	Overhead crane	A simply supported uniform Euler-Bernoulli beam carrying a crane (carriage and payload). The payload which was assumed to be suspended from the carriage on a massless rigid rod and restricted to motion in plane.	The differential equations of motion were derived using Hamilton's principle and operational calculus was used to determine the vibration of beam which was in turn, used to obtain the dynamics of suspended payload.	The position of the maximum deflection tends to drift to the right or the left of the beam centre depending on whether the operating speed is above or below this threshold. The magnitude of the maximum deflection tends to decrease with increasing drift from symmetry. The threshold speed and the location of the maximum beam deflection for a given carriage speed are observed to be functions of the beam vibration frequency.	[5]
4.	Overhead crane	Extension of work in [5] where beam carrying a crane that was allowed to travel in a direction perpendicular to its span. The point mass payload is attached to the carriage via a massless beam and was allowed both in-plane and out-of-plane motion	The Rayleigh-Ritz solution technique was used to obtain the equations of motion of the system which were solved with a modified Newmark method.	The pendulum length results showed that the dominant frequencies in the swing responses decreased with increasing pendulum length. The amplitude of swing angle increased with increasing payload mass. Minimal changes were observed in the swing angle frequencies for corresponding changes in payload mass.	[6]

Table 2.1: Continued

5.	Moored crane-ship	Sea waves and mooring forces	The boom was modeled based on finite element method, while the payload was modeled as a planar pendulum of point mass. The dynamic responses were investigated in time domain based on a Newmark method and an iterative method.	Large vibrations observed for the crane-ship with flexible boom. Crane-ship with flexible boom had a longer period of motion than that with the rigid boom.	[8]
6.	Gantry crane	Four time-variant moving point forces	The equivalent nodal forces for 1-D beam element. The problem was solved by standard finite element packages.	The technique of the equivalent nodal forces to represent the moving forces provided sensible, realistic results and generally applicable for other finite element packages.	[9]
7.	Gantry crane	The moving trolley and the swinging object, where the swing was assumed only in the plane with respect to the stationary framework. The hoisted object behaved as simple pendulum system and the centrifugal force was neglected. The motion of trolley was prescribed.	Concept of the equivalent moving mass for 3-D beam element. The problem was solved by means of the finite element and direct integration method, Newmark-β.	The axial and horizontal vibration responses of the static framework were as significant as the conventional vertical response. With small angles and planar swing, the influence of the swinging angle of the hoisted object on the vertical and axial dynamic responses of the structure was negligible, except the horizontal responses of the structure. He found out that it was very sensitive to the swinging angle of the hoisted object.	[10]

Table 2.1: Continued

8.	Tower crane	Slewing flexible jib structure when simultaneously traversed by a moving mass - carriage hoisting payload pendulum.	The jib structure was modeled as clamped-free Euler–Bernoulli beam attached to a rotating rigid hub or mast. Two tie bars of tower crane were modeled by two linear springs in the ‘‘in-plane” and ‘‘out-of-plane”. The payload was modeled as a sphere pendulum attached to via massless inextensible cable the carriage moving on the rotating beam. Non-linear coupled equations of the beam and the payload pendulum were derived by means of the Hamilton principle.	By using Ritz discretization method, the solutions for the in- and out-of-plane motions of the rotating beam were proposed. Some remarks were made on the equations of motion.	[11]
9.	Gantry crane	Moving trolley and the hoisted object	Concept of moving finite element method for 2-D beam element. The dynamic response was solved using the Newmark- β method.	The maximum axial displacements of the framework increased with the increase of the amplitude of the swinging angle of the hoisted object, except for vertical responses. The maximum axial and vertical dynamic responses of the framework was closely related to the cable length, where the largest maximum axial or vertical displacement would appear when the swinging frequency of the hoisted object associated with a certain cable length, was close to the natural frequency of framework in the axial and vertical direction.	[12]

Table 2.1: Continued

10.	Gantry crane	Four time-variant moving equivalent lumped masses	A combined finite element method and analytical technique for 2-D beam element. The dynamic response was evaluated by using mode superposition technique.	Extended work of [12], where The method had been validated with experimental results.	[13]
11.	Gantry crane	Technique in work [12] was utilized as moving load to the stationary framework.	Finite element method by means of conventional modal analysis for a scale laboratory model, and by using the scaling technique.	The scaling technique can provide sensible and realistic dynamic similarity between the full-size structure and a scale model.	[14]
12.	Tower crane	Comments on work [10]	Comments on work [10]	Correction for model of two tie bars proposed by [10] and suggested to consider the influence of tower stiffness and applied non-classical boundary condition.	[15]
13.	Bridge bucket unloader	Moving mass	Finite element method	A method for analyzing the dynamic response of a structural system with variable mass, damping and stiffness. The results were then verified with SAP software.	[16]

Table 2.1: Continued

14.	Tower crane	Acceleration and deceleration of hoisted payload.	The members of tower and boom structures were modeled as space truss or frame elements. Modal properties and dynamic responses, respectively, were computed by the Newmark method and subspace iteration method with QL algorithm.	Jib angles changed both the inertia and stiffness distribution of the whole structure, while the added bracings contribute mainly to the global stiffness of the system. Some modes were insensitive to the change of jib angle. Acceleration and deceleration of hoisted payload were significant on dynamic response of structure.	[17]
15.	Tower crane	Pendulum motion of payload, either pure planar or pure spherical motion.	The tower crane was modeled by finite element method, while the pendulum motion was represented as rigid-body kinetics. Lagrange's approach is used to derive the coupled dynamics equations based on a simple perturbation scheme and the assumption of small pendulum angle.	The dynamic responses of the tower crane were dominated by both the first few natural frequencies of crane structures and the pendulum motion of the payload. The DAF generally increase with the increase of the initial pendulum angle and the changes were just slightly nonlinear for the planar pendulum motion.	[18]
16.	Rail-guided cart with hoisted payload	Electrical motor as driving force	The linearly moving chart, driven by a travel mechanism was modeled as a discrete six DoF. The hoist drive was modeled as one DoF system. EoM of the cart elements were derived using Lagrange dynamics and solved by fourth-order Runge-Kutta.	The proposed model was verified with classical linearized 2 DoF model of pendulum with moving pivot.	[19]

Table 2.1: Continued

17.	Overhead crane	Hoisting motion	Girder of an overhead crane was modeled using 1D beam element and derived by Lagrange equations of the second order. They included the dynamic model of hoist mechanism into dynamic model of an overhead crane under lifting condition.	Investigation of the dynamics of an overhead crane lifting process in a vertical plane. They showed that non-stationary operating regimes introduced variable loads.	[20]
18.	Slewing crane	Extended work of [3]	Extended work of [3]	The horizontal inertial forces in the radial direction are of no less importance than the forces in the tangential direction. Based on that, a new coefficient of radial horizontal inertial force was introduced and a diagram for the rapid determination of this coefficient was calculated.	[21]
19.	Boom crane	Flexible soil foundation of the boom crane.	The dynamic models were derived using second order Lagrange equations and solved numerically.	The amplitudes of vibration of the whole crane during the rotation of the boom decrease with an increase in its rotational speed. Another finding was the proper selection of kinematic parameters, particularly the rotation, allows deflection to be minimized and the precision of positioning increased. The greater the rotational speed of the boom, the greater was the deflection of the wire rope.	[22]

Table 2.1: Continued

20.	Mobile crane	Hydraulic motion as driving force	Flexible boom of a mobile crane was modeled by the finite element method and modal variables were used as the elastic variables by utilizing modal transformation.	The boom motion time affected the crane dynamics. For low speed, the effect of flexibility was very small. When the speed was increased, the effect of flexibility was dominant.	[23]
21.	Over head crane	Uprising dynamics of an overhead crane carrying two trolleys	The main beam was modeled as flexible box beam, the trolley as a sphere mass, the uprising object as a rigid body and the wire rope as a flexible body.	Simulations results obtained from ADAMS from a specific example show good agreements with physical conditions	[24]
22.	Truck crane	Kinematic forcing such as: change of the telescopic boom length, rotation of the boom and the change of wire rope length.	The flexibility of the support system was modeled by elastic suspension and the load was considered as a particle. The equations of motion were solved by fourth-order Runge-Kutta.	The influence of the flexibility of the support system on the load motion.	[25]
23.	Hydraulic mobile crane	Response of the structure and the state parameters of drive system with kinematic forcing such as desired rotary speeds.	Concept of flexible multi-body and finite element method.	The simulation results showed that, in addition to the accelerations and decelerations of crane movements, the rotary speed had also significant influence on crane dynamic responses.	[26]
24.	Lattice mobile crane	Hoist speed, acceleration, and deceleration.	Hoisting rope system was modeled by nonlinear finite element, while the boom was modeled by Timoshenko beam element.	The proposed method was very convenient for simulation of the crane hoisting motion and control system.	[27]

Table 2.1 informs that three kinds of dynamic sources in the dynamic of crane systems carrying moving load. First source of dynamic load comes from moving subsystem of crane system itself as discussed in [2], [5], [6], [9]-[12] and other papers as stated in Table 2.1. The second source is driving force from power transmission as shown by Jerman *et al*. [4]. Ren *et al*. [8] uses the third source which comes from ocean waves and mooring forces. In addition to aforementioned references, experimental modal to find natural frequency of mobile gantry crane was conducted in [28], while forced vibration due to wind and earthquakes on container crane was studied by Wu *et al*. [29].

Further, among those references, Ref. [10] and [18] have investigated the dynamic responses of a 3D crane structure and closely relate to this thesis. Compared to Wu [10], dynamics of payload was not introduced, restricted to planar swing and without considering detailed two-sided interaction between gantry crane on the flexible crane framework. Besides that, Ju *et al*. [18] only studied the swinging motion of payload in tower crane with stationary trolley. They introduced small perturbation in solving payload dynamics for small angle of swing, rigid hoist cable and the motion of payload was restricted to pure planar and pure spherical motion. They also concerned only in dynamic responses of crane framework.

2.2.2 Research on Structural Systems Carrying Moving Load

Researches on elastic structures subjected to moving loads are abundant. A plenty of important citations related to moving load are shown in Table 2.2.

Table 2.2: Moving loads literature review

No.	Skeletal Structure Type	Moving Load Type	Method	Remarks	Ref.
1.	Beam	Moving mass	Analytical	A solution for a single-span beam carrying a moving mass was derived by approximating the total time derivative of the mass displacement with partial derivative and by using as a first approximation; the solution without the effect of the mass was fully assessed.	[30]

Table 2.2: Continued

2.	Beam	Moving mass	Analytical	A simply supported elastic single-span beam under random loads moving with variable speeds. The approach was based on the Euler-Bernoulli's beam theory. The results showed that the acceleration tends to induce larger deflections, while the deceleration smaller ones. The effect of a variable speed was significant for the deflection of the beam.	[31
3.	Beam	Moving vehicles	Analytical	The simulations showed that the influence of centripetal and Coriolis forces, together with vehicle's mass rotatory inertia of a simply supported light bridge under a moving vehicle of constant magnitude and velocity was significant and had to be considered in dynamic analysis.	[32]
4.	Beam	Moving mass	Analytical	The onset of separation between the moving mass and by using the integro-differential equation of motion and modal analysis method. Numerical tests revealed that the separation could occur easily and had significant effect on the dynamic responses of the beam especially at high velocity of the moving mass.	[33], [34]
5.	Beam	Moving mass	Analytical	The possibility of the mass separating from the beam by monitoring the contact forces between the mass and the beam during the motion. The equation of motion of Euler beam acted upon by a concentrated mass moving at a constant speed was formulated by using the Lagrange approach and the assumed mode method. It was found that separation of the mass from the beam might occur for a relatively slow speed and small mass when the beam was clamped at both ends.	[35
6.	Beam	Moving mass	Analytical	The equation of motion for a Timoshenko beam acted upon by a concentrated mass moving at a various prescribed constant speed was formulated by using the Lagrange approach and AMM. It was found that separation of the mass from the beam might occur for high axial speeds of the mass and such a separation can be suppressed by a Winkler foundation of large stiffness.	[36

Table 2.2: Continued

7.	Beam	Moving mass	Analytical	Under an accelerating mass, It was found that separation of the mass from the beam might occur for a Timoshenko beam when the travelling speed of the mass was large due to large initial travelling speed or large prescribed acceleration.	[37]
8.	Beam	Moving mass	Analytical	It was confirmed that the deflection under the moving load computed using the "moving-force formulation" was not always an upper bound solution for the corresponding "moving force moving mass" formulation for both the Euler beams and Timoshenko beams.	[38]
9.	Beam	Moving mass	Analytical	Timoshenko beam traversed by uniform partially distributed moving masses was investigated. Equations of motion were solved by using a finite difference based algorithm. It was observed that by increasing the length of the load distribution, a decrease in the maximum dynamic deflection of the beam was obtained which was essentially the result of a decrease in time during which the total load acted on the beam.	[39]
10	Beam	Moving mass	Analytical	The multi-span continuous beam traversed by a moving mass at a constant velocity was investigated using Euler-Bernoulli beam theory. Eigen function expansion accompanied by the direct integration method was used for the solution. When the velocity parameter exceeded about 0.5, all the spans of continuous beams seem to change its behavior and their local peaks showed an increasing tendency with the velocity. In the calculated range of velocity parameter, the inertia of moving mass does not significantly affect DAF when the value of the mass ratio was less than 0.1.	[40]

Table 2.2: Continued

11.	Beam	Moving mass	Finite Difference Method and perturbation technique	Investigation of the longitudinal and transverse motions of a finite elastic beam traversed by a moving mass was studied. The results showed that the effect of the friction force between mass and the beam on the longitudinal motion was to be significant.	[41
12.	Beam	Moving force	Combined analytical and numerical method	The determination of unique amplitude-velocity dependence functions for simply supported (SS) and clamped-clamped (CC) for Euler-Bernoulli beams. There existed a unique function describing the dependence of the maximum response of an arbitrary beam with given boundary conditions on the velocity of the traveling force.	[42
13.	Beam	Moving mass	Combined analytical and numerical method	The influence of various parameters such as forward force, retard force, friction and convective acceleration of the interface between the moving mass and the simply supported Euler-Bernoulli beam was investigated. The applied forward force amplifies the speed of the mass and the displacement of the beam. The ability to bring the mass to a halt at a desired point on the beam was accomplished by applying a constant reverse force to the mass and/or increasing the friction between the mass and the beam after the mass had achieved specified condition.	[43
14.	Beam	Moving mass	Finite element method	Continuum discretization for finite element models analyzing a moving load on an elastic beam was investigated. The results indicated that the model accuracy could be maintained at an acceptable level provided that, in general, the number of elements used in discretized the support structure continuum is at least two to eight times greater than the number used in static analysis.	[44

Table 2.2: Continued

15.	String & Beam	Moving mass and moving force	Finite Element method	The space-time finite element method was proposed for the discrete element of the string and the Bernoulli-Euler beam. The perfect coincidence with the semi-analytical solutions proved the efficiency of the space-time approach. The solution method can easily be implemented in the classical finite element code.	[45]
16.	Planar structure	Moving force	force-based finite element	The use of force-based finite elements to analyze moving force in planar structures was developed. They proposed new numerical integration approach called Gauss-Lobatto integration. Accurate results for the moment and shear demand history at specified locations in a structure.	[46]
17.	Beam	Moving mass	Classical modal analysis	A new correction procedure for dynamic analysis of Euler-Bernoulli beam under moving loads was proposed. The Solutions were obtained by using classical modal analysis. Numerically, the proposed corrected solution improved the stress response resolution. However, it required the knowledge of the frequency content of the forcing function in order to guarantee the robustness their method.	[47]
18.	Beam	Moving force	Analytical	The non-linear dynamics of an Euler-Bernoulli beam under moving loads was studied. The results showed that the load inertia of moving load could only be neglected under conditions: when the load velocity was higher than that which leaded to the resonance in the beam and when the moving mass was very small compared to the mass of the beam. When non-linearity came into play, beam deflection and the resonance velocity of the moving load increased.	[48]

Table 2.2: Continued

19.	Beam	Moving force	Analytical	The dynamic response of multi-span shape memory alloy (SMA) beams subjected to a moving force was presented. The important results were concluded: unlike the isotropic viscously damped beam, SMA beam was significantly nonlinear, its behavior changed with respect to the moving load and higher values of the moving load caused more damping effect and less Young's modulus of the SMA.	[49]
20.	Beam	Moving mass	Combined analytical and numerical method	The dynamic behavior of a flexible cantilever beam carrying a moving mass-spring was investigated. The equations of motion were derived by Hamilton's principle, solved numerically using the Galerkin method and automatic ODE solver. The numerical results were compared with a closed-form analytical solution obtained using a perturbation method. The numerical solutions showed that when the motion was predominantly bi-periodic, the results matched well. They also identified regions of strong non-linear coupling between the beam and the moving mass.	[50]
21.	Beam	Moving mass	Analytical	A clamped-free flexible beam rotating in a horizontal plane and carrying a moving mass by the Euler-Bernoulli beam theory was modeled. The equations of motion were derived by Hamilton's principle. The numerical bisection method was used to solve for the vibration frequencies. The modal frequencies as functions of beam angular velocity and mass position for different values of moving mass. When angular velocity of beam was zero, modal frequencies decreased or remain approximately constant with increase in values of moving mass. Increasing of angular velocity of beam, the modal frequency decreased with increase in values of moving mass.	[51]

Table 2.2: Continued

22.	Beam	Moving mass	Analytical	Extended work of [51], where the equations were solved numerically using the fourth-order Runge-Kutta method. The peak deflections increased with increase in mass and decrease with increase in mass travelling time. A decrease in the mass travelling time caused an increase in the steady state vibration amplitude under all conditions.	[52]
23.	Beam	Moving mass	Analytical	A simple and practical approximate technique for determining the time response of beam with internal hinges and different boundary condition was formulated. The theories and the results were based on the Bernoulli-Euler beam and the governing equations were derived by using Lagrange's equation. The results were then compared with a general-purpose nonlinear dynamic finite element program.	[53]
24.	Beam	Moving mass	Analytical	The development of identification method of moving loads on bridges was conducted under Euler-Bernoulli beam. To evaluate the proposed identification methods, a series of experiments had been conducted.	[54]
25.	Bar	Moving force	Analytical	New method for the stationary response of an infinite bar posed on a Winkler foundation under constant moving loads was proposed. The bar was discretized by the Galerkin method and solved using the semi-analytical and the finite element method. Comparing with numerical solutions with analytical ones showed that the proposed method was valid for all values of load speed.	[55]
26.	Beam	Moving harmonic load	Analytical	Similar with work [55], Numerical approach to the stationary solution of infinite Euler-Bernoulli beams posed on Winkler foundations under moving harmonic loads was proposed.	[56]

Table 2.2 shows the development of concept of moving load during the years from 1996 until 2008. Mostly, researchers use analytical method to solve moving load problem and confined to Euler-Bernoulli or Timoshenko type beam structure. The methods to calculate the dynamic responses still expand dynamically, not only for finding the dynamic response, but also the methods for identification system purposes as shown in Ref. [54]. Mostly, beam structures are analyzed with under condition that beam is in stationary position, but Ref. [50]-[52] also investigate the dynamics of beam which has angular velocity (large deformation) under moving load.

2.2.3 Researches on Control of Flexible Crane System

Recently, much attention has been placed on the modeling of dynamics and control of flexible structures. A number of published papers deal with the applications of control theory in flexible structures without moving load. Selected references can be referred in [57]-[61]. However, it is still rare on application of flexible crane system. Generally, control of crane system is implemented with rigid body assumption, either in simulation or real time as demonstrated in [62]-[69]. Papers relate to the case of flexible structures with a moving load and crane system is shown in Table 2.3.

Table 2.3: Control of flexible crane system literature review

No.	System type	Controller	Remarks	Ref.
1.	Cantilever beam under a moving mass	Adaptive fuzzy control	The dynamic response model of the system type was solved by the Duhamel integration and iterative procedure by the step-by step method. The experimental showed that smart material could suppress actively the time-varying flexible structure vibration.	[70]
2.	Gantry crane with flexible cable	Proportional, Derivative and coupling amplification (PDC)	Theory and experiment for position control of the system type was conducted, where Galerkin approach was used to incorporate spatially varying tension and damping. The governing partial differential equations horizontally-translating gantry, flexible cable and payload were derived using Lagrange method. Experimental results showed accurate position regulation and good cable vibration damping with PDC controller.	[71]

Table 2.3: Continued

3.	A crane mounted on a tower-like flexible structure.	H_∞	Governing equations were derived using Lagrange's equation including Rayleigh dissipation function. They applied H_∞ controller to suppress the vibration of tower and the sway of the load in addition to control the positions of crane. The control experiment showed that the controller was effective for the control of the tower crane.	[72]
4.	An Euler-Bernoulli beam with an attached mass rolling on an initially curved beam	Linear Quadratic Regulator (LQR)	A simple closed-loop feedback control combined with the coupled non-linear equations of motion was derived by Newtonian mechanics. The approximate solution of the beam-mass system could be obtained by employing Galerkin method. Results of their study showed that the vibrations of the system can be suppressed significantly even if a simplified control model was applied.	[73]
5.	Nonlinear beam under moving force	Time delay feedback	Time delay feedback controller to control the bifurcation in nonlinear beam under moving force was applied. The bifurcation equation of the nonlinear dynamic system was obtained using the perturbation method. The result indicated that time delay feedback controller might work well to eliminate the bifurcation.	[74]
6.	Moving elastic beam fixed on a moving chart carrying a moving mass	Open-loop response	The open-loop response of moving elastic beam fixed on a moving chart carrying a moving mass in tracking the pre-designed path of the moving mass was carried out. The coupled dynamic equations were obtained from Hamilton's principle and solved by unconstrained modal analysis. The simulated results showed that their proposed method can be applied to analyze the dynamic behavior and to design the model-based controller to suppress the vibration of the elastic beam.	[75]
7.	Flexible beam mounted on an elastic base.	Independent modal space control (IMSC)	The beam was analyzed using a finite element approach, where the system equations were expressed as state-space equations. IMSC was applied for modal decoupling of the system and design of a vibration controller. They demonstrated that the control strategy was effective for vibration suppression of the beam system under any of types of disturbances.	[76]

Table 2.3: Continued

8.	Container cranes with flexible cable	A control law based upon the Lyapunov's second method.	The container crane with flexible cable was modeled as hybrid PDE-ODE system. The dynamics of the moving system was derived as a cable with tension caused by payload using Hamilton's principle. They revealed that a time-varying control force and a suitable passive damping at the actuator can successfully suppress the transverse vibrations.	[77]
9.	Cable-driven crane	Input shaping	Input shaping could counteract the influences of vertical acceleration on cable-driven crane.	[78]
10.	Quay-side container crane with flexible hoist cable	Delayed feedback	It was demonstrated that using new frequency approximation can improve the performance of a delayed feedback controller.	[79]

2.3 Application of Finite Element Method in Moving Load for Space Frame Structure

A "moving load" refers to a load that varies in time and space, whereas the conventional static load varies only in space, while a stationary oscillatory load varies only in time. In general, moving load can be classified into three categories; the moving force, moving mass and moving oscillator model. In this, the trolley construction for cranes is rigid and moving oscillator model can be ignored as mentioned in [2].

Finite element method has been employed in deriving the equations of motion for moving load model on skeletal structures [9]-[13], [45]-[47]. That is because the method provides very broad capabilities and versatility in the modeling process and is chosen in this thesis to simulate the dynamic behavior of gantry crane system. The concept of moving load is derived based on those references, where the concept is developed for space frame.

2.3.1 Equivalent Nodal Forces for Space Frame Structure

Moving force neglects the inertia forces of a moving mass and does not consider dynamic interaction between moving mass and structure. An element of space frame element which traversed by a point force is shown in Figure 2.1.

The governing equation of motion can be obtained through the application of the finite element method for MDoF structural system, geometrically and materially linear dynamic is represented as follows [91].

$$[M]\{\ddot{q}\}+[C]\{\dot{q}\}+[K]\{q\}=\{F(t)\} \tag{1}$$

where $[M]$, $[C]$, $[K]$ are representing global mass, damping and stiffness matrices of the beam, $\{q\}$ is the nodal displacement vector and its time derivative and $\{F(t)\}$ is the external force vector.

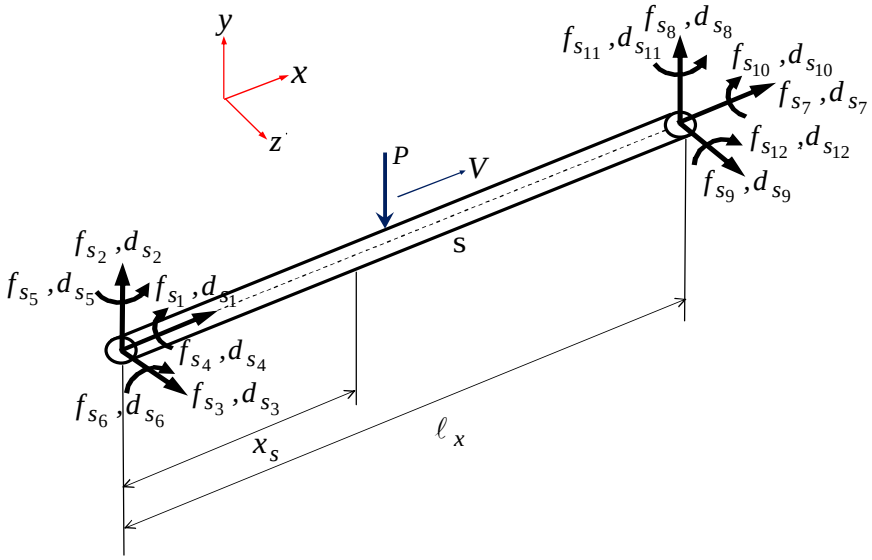

Figure 2.1: Equivalent nodal forces of the *s*-th space frame element

The concentrated load traveling across the beam is handled by modifying the external load $\{F(t)\}$ in Equation (1) into the equivalent nodal forces $f_{sk}(k=1-12)$ as shown by in Figure 2.1, where $s_k(k=1-12)$ are the numberings for the twelve degrees of freedom of the *s*-th space frame element on which the moving load applied and given as follows [10].

$$[M]\{\ddot{q}\}+[C]\{\dot{q}\}+[K]\{q\}=\{N_k\}^T P=\{f_{s_k}(t)\}$$
$$=\left[f_{s_1}(t)\quad f_{s2}(t)\quad f_{s_3}(t)\quad f_{s_4}(t)\quad f_{s_5}(t)\quad f_{s_6}(t)\quad f_{s_7}(t)\quad f_{s_8}(t)\quad f_{s_9}(t)\quad f_{s_{10}}(t)\quad f_{s_{11}}(t)\quad f_{s_{12}}(t)\right]^T \tag{2}$$

Term P is the magnitude of the applied concentrated load and $N_k(k=1-12)$ is the transposition of the shape functions.

Since this structure is space frame, then the shape functions of space frame element are $\{N_k\}=[N_1\quad N_2\quad N_3\quad N_4\quad N_5\quad N_6\quad N_7\quad N_8\quad N_9\quad N_{10}\quad N_{11}\quad N_{12}]$. The shape functions and their derivatives are shown in Table 2.4.

Table 2.4: The shape functions and their derivatives of space frame element [91]

k	N	N'	N''
1.	$1-\varsigma$	$-\frac{1}{\ell}$	0
2.	$1-3\varsigma^2+2\varsigma^3$	$\frac{-6\varsigma+6\varsigma^2}{\ell_x}$	$\frac{-6+12\varsigma}{\ell_x^2}$
3.	$1-3\varsigma^2+2\varsigma^3$	$\frac{-6\varsigma+6\varsigma^2}{\ell_x}$	$\frac{-6+12\varsigma}{\ell_x^2}$
4.	$1-\varsigma$	$-\frac{1}{\ell_x}$	0
5.	$\left[-\varsigma+2\varsigma^2-\varsigma^3\right]\ell_x$	$-1+4\varsigma-3\varsigma^2$	$\frac{4-6\varsigma}{\ell_x}$
6.	$\left[\varsigma-2\varsigma^2+\varsigma^3\right]\ell_x$	$1-4\varsigma+3\varsigma^2$	$\frac{-4+6\varsigma}{\ell_x}$
7.	ς	$\frac{1}{\ell_x}$	0
8.	$3\varsigma^2-2\varsigma^3$	$\frac{6\varsigma-6\varsigma^2}{\ell}$	$\frac{6-12\varsigma}{\ell_x^2}$
9.	$3\varsigma^2-2\varsigma^3$	$\frac{6\varsigma-6\varsigma^2}{\ell_x}$	$\frac{6-12\varsigma}{\ell_x^2}$
10.	ς	$\frac{1}{\ell_x}$	0
11.	$\left[\varsigma^2-\varsigma^3\right]\ell_x$	$2\varsigma-3\varsigma^2$	$\frac{2-6\varsigma}{\ell_x}$
12.	$\left[-\varsigma^2+\varsigma^3\right]\ell_x$	$-2\varsigma+3\varsigma^2$	$\frac{-2+6\varsigma}{\ell_x}$

The parameter ς in the table is derived as follows [9].

$$\varsigma = \frac{x_S}{\ell_X} \tag{3}$$

where ℓ_X is the length of the *s*-th beam element and x_S is local position of the moving force from the left end of the *s*th beam element, at time t, as it can be seen from Figure 2.1. In addition, the position, velocity and acceleration of the point mass within the structure at any time is assumed to be,

$$x = x_0 + V_0 \cdot t + \frac{1}{2} \cdot a_0 \cdot t^2; \quad \dot{x} = V_0 + a \cdot t; \quad \ddot{x} = a_0 \tag{4}$$

where: x_0 is the initial position of moving load

x is the global position of moving load and its time derivatives

V_0 is the initial velocity of moving load

a_0 is the initial acceleration of moving load

The local position of the concentrated force P can be converted into the global position of as the function of x, i.e.,

$$\varsigma = \frac{x_S}{\ell_X} = \frac{x(t) - (s-1)\ell_X}{\ell_X} \tag{5}$$

where the numbering for space frame element on which the concentrated force P applies at time t is determined as follows.

$$s = \left(Integer\ part\ of\ \frac{x(t)}{\ell_X} \right) + 1 \tag{6}$$

Details about the equivalent nodal forces can be referred in [9] and [44]. Because the inertial effects of the moving load are not considered, overall matrices property of Equation (1) is time-independent.

2.3.2 Moving Finite Element for Space Frame Structure

Inertial effects of moving load can be accounted by extending moving point force model into moving point mass, which is assumed that it is always remain in contact with structure as depicted in Figure 2.2.

This model affects the magnitude and distributions of the external force. It also changes the conventional constant overall mass, damping and stiffness matrices for the entire system due to the time dependent of the magnitude and location of the moving mass. That is the concept of moving finite element developed by Wu [12] to take into account the inertial effects of the moving load for portal frame. The concept of moving finite element is then developed for space frame structure as depicted in Figure 2.2.

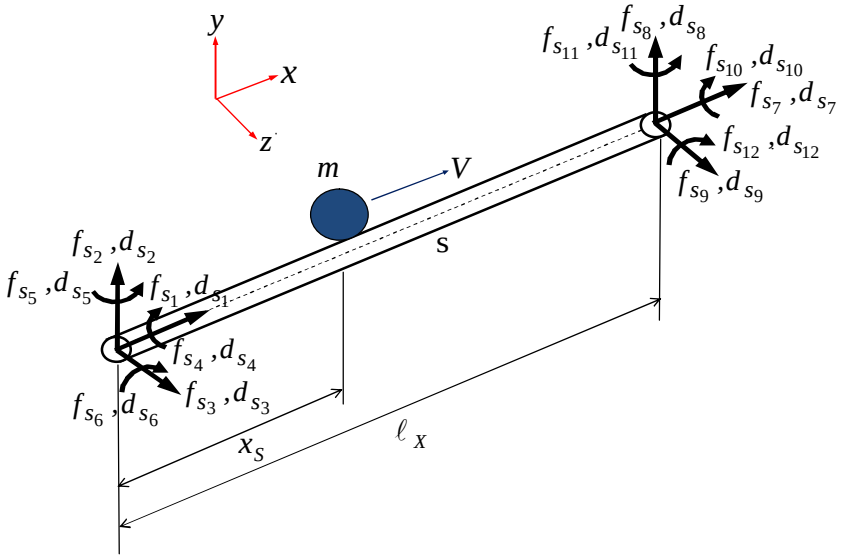

Figure 2.2: Moving point mass at the *s*-th space frame element [9]

The axial (x), vertical (y) and lateral (z) displacement of space frame element at position x, can be obtained as follows.

$$u = N_1 d_{s_1} + N_7 d_{s_7} \tag{7a}$$

$$v = N_2 d_{s_2} + N_6 d_{s6} + N_8 d_{s_8} + N_{12} d_{s_{12}} \tag{7b}$$

$$w = N_3 d_{s_3} + N_5 d_{s5} + N_9 d_{s_9} + N_{11} d_{s_{12}} \tag{7c}$$

where $d_{s\,i} = (i = 1-12)$ are the displacements for the nodes of the space frame element at which the moving mass locates. Thus, the Equation (7) can be rewritten as follows.

$$u(x,t) = \{N_k\}_u \{d_{s_k}\}_u \tag{8a}$$

$$v(x,t) = \{N_k\}_v \{d_{s_k}\}_v \tag{8b}$$

$$w(x,t) = \{N_k\}_w \{d_{s_k}\}_w \tag{8c}$$

Terms $\{N_k\}_u \quad u = k = 1,7$, $\{N_k\}_v \quad v = k = 2,6,8,12$ and $\{N_k\}_w \quad w = k = 3,5,9,11$ are shape functions associated with translation degree of freedoms in three directions axial (x), vertical (y) and lateral (z) and terms $\{d_{s_k}\}_u, \{d_{s_k}\}_v, \{d_{s_k}\}_w$ are displacements in three directions. Terms $(u(x,t), v(x,t), w(x,t))$ depend on position x and time t.

Derivatives of $u(x,t)$ with respect to time t and position x are:

$$\begin{aligned}
\frac{\partial u(x,t)}{\partial t} &= \frac{\partial u(x,t)}{\partial x}\frac{\partial x}{\partial t} + \frac{\partial u(x,t)}{\partial t}\frac{\partial t}{\partial t} \\
&= u'(x,t)\dot{x} + \dot{u}(x,t) \\
\frac{\partial^2 u(x,t)}{\partial t^2} &= \frac{\partial u'(x,t)}{\partial x}\frac{\partial x}{\partial t}\dot{x} + \frac{\partial u'(x,t)}{\partial t}\frac{\partial t}{\partial t}\dot{x} + u'(x,t)\frac{\partial \dot{x}}{\partial t} + \frac{\partial \dot{u}(x,t)}{\partial x}\frac{\partial x}{\partial t} + \frac{\partial \dot{u}(x,t)}{\partial t}\frac{\partial t}{\partial t} \\
&= u''(x,t)\dot{x}^2 + 2\dot{u}'(x,t)\dot{x} + u'(x,t)\ddot{x} + \ddot{u}(x,t)
\end{aligned} \tag{9a}$$

Derivatives of $v(x,t)$ with respect to time t and position x are:

$$\begin{aligned}
\frac{\partial v(x,t)}{\partial t} &= \frac{\partial v(x,t)}{\partial x}\frac{\partial x}{\partial t} + \frac{\partial v(x,t)}{\partial t}\frac{\partial t}{\partial t} \\
&= v'(x,t)\dot{x} + \dot{v}(x,t) \\
\frac{\partial^2 v(x,t)}{\partial t^2} &= \frac{\partial v'(x,t)}{\partial x}\frac{\partial x}{\partial t}\dot{x} + \frac{\partial v'(x,t)}{\partial t}\frac{\partial t}{\partial t}\dot{x} + v'(x,t)\frac{\partial \dot{x}}{\partial t} + \frac{\partial \dot{v}(x,t)}{\partial x}\frac{\partial x}{\partial t} + \frac{\partial \dot{v}(x,t)}{\partial t}\frac{\partial t}{\partial t} \\
&= v''(x,t)\dot{x}^2 + 2\dot{v}'(x,t)\dot{x} + v'(x,t)\ddot{x} + \ddot{v}(x,t)
\end{aligned} \tag{9b}$$

Derivatives of $w(x,t)$ with respect to time t and position x are:

$$\begin{aligned}
\frac{\partial w(x,t)}{\partial t} &= \frac{\partial w(x,t)}{\partial x}\frac{\partial x}{\partial t} + \frac{\partial w(x,t)}{\partial t}\frac{\partial t}{\partial t} \\
&= w'(x,t)\dot{x} + \dot{w}(x,t) \\
\frac{\partial^2 w(x,t)}{\partial t^2} &= \frac{\partial w'(x,t)}{\partial x}\frac{\partial x}{\partial t}\dot{x} + \frac{\partial w'(x,t)}{\partial t}\frac{\partial t}{\partial t}\dot{x} + w'(x,t)\frac{\partial \dot{x}}{\partial t} + \frac{\partial \dot{w}(x,t)}{\partial x}\frac{\partial x}{\partial t} + \frac{\partial \dot{w}(x,t)}{\partial t}\frac{\partial t}{\partial t} \\
&= w''(x,t)\dot{x}^2 + 2\dot{w}'(x,t)\dot{x} + w'(x,t)\ddot{x} + \ddot{w}(x,t)
\end{aligned} \tag{9c}$$

Due to the point mass, m is moving along a vibrating path, then Coriolis acceleration will occur as shown in Equations (9). An example, Equation (9b) is applied to the general element displacement in Equation (8b) yields:

$$\frac{\partial v(x,t)}{\partial x} = \{N_k{}'\}\{d_{s_k}\}_v, \frac{\partial^2 v(x,t)}{\partial x^2} = \{N_k{}''\}\{d_{s_k}\}_v$$
$$\frac{\partial v(x,t)}{\partial t} = \{N_k\}\{\dot{d}_{s_k}\}_v, \frac{\partial^2 v(x,t)}{\partial t^2} = \{N_k\}\{\ddot{d}_{s_k}\}_v \tag{10}$$
$$\frac{\partial^2 v(x,t)}{\partial x \partial t} = \{N_k{}'\}\{\dot{d}_{s_k}\}_v$$

This is also applicable for in Equation (8a) and Equation (8c), where the terms $\{N_k{}'\}$and $\{N_k{}''\}$, indicate the partial derivative of shape functions with respect to x. By substituting Equation (4) into Equations (9), an expression for the acceleration of the point mass, $(\ddot{u}(x,t),\ddot{v}(x,t),\ddot{w}(x,t))$ can be obtained.

$$\begin{aligned}\ddot{u}(x,t) = {} & (\dot{x}+\ddot{x}t)^2\{u_{s_k}\}_u\{N_k{}''\} + 2(\dot{x}+\ddot{x}t)\{\dot{u}_{s_k}\}_u\{N_k{}'\} \\ & + \ddot{x}\{u_{s_k}\}_u\{N_k{}'\} + \{\ddot{u}_{s_k}\}_u\{N_k\}\end{aligned} \tag{11a}$$
$$\begin{aligned}\ddot{v}(x,t) = {} & (\dot{x}+\ddot{x}t)^2\{v_{s_k}\}_v\{N_k{}''\} + 2(\dot{x}+\ddot{x}t)\{\dot{v}_{s_k}\}_v\{N_k{}'\} \\ & + \ddot{x}\{v_{s_k}\}_v\{N_k{}'\} + \{\ddot{v}_{s_k}\}_v\{N_k\}\end{aligned} \tag{11b}$$
$$\begin{aligned}\ddot{w}(x,t) = {} & (\dot{x}+\ddot{x}t)^2\{w_{s_k}\}_w\{N_k{}''\} + 2(\dot{x}+\ddot{x}t)\{\dot{w}_{s_k}\}_w\{N_k{}'\} \\ & + \ddot{x}\{w_{s_k}\}_w\{N_k{}'\} + \{\ddot{w}_{s_k}\}_w\{N_k\}\end{aligned} \tag{11c}$$

Equations (11) represent the acceleration of the point mass in terms of the shape functions, nodal displacements and the velocity and acceleration of the point mass. The equations of the motion for a point mass traversing an elastic beam structure can be obtained by substituting Equations (11) into Equation (1) by replacing the point force into the point mass yields:

$$\begin{aligned}&\Big[[M] + m\big(\{N_k\}^T\{N_k\}\big)\Big]\{\ddot{q}\} + \\ &\Big[[C] + 2m(\dot{x}+\ddot{x}t)\big(\{N_k\}^T\{N_k{}'\}\big)\Big]\{\dot{q}\} + \\ &\Big[[K] + m(\dot{x}+\ddot{x}t)^2\big(\{N_k\}^T\{N_k{}''\}\big) + m\ddot{x}\big(\{N_k\}^T\{N_k{}'\}\big)\Big]\{q\} = \big(\{N_k\}^T\big)mg\end{aligned} \tag{12}$$

If the point mass is constrained to move at a constant velocity $V = \dot{x}$, the equation of motion can be written in Equation (13).

$$\begin{aligned}&\left[[M]+m\left\{\{N_k\}^T\{N_k\}\right\}\right]\{\ddot{q}\}+\\&\left[[C]+2mV\left\{\{N_k\}^T\{N_k{}'\}\right\}\right]\{\dot{q}\}+\\&\left[[K]+mV^2\left\{\{N_k\}^T\{N_k{}''\}\right\}\right]\{q\}=\left\{\{N_k\}^T\right\}mg\end{aligned}\tag{13}$$

The system matrices in Equation (13) are time variant, with the entries being directly dependent upon the position of the point mass along the beam. The coupling terms in Equation (13), $m\left\{\{N_k\}^T\right\}\{N_k\}$, $2mV\left\{\{N_k\}^T\right\}\{N_k{}'\}$, $mV^2\left\{\{N_k\}^T\right\}\{N_k{}''\}$ and $\left\{\{N_k\}^T\right\}mg$ are inertial, Coriolis, centrifugal force and gravitational load of moving mass, respectively, which is time dependent and move within the structural matrices as the point mass travels from one element to another. The moving finite element of space frame can be rewritten as mass, damping and stiffness matrices in the following equations.

$$[m]=m\left\{\{N_k\}^T\right\}\{N_k\}=m\begin{bmatrix}N_1^2&0&0&0&0&0&N_1N_7&0&0&0&0&0\\0&N_2^2&0&0&0&N_2N_6&0&N_2N_8&0&0&0&N_2N_{12}\\0&0&N_3^2&0&N_3N_5&0&0&0&N_3N_9&0&N_3N_{11}&0\\0&0&0&N_4^2&0&0&0&0&0&0&0&0\\N_5N_3&0&0&0&N_5^2&0&0&0&N_5N_9&0&N_5N_{11}&0\\0&0&0&0&0&N_6^2&0&N_6N_8&0&0&0&N_6N_{12}\\N_7N_1&0&0&0&0&N_8N_6&N_7^2&0&0&0&0&0\\0&N_8N_2&0&0&0&0&0&N_8^2&0&0&0&N_8N_{12}\\0&0&N_9N_3&0&N_9N_5&0&0&0&N_9^2&0&N_9N_{11}&0\\0&0&0&0&0&0&0&0&0&N_{10}^2&0&0\\0&0&N_{11}N_3&0&N_{11}N_5&0&0&0&N_{11}N_9&0&N_{11}^2&0\\0&N_{12}N_2&0&0&0&N_{12}N_6&0&N_{12}N_8&0&0&0&N_{12}^2\end{bmatrix}\tag{14}$$

$$[c]=2mV\left\{\{N_k\}^T\right\}\{N_k{}'\}=2mV\begin{bmatrix}N_1N_1'&0&0&0&0&0&N_1N_7'&0&0&0&0&0\\0&N_2N_2'&0&0&0&N_2N_6'&0&N_2N_8'&0&0&0&N_2N_{12}'\\0&0&N_3N_3'&0&N_3N_5'&0&0&0&N_3N_9'&0&N_3N_{11}'&0\\0&0&0&N_4N_4'&0&0&0&0&0&0&0&0\\N_5N_1'&0&0&0&N_5N_5'&0&0&0&N_5N_9'&0&N_5N_{11}'&0\\0&0&0&0&0&N_6N_6'&0&N_6N_8'&0&0&0&N_6N_{12}'\\N_7N_1'&0&0&0&0&N_8N_6'&N_7N_7'&0&0&0&0&0\\0&N_8N_2'&0&0&0&0&0&N_8N_8'&0&0&0&N_8N_{12}'\\0&0&N_9N_3'&0&N_9N_5'&0&0&0&N_9N_9'&0&N_9N_{11}'&0\\0&0&0&0&0&0&0&0&0&N_{10}N_{10}'&0&0\\0&0&N_{11}N_3'&0&N_{11}N_5'&0&0&0&N_{11}N_9'&0&N_{11}N_{11}'&0\\0&N_{12}N_2'&0&0&0&N_{12}N_6'&0&N_{12}N_8'&0&0&0&N_{12}N_{12}'\end{bmatrix}\tag{15}$$

(3.22)

$$[k] = mV^2 \left\{ \{N_k\}^T \{N_k''\} \right\}$$

$$= mV^2 \begin{bmatrix}
N_1N_1'' & 0 & 0 & 0 & 0 & 0 & N_1N_7'' & 0 & 0 & 0 & 0 & 0 \\
0 & N_2N_2'' & 0 & 0 & 0 & N_2N_6'' & 0 & N_2N_8'' & 0 & 0 & 0 & N_2N_{12}'' \\
0 & 0 & N_3N_3'' & 0 & N_3N_5'' & 0 & 0 & 0 & N_3N_9'' & 0 & N_3N_{11}'' & 0 \\
0 & 0 & 0 & N_4N_4'' & 0 & 0 & 0 & 0 & 0 & 0 & 0 & 0 \\
N_5N_1'' & 0 & 0 & 0 & N_5N_5'' & 0 & 0 & 0 & N_5N_9'' & 0 & N_5N_{11}'' & 0 \\
0 & 0 & 0 & 0 & 0 & N_6N_6'' & 0 & N_6N_8'' & 0 & 0 & 0 & N_6N_{12}'' \\
N_7N_1'' & 0 & 0 & 0 & 0 & N_8N_6'' & N_7N_7'' & 0 & 0 & 0 & 0 & 0 \\
0 & N_8N_2'' & 0 & 0 & 0 & 0 & 0 & N_8N_8'' & 0 & 0 & 0 & N_8N_{12}'' \\
0 & 0 & N_9N_3'' & 0 & N_9N_5'' & 0 & 0 & 0 & N_9N_9'' & 0 & N_9N_{11}'' & 0 \\
0 & 0 & 0 & 0 & 0 & 0 & 0 & 0 & 0 & N_{10}N_{10}'' & 0 & 0 \\
0 & 0 & N_{11}N_3'' & 0 & N_{11}N_5'' & 0 & 0 & 0 & N_{11}N_9'' & 0 & N_{11}N_{11}'' & 0 \\
0 & N_{12}N_2'' & 0 & 0 & 0 & N_{12}N_6'' & 0 & N_{12}N_8'' & 0 & 0 & 0 & N_{12}N_{12}''
\end{bmatrix} \tag{16}$$

2.4 Numerical Integration Methods

2.4.1 Newmark-β

Newmark's method [80] has been applied to the dynamic analysis of many practical engineering structures. In its application, it has been modified and improved by many other researchers. The method is based on the assumption that the acceleration varies linearly between two instants of time. The derivation can be illustrated by using the Taylor's series provides a rigorous approach to obtain the following two additional equations.

$$\begin{aligned}
q_t &= q_{t-\Delta t} + \Delta t \dot{q}_{t-\Delta t} + \frac{\Delta t^2}{2} \ddot{q}_{t-\Delta t} + \frac{\Delta t^3}{2} \dddot{q}_{t-\Delta t} + \ldots \\
\dot{q}_t &= \dot{q}_{t-\Delta t} + \Delta t \ddot{q}_{t-\Delta t} + \frac{\Delta t^3}{2} \dddot{q}_{t-\Delta t} + \ldots
\end{aligned} \tag{17}$$

Newmark truncated these equations and expressed them in the following form.

$$\begin{aligned}
q_t &= q_{t-\Delta t} + \Delta t \dot{q}_{t-\Delta t} + \frac{\Delta t^2}{2} \ddot{q}_{t-\Delta t} + \beta \Delta t \dddot{q}, \\
\dot{q}_t &= \dot{q}_{t-\Delta t} + \Delta t \ddot{q}_{t-\Delta t} + \gamma \Delta t \dddot{q},
\end{aligned} \tag{18}$$

If the acceleration is assumed to be linear within the time step, the following equation can be written:

$$\dddot{q} = \frac{\ddot{q}_t - \ddot{q}_{t-\Delta t}}{\Delta t}, \tag{19}$$

The substitution of Equation (19) into Equation (18) produces Newmark's equations in standard form.

$$q_t = q_{t-\Delta t} + \Delta t \dot{q}_{t-\Delta t} + \left(\frac{1}{2} - \beta\right)\Delta t^2 \ddot{q}_{t-\Delta t} + \beta \Delta t^2 \ddot{q}_t,$$
$$\dot{q}_t = \dot{q}_{t-\Delta t} + (1-\gamma)\Delta t \ddot{q}_{t-\Delta t} + \gamma \Delta t \ddot{q}_t, \tag{20}$$

Normally, model of large real structures contain a large number of periods which are smaller than the integration time step. Unconditionally stable of all time steps for numerical integration method is essential. By specifying different integration parameters, a number of different direct numerical integration methods are possible to be used. In this thesis, Newmark integration method is used with the integration parameters β=0.25 and γ=0.5, which lead to constant-average acceleration approximation.

2.4.2 Fourth-Order Runge-Kutta

Estimating the value of the solution y_{n+1} at a time interval Δt by using derivative information at a single point y_n is the method of Runge-Kutta, as long as the value of y_n is defined. This method is repeated over the entire range of interest $(n = 0, 1, 2, 3, ...N)$ to estimate the solution. One of the most popular Runge-Kutta methods is the fourth-order method, which requires four function evaluations per time step [81].

$$y_{n+1} = y_n + \Delta t(k_1 + 2k_2 + 2k_3 + k_4)/6 \tag{21}$$

Terms k_i are estimates of the first derivatives of y at four locations in the integration time interval. Because all k_i depend on previous calculated values, this method is explicit. The fourth-order Runge-Kutta has the same accuracy as a fourth-order Taylor series, makes it widely accepted method in numerical integration of non-linear differential equation. Many practitioners use the fourth-order Runge-Kutta as the default integration method. In this thesis, fourth-order Runge-Kutta method is utilized.

2.5 Control Methods

All cranes use cables to support the payload. Because the traverse motion of trolley during transport operations, the payload has the tendency to swing naturally due to traverse motion of trolley. The swinging motion reduces the speed, accuracy and safety requirements of crane operations. It lowers the speed of crane operations because the payload swing must be avoided before the payload can be safely lowered into specified position. The swings make it difficult to perform alignment, fine position, or other accuracy driven task. Swing effect also causes safety problems to the crane framework. That's why control methods are needed to suppress the effects and it will be discussed in the following subsection.

2.5.1 Zero-Vibration-Derivative-Derivative (ZVDD)

Input shaping is an easy and effective way to reduce payload swing in cranes and has been implemented on several large cranes [78], [82]-[84]. It is a feed-forward control technique by convolving the desired command with a sequence of impulses known as input shapers. Figure 2.3 shows how the input shaping works.

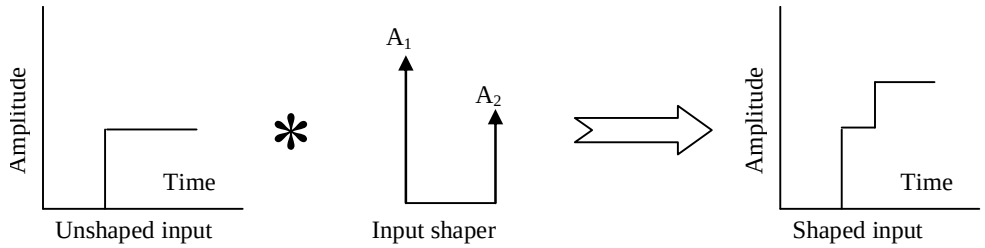

Figure 2.3: Input shaping process [84]

The goal of input shaping design is to determine the amplitudes and the impulse time locations such that the shaped command make the total response become zero vibration.

There are a number of schemes to design input shapers. In this thesis, Zero Vibration-Derivative-Derivative (ZVDD) input shapers are selected to be one of the control method in this study. ZVDD consist of four impulses.

The amplitude of the impulse and the time location of ZVDD shaper are as follows:

$$
\begin{aligned}
A_1 &= \frac{1}{1+3K+3K^2+K^3}, \qquad at \quad t_1 = 0, \\
A_2 &= \frac{3K}{1+3K+3K^2+K^3}, \qquad at \quad t_1 = \frac{\pi}{\omega_n\sqrt{1-\zeta^2}}, \\
A_3 &= \frac{3K^2}{1+3K+3K^2+K^3}, \qquad at \quad t_1 = \frac{2\pi}{\omega_n\sqrt{1-\zeta^2}}, \\
A_4 &= \frac{K^3}{1+3K+3K^2+K^3}, \qquad at \quad t_1 = \frac{3\pi}{\omega_n\sqrt{1-\zeta^2}},
\end{aligned}
\tag{22}
$$

where:

$$
\begin{aligned}
K &= e^{-\frac{\zeta\pi}{\sqrt{1-\zeta^2}}}, \\
\Delta t &= \frac{\pi}{\omega_n\sqrt{1-\zeta^2}}, \\
D &= 1+3K+3K^2+K^3,
\end{aligned}
\tag{23}
$$

The derivation of Equation (22) and (23) can be referred to [84].

2.5.2 Fuzzy Logic Controller (FLC)

The field of fuzzy system and control has seen great progress, motivated by practical success in controlling industrial processes. The fuzzy controller uses a form of quantification of imprecise information (input fuzzy sets) to generate by an inference scheme, which is based on a knowledge base of control force to be applied to the system.

The benefit of this quantification is that fuzzy sets can be represented by a unique linguistic expression, such as small, medium, or large. The linguistic representation of a fuzzy set is known as a term, and a collection of such terms defines a term-set, or a linguistic control strategy. The logical controller is comprised of four primary components as shown in Figure 2.4.

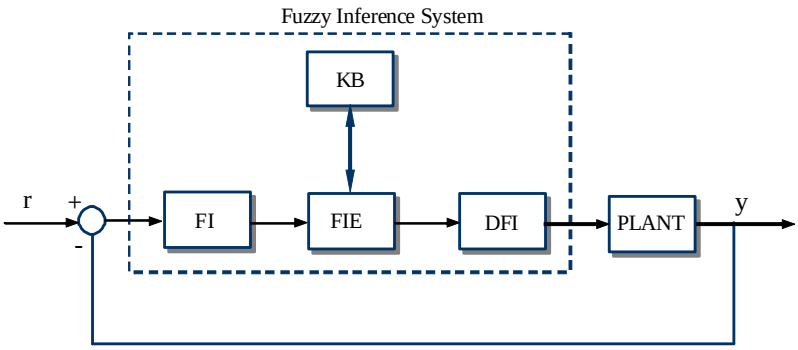

Figure 2.4: Block diagram of Fuzzy logic controller [85]

- Fuzzification Interface, FI

Fuzzification is defined as mapping of measured input domain into fuzzy values in certain domain. This process consists of taking input variables and calculating its fuzzy values based on respective membership function. Input variables must belong to universe of discourse of membership function which generates membership degree between 0 and 1.

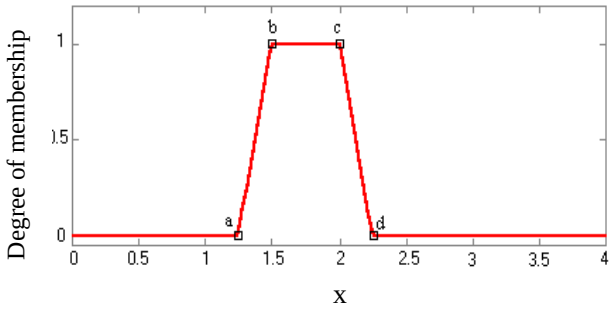

Figure 2.5: Trapezoidal membership function [86]

Input variable of fuzzy control in Figure 2.4 is the error between output y and set-point r. If this error is denoted by x and belongs to the universe of discourse X, then a fuzzy set A in X is defined as a set of ordered pairs.

$$A = \{x, \mu_A(x) \mid x \in X\} \tag{24}$$

Term $\mu_A(x)$ is called the membership function of X in A. The membership function maps each element of X to a membership degree between 0 and 1. Membership function has several forms, such as triangular, trapezoidal, gaussian, sigmoidal and etc.

Triangular and trapezoidal membership functions are general used in fuzzy control due to their simple function. Basically, triangular membership function is specific form of trapezoidal. Trapezoidal membership function is defined by four parameters $\{a, b, c, d\}$ as shown in Figure 2.5, where degree of membership function is calculated as follows.

$$trapezoidal(x; a,b,c,d) = \begin{cases} 0, & x \le a \\ \dfrac{x-a}{b-a}, & a \le x \le b \\ 1, & b \le x \le c \\ \dfrac{d-x}{d-c}, & c \le x \le d \\ 0, & x \le d \end{cases} \tag{25}$$

If the input variable for fuzzy inference system is more than one, ex. x and y, then fuzzy set operations are needed. Fuzzy set operations use logical connective operators such as AND (conjunction), OR (disjunction) or NOT (complement). Logical operations are described as below:

1. T-norm operation '$\otimes$'

T-norm operation '$\otimes$' is defined as intersection operation of two sets as follows.

$$\mu_{A\cap B} = T(\mu_A(x), \mu_B(y)) = \mu_A(x) \otimes \mu_B(y) \tag{26}$$

T-norm must satisfy the following requirements:

$$x \otimes y = \begin{cases} min[x,y], \\ xy, \\ max[0, x+y-1], \end{cases} \tag{27}$$

where $x, y \in [0,1]$.

2. T-conorm'$\oplus$'

T-conorm operation '$\oplus$' is defined as union operation of two sets as follows.

$$\mu_{A\cap B} = T(\mu_A(x), \mu_B(y)) = \mu_A(x) \oplus \mu_B(y) \tag{28}$$

T-conorm must satisfy the following requirements:

$$x \otimes y = \begin{cases} max[x,y], \\ x+y-xy, \\ min[0, x+y-1], \end{cases} \tag{29}$$

where $x, y \in [0,1]$.

3. The complement operator is represented by

$$\mu_{\bar{A}}(x) = 1 - \mu_A(x), \quad or \quad \mu_{\bar{B}}(y) = 1 - \mu_B(y) \tag{30}$$

- Fuzzy Inference Engine, FIE and Knowledge Base, KB

After degree of membership for input and output variables is determined, if-then rules are generated to connect between input and output variables. In this stage, decision making is conducted based on fuzzified input variables based on knowledge bases. These knowledge bases are generated through intuitions which are extracted from knowledge of control designer to achieve specified performance of controller.

Fuzzy f-then rules, denoted by R are groups of if-then rules which are presented as follows.

$$R = \left[R^{(1)}, R^{(2)}, ..., R^{(M)}\right] \tag{31}$$

with

$$\begin{aligned} R^{(\ell)} &: IF \left(x_i is\ F_i^{\ell}\ and \ldots and\ x_p\ is\ F_p^{\ell}\right) \\ &THEN \left(y_i\ is\ G_i^{\ell}, \ldots, y_q\ is\ G_q^{\ell}\right) \end{aligned} \tag{32}$$

In Equation (32), $x = (x_1, \ldots, x_n)^T$ is input vector and $y = (y_1, \ldots, y_n)^T$ is output vector in fuzzy system. Terms F_i^{ℓ} and G_j^{ℓ} are fuzzy sets symbol in U_i and V_j, where $1 \le p \le n$, $1 \le q \le m$ and $\ell = 1, 2, \ldots, m$. Based on equation above, $R^{(\ell)}$ can be decomposed in q rules:

$$R^{(\ell)} = \left[R_1^{(\ell)}, ..., R_q^{(\ell)}\right] \tag{33}$$

where

$$\begin{aligned} R_j^{(\ell)} &: IF \left(x_i is\ F_i^{\ell}\ and \ldots and\ x_p\ is\ F_p^{\ell}\right) \\ &THEN \left(y_j\ is\ G_j^{\ell}\right) \end{aligned} \tag{34}$$

with j = 1, 2,…,q.

Interpreting an if-then rule involves distinct parts. Firstly, evaluating the “IF” part or called antecedent which involves fuzzifying the input and applying any necessary fuzzy operators.

Secondly, applying that result to the "THEN" part or called consequent. This process is called implication. Example: say A and B are fuzzy sets in universe of discourse, X and Y, then fuzzy implication $A \to B$ or "IF A then B", defined as fuzzy sets in $X \times Y$ with degree of membership.

$$\mu_{A \to B}(x, y) = \mu_A(x) \otimes \mu_B(x, y) \tag{35}$$

Fuzzy inference is the process of formulating the mapping from given input to an output using fuzzy logic. The mapping then provides a basis, from which decisions can be made or patterns discerned. The process of fuzzy inference involves membership function, fuzzy logic operator, and if-then rules. In general, one rule by itself does not do much good. Two or more rules are needed to achieve control performance. The output of each rule is a fuzzy set. The output fuzzy sets for each rule are then aggregated into a single output fuzzy set.

Fuzzy inference engine uses fuzzy rules to map fuzzy set in U into fuzzy set in V based on fuzzy operators. In FIE, "IF" part of $R_i^{(\ell)}$ is taken as Cartesian product of $F_1^\ell, ..., F_p^\ell$, while $R_j^{(\ell)}$ is taken as implication of $F_1^\ell \times ... \times F_p^\ell \to G_j^\ell$. Example: A is fuzzy set in U, and then every $R_j^{(\ell)}$ from equation above will determine a fuzzy set $A \circ R_j^{(\ell)}$ in V_j based on following supstar composition.

$$\begin{aligned} \mu_{A \circ R_j^{(\ell)}}(y_j) &= \sup_{\underline{x} \in U} \left[\mu_A(\underline{x}) \otimes \mu_{F_i^\ell \times ... \times F_p^\ell \to G_j^\ell}(\underline{x, y_j}) \right] \\ &= \sup_{\underline{x} \in U} \left[\mu_A(\underline{x}) \otimes \mu_{F_1^\ell}(x_1) \otimes ... \otimes \mu_{F_p^\ell}(x_p) \otimes \mu_{G_j^\ell}(y_j) \right] \end{aligned} \tag{36}$$

where $y_j \in V_j$. Final fuzzy set $A \circ R_j \left(R_j = \left[R_j^{(1)}, ... R_j^{(M)} \right] \right)$ in V_j is determined by FIE which is obtained through combining Equation (36) for $\ell = 1,2,...,M \quad \ell = 1,2,\ldots,m$ by using T-conorm $\oplus$.

$$\mu_{A \circ R_j}(y_j) = \mu_{A \circ R_j^1}(y_j) \oplus ... \oplus \mu_{A \circ R_j^N}(y_j) \tag{37}$$

Based on equations above, FIE is to map fuzzy set A in U into fuzzy set $A \circ R$ in V by following relationship.

$$\mu_{A \circ R}(\underline{y}) = \left(\mu_{A \circ R_1}(y_1), ..., \mu_{A \circ Rm}(y_m) \right)^T \tag{38}$$

Since the decisions are based on the testing of all of the rules in a FIE, the rules must be combined in some manner in order to make decision.

Aggregation is the process by which the fuzzy sets that represents the outputs of each rules are combined into a single fuzzy set. The input of the aggregation process is the list of truncated output functions returned by the implication process for each rule. The output of the aggregation process is one fuzzy set for each output variable. The general operators for aggregation are max (maximum) and sum (simply the sum of each rule's output set). Finally the resulting set is defuzzified or resolved to a single number as described in the following description.

- Defuzzification Interface, DFI

The input for the defuzzification process is a fuzzy set (the aggregate output fuzzy set) and the output is a single number. As much as fuzziness helps the rule evaluation during the inference system, the final desired output for each variable is generally a single number. However, the aggregate of a fuzzy set encompasses a range of output values, and so must be defuzzified in order to resolve a single output value from the set. Defuzzification based on centroid calculation is employed in this thesis due to its popularity. The calculation is presented as follows.

$$y_j = \frac{\sum_{\ell=1}^{m} \bar{y}_j^{\ell} \left(\mu_{AoR_j^{(\ell)}} \left(\bar{y}_j^{\ell} \right) \right)}{\sum_{\ell=1}^{m} \left(\mu_{AoR_j^{(\ell)}} \left(\bar{y}_j^{\ell} \right) \right)} \tag{39}$$

where $\bar{y}_j^{\ell}$ is point in V_j when $\mu_{G_j^{\ell}}(y_j)$ achieves maximum value. Value of $\mu_{A \circ R_j^{(\ell)}}(y_j)$ in above equation is equation obtained from Equation (37), where j = 1, 2,…,m.

Based on inference process, there are several inference systems of fuzzy logic in its application. In this thesis, Mamdani is chosen as fuzzy inference system. That is because this fuzzy inference system is intuitive compared then other types of inference system [86]. Overall, this inference system is shown in Figure 2.6.

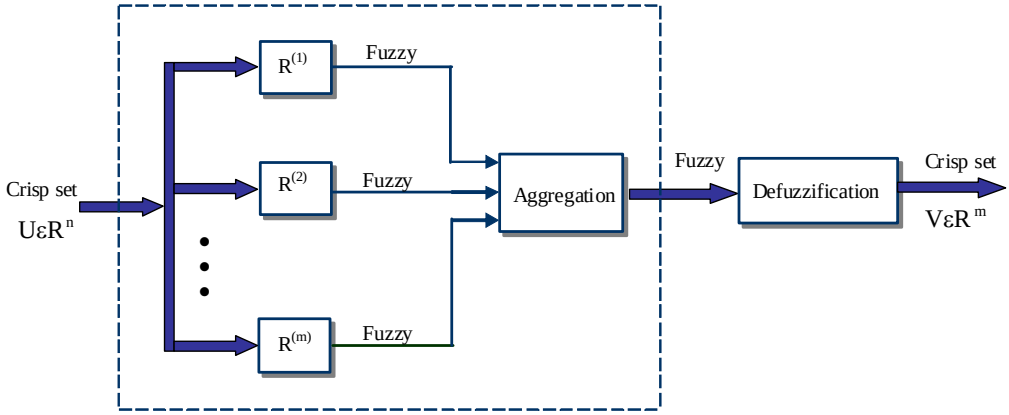

Figure 2.6: Mamdani fuzzy inference system [86]

2.5.3 Proportional Integral Derivative (PID)

PID controllers are a simple feed-back control technique that is very common in industrial control application. PID controller consists of three separate parameters, namely Proportional (P), Integral (I) and Derivative (D). Those gains are designed to track the process variable into the desired value (set-point) by giving corrective action in order to match between the process variable with the desired variable.

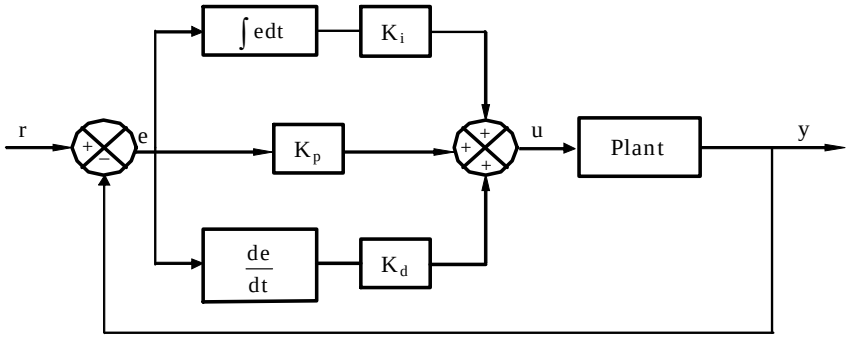

Figure 2.7: Block diagram of PID controller [87]

Based on the block diagram shown in Figure 2.7, output of PID controllers is as follows:

$$u(t) = K_p e(t) + K_i \int e(t)\,dt + K_d \frac{de(t)}{dt} \tag{40}$$

where u(t) is control action. Error e between the output y and set-point r will be manipulated by gains of proportional (K_p), integral (K_i) and derivative (K_d).

The controlled process variable can become unstable and high overshoot can occur, when the gains of proportional, integral and derivative are not optimally set. Since PID controllers are linear, their performance in nonlinear system may or may not be optimal. PID controller performance may be enhanced effectively by combining it with other controller methods to be adaptive and robust. In some applications, K_d is turned off, and it is known as PI controller. Vice versa, if the K_i is turned off, and then it is known as PD controller.

2.6 Summary

Researches relate with dynamic of crane system carrying a moving load are present in Table 2.1. This table contains the type of crane systems which studied by many researchers. Dynamic response of respective crane system is generally obtained numerically either analytical or numerical method. The corresponding references in conjunction with the title of this thesis are [5]-[6] and [9]-[12].

The literature review is extensive for vibration of structural system due to moving load The methods to calculate the dynamic responses still expand dynamically, as seen in Table 2.2. This table covers only selected papers to represent the progress research of moving load.

Active control for flexible structure can be found in Table 2.3. It is shown that the application of control system is still rare on flexible crane system. The accessed literatures inform that references in [72], [77] and [79] have implemented control method in flexible crane system.

Selected background materials for supporting theory are presented which cover the concept of equivalent nodal forces and moving finite element for space frame, theory of utilized numerical integration and control methods.

CHAPTER 3

METHODOLOGY

3.1 Gantry Crane System Description

Gantry crane system can be divided into two subsystems, namely gantry crane and stationary crane framework. Gantry crane incorporates interaction among trolley, wire rope as hoist cable and payload which is manipulated by trolley and hoist mechanism. The payload is grabbed using hook system, which is then hoisted from trolley by means of cable. For simplicity of the characteristics of the physical gantry crane, several assumptions are put forward to the proposed dynamical model. Mass of trolley and payload are modeled as lumped mass which is connected by elastic hoist cable. Payload and its cable behave as pendulum model as depicted in Figure 3.1. The payload has two swing angles with respect to the inference frame: θ is denoted as angle between the x_T-axis and $x_T y_T$-plane, while notation φ is the angle between the cable to $x_T y_T$-plane. The payload swings either small or large swing angles. Friction between trolley and the top beam of crane framework, hoist cable and drum in hoist system and dynamics of trolley and hoist drive mechanism are not considered.

Some gantry cranes are equipped with wheels and may run along a parallel pair of rails, as shown in Figure 1.1, while the others are not. According to Wu [10], even it is equipped with wheels; the vibration effect of the entire crane framework can be negligible because of low and constant speed. This assumption makes the supports of crane framework can be fixed to the ground, as shown in Figure 3.1. It is noted that the figure above is a simplified model of gantry crane system which is depicted in Figure 1.1. Structural members of crane framework have constant cross-sections, materially and geometrically linear so it is only applicable for small deformation.

Because the crane framework is categorized as space frame, the used structural element for crane framework is 3D beam element.

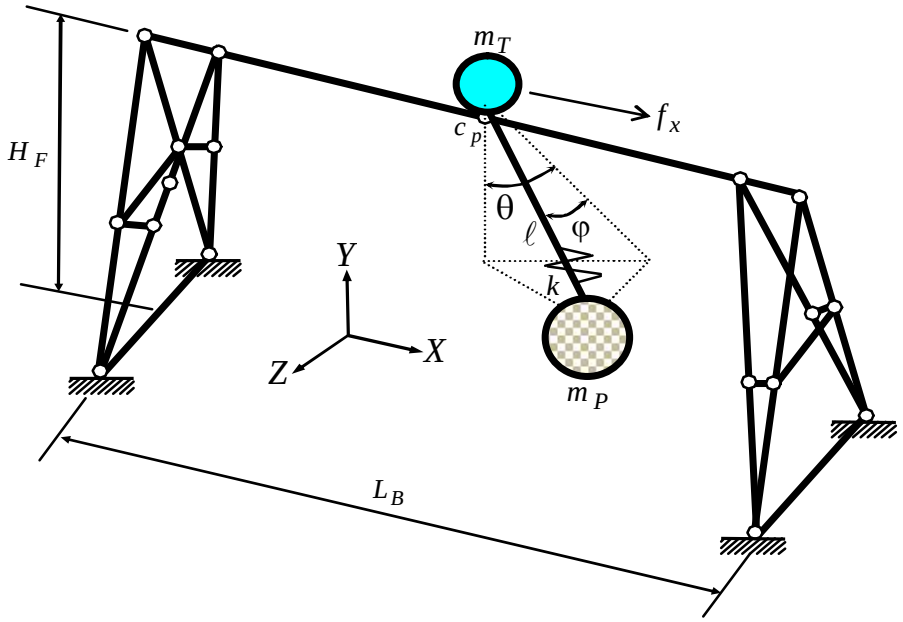

Figure 3.1: Model of flexible gantry crane system

3.2 Dynamic Analysis Scheme

The dynamic analysis stage is illustrated in the scheme shown in Figure 3.2. The derivation of dynamic model for a flexible gantry crane system is the first step in model-based research. To obtain the equations of motion, gantry crane system is described in Section 3.1 and discussed further in Chapter IV including the proposed numerical solver. To investigate the behavior of the flexible gantry crane system, the simulations are performed in three stages, namely static, modal and transient analysis.

Modal analysis is the stage to calculate the natural frequencies and corresponding modes of vibration for the crane framework. Transient analysis is conducted under three different cases, namely swinging payload with stationary trolley, stationary payload with moving trolley and moving trolley with swinging payload.

The results are time histories of framework and payload swinging as functions of limited set parameters for quite simple but representative for the dynamics of the gantry crane. Time history of gantry crane response are verified with the rigid model of gantry crane, while the time history of crane framework response is measured at the central point c_P of the top beam and as comparison, static analysis is used. The detail flowchart of dynamic analysis is given in Appendix A.

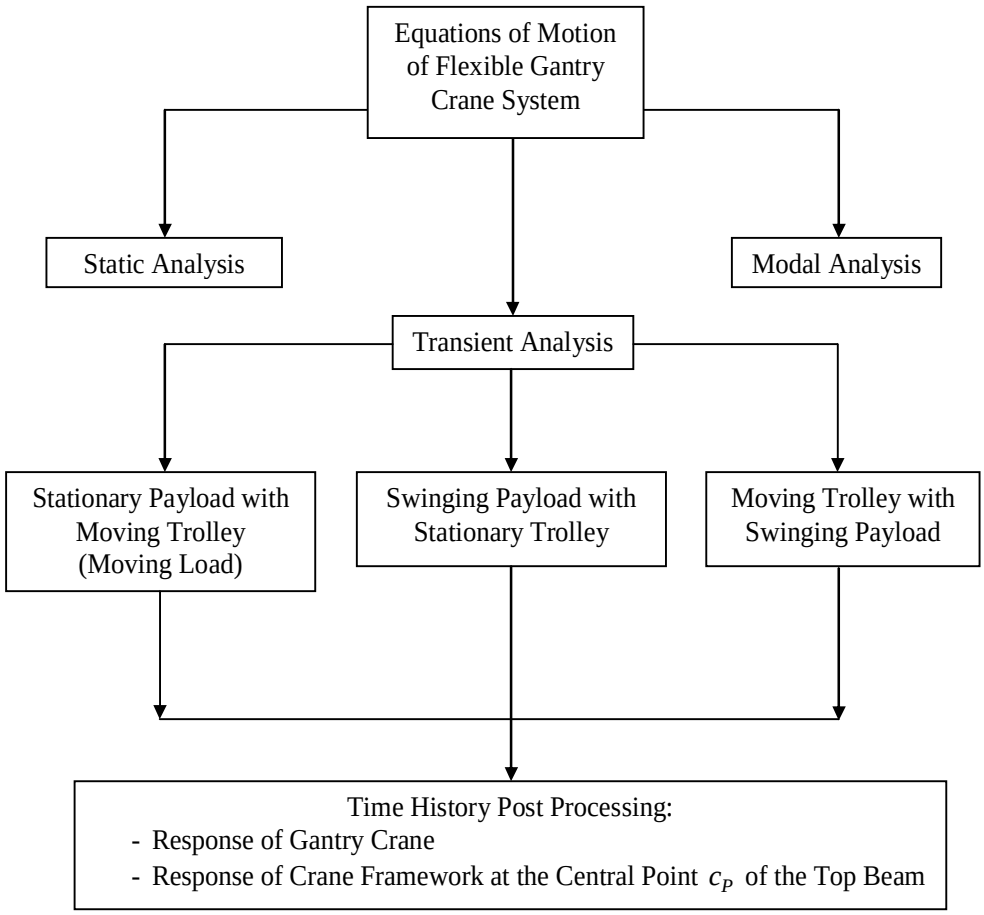

Figure 3.2: Dynamic analysis stage

3.3 Control System Methods

The control system strategy is illustrated in the scheme shown in Figure 3.3. Control methods are utilized to suppress dynamical effect of gantry crane motion and the effect of structural flexibility. Because of model-based control, plant model in

controller design and simulations are taken from equations of motion of flexible gantry crane system (see Chapter IV for detail).

Zero-Vibration-Derivative-Derivative (ZVDD) is employed as open-loop control system, while PID and FLC are applied as controller for closed-loop control system. Performance of the three controllers are evaluated in capability of transferring the payload and suppressing the swing response of the payload simultaneously, with the flexibility of crane framework and hoist cable are taken into account into the plant model. Control simulations are conducted to show the effect of structural flexibility on controller performance compared to rigid model assumption.

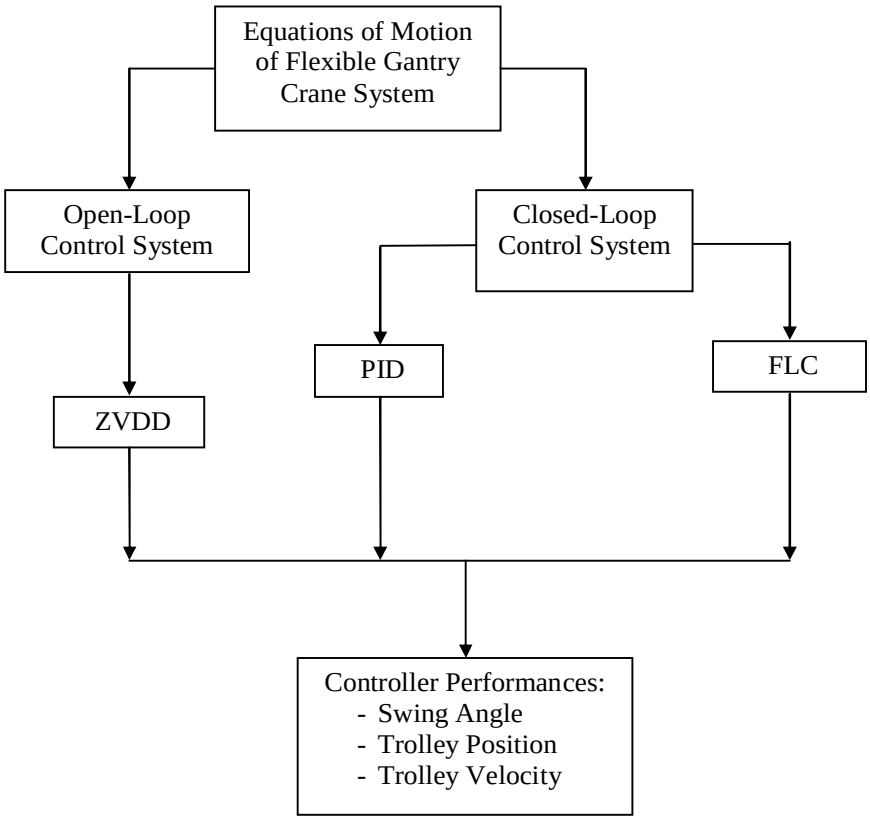

Figure 3.3: Control system strategy

CHAPTER 4

SYSTEM MODELING

4.1 Introduction

The goal of this chapter is to derive the equations of motion of gantry crane. Finite element method is utilized to model the framework and is applied in Section 4.2. Dynamics of flexible gantry crane is derived using Lagrange's equations in conjunction with moving finite element method, and applied in Section 4.3. Both equations of motion of gantry crane and framework are then combined to form integrated finite element formulation. Some cases are discussed based on the derived equations and described in Section 4.4. To solve the integrated equations, the numerical approach is presented in Section 4.5. Finally, summary for this chapter is written in Section 4.6.

4.2 Dynamics of Crane Framework

The crane framework model is established by the finite element method, where the structural information of the framework can be expressed through the direct stiffness method. By using the direct stiffness method, the model can be established just by introducing the global mass, damping and stiffness matrices of the crane framework. When the framework is modeled using finite element method, then the equations of motion will take the form, in geometrically and materially linear dynamic is the same with Equation (1) and rewritten as follows [9]:

$$[M_{st}]\{\ddot{q}_{st}(t)\} + [C_{st}]\{\dot{q}_{st}(t)\} + [K_{st}]\{q_{st}(t)\} = \{F_{st}(t)\}, \tag{41}$$

where $[M_{st}]$, $[C_{st}]$, $[K_{st}]$ are mass, damping and stiffness matrices of the crane framework, respectively. Terms $\{\ddot{q}_{st}(t)\}$, $\{\dot{q}_{st}(t)\}$, $\{q_{st}(t)\}$ are the acceleration, velocity and displacement vectors for the whole framework, respectively.

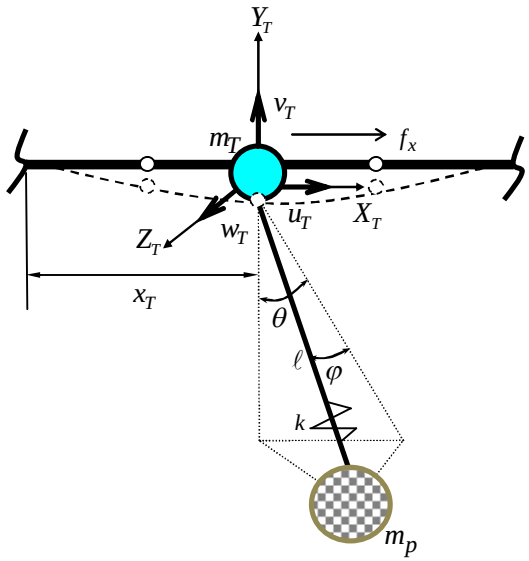

Figure 4.1: Traverse motion of flexible gantry crane model with elastic deformation of crane framework

Term $\{F_{st}(t)\}$ is the external force of gantry crane on the crane framework through the contact point between the trolley and crane framework.

These external forces vector traverse to the every node along the top beam of crane framework, make its position is time-variant as shown in Figure 4.1. The external forces can be tackled by modification of $\{F_{st}(t)\}$ in Equation (41) as per Equation (2) and can be rewritten [44]:

$$[M_{st}]\{\ddot{q}_{st}(t)\}+[C_{st}]\{\dot{q}_{st}(t)\}+[K_{st}]\{q_{st}(t)\}=\{N_k\}^T f_0 \tag{42}$$

where N_k are the shape functions of space frame element as written in Table 2.4 and f_0 is external forces acting on the top beam of crane framework.

By assuming that the gantry crane is always in contact with the top beam, there will be transmitted force to the crane framework from gantry crane through the cable and vice versa.

To calculate the external forces which cover the inertial force of gantry crane and swing effect of payload at the contact point between trolley and crane framework, Lagrange's equations will be employed and derived in the following section.

4.3 Dynamics of Flexible Gantry Crane

The equations of motion of flexible gantry crane as moving lumped mass with swing effect from payload on flexible crane framework can be derived by Lagrange's equations, with the following form:

$$\frac{d}{dt}\left(\frac{\partial L}{\partial \dot{q}}\right) - \frac{\partial L}{\partial q} + \frac{\partial F}{\partial \dot{q}} = f_i, \qquad \textbf{(43)}$$
$$q = \left(u_T, v_T, w_T, x_T, \theta, \varphi, \delta\right), \dot{q} = \left(\dot{u}_T, \dot{v}_T, \dot{w}_T, \dot{x}_T, \dot{\theta}, \dot{\varphi}, \dot{\delta}\right)$$

where the first three terms of $q = \left(u_T, v_T, w_T, x_T, \theta, \varphi, \delta\right)$ are defined as the generalized coordinates to describe the elastic deformation in the three directions in terms of equivalent nodal displacements and the rest is trolley and payload motion. General velocity of the system is $\dot{q} = \left(\dot{u}_T, \dot{v}_T, \dot{w}_T, \dot{x}_T, \dot{\theta}, \dot{\varphi}, \dot{\delta}\right)$. The Lagrangian L is defined as $L = K - P$, where K is kinetics energy and P is potential energy of system. Generalized force is denoted as f_i, where they are f_x, f_y and f_z applied input force for the *x*, *y* and *z* motions respectively.

The position vector of trolley r_T and payload r_p as shown in Figure 4.1 can be expressed as follows.

$$r_T = \left(x_T(t) + u(x_T, t)\right) \cdot i + v(x_T, t) \cdot j + \left(H_F + w(x_T, t)\right) k \qquad \text{(44a)}$$

$$r_P = \left(x_T(t) + u(x_T, t) + \left(\ell_P + \delta\right) \sin\theta \cos\varphi\right) i + \left(v(x_T, t) - \left(\ell_P + \delta\right) \cos\theta \cos\varphi\right) j + \left(H_F + w(x_T, t) - \left(\ell_P + \delta\right) \sin\varphi\right) k \qquad \text{(44b)}$$

where i, j and k are unit vectors along the-x-, y-, and z-axis, respectively. For convenience, elastic displacements in Equations (44) can be expressed in term:

$$u_T = u(x_T, t) = u(x,t)\big|_{x=x_T},\ v_T = v(x_T, t) = v(x,t)\big|_{x=x_T},\ w_T = w(x_T, t) = w(x,t)\big|_{x=x_T} \qquad \text{(44c)}$$

where term x_T is position of moving trolley carrying a swinging payload in time dependent manner and so are terms u_T, v_T, w_T. Referring to Equations (44), the flexibility of crane framework (u_T, v_T, w_T) and hoist cable (δ) is introduced in the position vector of trolley and payload. The velocity vector of trolley and payload can be obtained by deriving r_T and r_P respective to time as follows.

$$\dot{r}_T = (\dot{x}_T + \dot{u}_T)\cdot i + (\dot{v}_T)\cdot j + (\dot{w}_T)\cdot k \tag{45a}$$

$$\begin{aligned}\dot{r}_P = {} & \left(\dot{x} + \dot{u}_T + (\ell_P \cos\theta\cos\varphi + \delta\cos\theta\cos\varphi)\dot{\theta} - (\ell_P \sin\theta\sin\varphi + \delta\sin\theta\sin\varphi)\dot{\varphi} + \sin\theta\cos\varphi\dot{\delta}\right) i \\ & + \left(\dot{v}_T + (\ell_P \sin\theta\cos\varphi + \delta\sin\theta\cos\varphi)\dot{\theta} + (\ell_P \cos\theta\sin\varphi + \delta\cos\theta\sin\varphi)\dot{\varphi} - \cos\theta\cos\varphi\dot{\delta}\right) j \\ & + \left(\dot{w}_T - (\ell_P \cos\varphi + \delta\cos\varphi)\dot{\varphi} - \sin\varphi\dot{\delta}\right) k\end{aligned} \tag{45b}$$

The flexibility of hoist cable is modeled as one linear spring with stretched length ℓ. This is sufficient approach since the cable is assumed to be in tension during normal crane operation [79]. The linear spring force of hoist cable is as follows.

$$F_k = k\delta = k(\ell - \ell_p) \tag{45c}$$

It is noted that notation k is cable stiffness, while ℓ_p is unstreched hoist cable. Notation x_T and its derivative indicate trolley position and velocity, while δ and its derivative indicate hoist cable displacement and velocity. The total kinetics energy of the system K in terms of generalized coordinates and velocities is

$$K = K_T + K_P = \tfrac{1}{2} m_T \cdot \dot{r}_T{}^2 + \tfrac{1}{2} m_p \cdot \dot{r}_p{}^2; \quad K_T = \tfrac{1}{2} m_T (\dot{u}_T^2 + \dot{v}_T^2 + \dot{w}_T^2 + \dot{x}_T^2 + 2\dot{u}_T\dot{x}_T)$$

$$K_P = \tfrac{1}{2} m_p \begin{pmatrix} \dot{u}_T^2 + \dot{v}_T^2 + \dot{w}_T^2 + \dot{x}_T^2 + 2\dot{u}_T\dot{x}_T \\ + 2\begin{pmatrix} \ell_P \cos\theta\cos\varphi\dot{\theta} - \ell_P \sin\theta\sin\varphi\dot{\varphi} + \sin\theta\cos\varphi\dot{\delta} + \delta\cos\theta\cos\varphi\dot{\theta} \\ - \delta\sin\theta\sin\varphi\dot{\delta} \end{pmatrix}\dot{x}_T \\ + 2\begin{pmatrix} \ell_P \cos\theta\cos\varphi\dot{\theta} - \ell_P \sin\theta\sin\varphi\dot{\varphi} + \sin\theta\cos\varphi\dot{\delta} + \delta\cos\theta\cos\varphi\dot{\theta} \\ - \delta\sin\theta\sin\varphi\dot{\delta} \end{pmatrix}\dot{u}_T \\ + 2\begin{pmatrix} \ell_P \sin\theta\cos\varphi\dot{\theta} + \ell_P \cos\theta\sin\varphi\dot{\varphi} - \cos\theta\cos\varphi\dot{\delta} + \delta\sin\theta\cos\varphi\dot{\theta} \\ + \delta\cos\theta\sin\varphi\dot{\delta} \end{pmatrix}\dot{v}_T \\ - 2(\ell_P \cos\varphi\dot{\varphi} + \sin\varphi\dot{\delta} + \delta\cos\delta\dot{\varphi})\dot{w}_T \\ + \ell_P{}^2\dot{\varphi}^2 + \ell_P{}^2\cos^2\varphi\dot{\theta}^2 + \dot{\delta}^2 + \delta^2\cos^2\varphi\dot{\theta}^2 + \delta^2\dot{\varphi}^2 + 2\ell_P\delta\cos^2\varphi\dot{\theta}^2 + 2\ell_P\delta\dot{\varphi}^2 \end{pmatrix}$$

$$K = \tfrac{1}{2}\left(m_T + m_p\right)\left(\dot{u}_T^2 + \dot{v}_T^2 + \dot{w}_T^2 + \dot{x}_T^2 + 2\dot{u}_T\dot{x}_T\right)$$
$$\tfrac{1}{2}m_p\begin{pmatrix}\dot{u}_T^2 + \dot{v}_T^2 + \dot{w}_T^2 + \dot{x}_T^2 + 2\dot{u}_T\dot{x}_T \\ +2\left(\ell_P\cos\theta\cos\varphi\dot{\theta} - \ell_P\sin\theta\sin\varphi\dot{\varphi} + \sin\theta\cos\varphi\dot{\delta} + \delta\cos\theta\cos\varphi\dot{\theta} - \delta\sin\theta\sin\varphi\dot{\delta}\right)\dot{x}_T \\ +2\left(\ell_P\cos\theta\cos\varphi\dot{\theta} - \ell_P\sin\theta\sin\varphi\dot{\varphi} + \sin\theta\cos\varphi\dot{\delta} + \delta\cos\theta\cos\varphi\dot{\theta} - \delta\sin\theta\sin\varphi\dot{\delta}\right)\dot{u}_T \\ +2\left(\ell_P\sin\theta\cos\varphi\dot{\theta} + \ell_P\cos\theta\sin\varphi\dot{\varphi} - \cos\theta\cos\varphi\dot{\delta} + \delta\sin\theta\cos\varphi\dot{\theta} + \delta\cos\theta\sin\varphi\dot{\delta}\right)\dot{v}_T \\ -2\left(\ell_P\cos\varphi\dot{\varphi} + \sin\varphi\dot{\delta} + \delta\cos\delta\dot{\varphi}\right)\dot{w}_T \\ +\ell_P{}^2\dot{\varphi}^2 + \ell_P{}^2\cos^2\varphi\dot{\theta}^2 + \dot{\delta}^2 + \delta^2\cos^2\varphi\dot{\theta}^2 + \delta^2\dot{\varphi}^2 + 2\ell_P\delta\cos^2\varphi\dot{\theta}^2 + 2\ell_P\delta\dot{\varphi}^2\end{pmatrix} \tag{46a}$$

where K_T and K_P are the kinetics energy of the trolley and payload, respectively. The total potential energy of the system P is

$$\begin{aligned} P &= P_T + P_P + P_K \\ &= \left(m_T + m_p\right)gH_F + \left(m_T + m_p\right)gv_T - m_p g\left(\ell_P + \delta\right)\cos\theta\cos\varphi + \tfrac{1}{2}k\delta^2 \end{aligned} \tag{46b}$$

where P_T, P_P and P_K are the potential energy of the trolley, the potential energy of the payload and cable, respectively. Notations m_T, m_P and g are the mass of the trolley, payload and the acceleration of gravity, respectively. Using the Lagrangian operator, the following equation is derived as Equation (47a).

$$L = K - P,$$
$$L = \tfrac{1}{2}\left(m_T + m_p\right)\left(\dot{u}_T^2 + \dot{v}_T^2 + \dot{w}_T^2 + \dot{x}_T^2 + 2\dot{u}_T\dot{x}_T\right) +$$
$$\tfrac{1}{2}m_p\begin{pmatrix}\dot{u}_T^2 + \dot{v}_T^2 + \dot{w}_T^2 + \dot{x}_T^2 + 2\dot{u}_T\dot{x}_T \\ +2\left(\ell_P\cos\theta\cos\varphi\dot{\theta} - \ell_P\sin\theta\sin\varphi\dot{\varphi} + \sin\theta\cos\varphi\dot{\delta} + \delta\cos\theta\cos\varphi\dot{\theta} - \delta\sin\theta\sin\varphi\dot{\delta}\right)\dot{x}_T \\ +2\left(\ell_P\cos\theta\cos\varphi\dot{\theta} - \ell_P\sin\theta\sin\varphi\dot{\varphi} + \sin\theta\cos\varphi\dot{\delta} + \delta\cos\theta\cos\varphi\dot{\theta} - \delta\sin\theta\sin\varphi\dot{\delta}\right)\dot{u}_T \\ +2\left(\ell_P\sin\theta\cos\varphi\dot{\theta} + \ell_P\cos\theta\sin\varphi\dot{\varphi} - \cos\theta\cos\varphi\dot{\delta} + \delta\sin\theta\cos\varphi\dot{\theta} + \delta\cos\theta\sin\varphi\dot{\delta}\right)\dot{v}_T \\ -2\left(\ell_P\cos\varphi\dot{\varphi} + \sin\varphi\dot{\delta} + \delta\cos\delta\dot{\varphi}\right)\dot{w}_T \\ +\ell_P{}^2\dot{\varphi}^2 + \ell_P{}^2\cos^2\varphi\dot{\theta}^2 + \dot{\delta}^2 + \delta^2\cos^2\varphi\dot{\theta}^2 + \delta^2\dot{\varphi}^2 + 2\ell_P\delta\cos^2\varphi\dot{\theta}^2 + 2\ell_P\delta\dot{\varphi}^2\end{pmatrix} -$$
$$\left(m_T + m_p\right)gv_T + m_p g\left(\ell_P + \delta\right)\cos\theta\cos\varphi - \tfrac{1}{2}k\delta^2$$

(47a)

Due to terms $\left(u_T, v_T, w_T\right)$ are displacements of crane framework at position x_T and time t, then

$$\frac{\partial u_T}{\partial t} = \frac{\partial u_T}{\partial x_T}\frac{\partial x_T}{\partial t} + \frac{\partial u_T}{\partial t}, \frac{\partial v_T}{\partial t} = \frac{\partial v_T}{\partial x_T}\frac{\partial x_T}{\partial t} + \frac{\partial v_T}{\partial t}, \frac{\partial w_T}{\partial t} = \frac{\partial w_T}{\partial x_T}\frac{\partial x_T}{\partial t} + \frac{\partial w_T}{\partial t} \tag{47b}$$

First, the equation of motion associates with the generalized coordinate $q = u_T$ is derived as follows.

$$\frac{d}{dt}\left(\frac{\partial L}{\partial \dot{u}_T}\right) - \frac{\partial L}{\partial u_T} + \frac{\partial F}{\partial \dot{u}_T} = 0$$

$$\left(m_T + m_p\right)\left(\ddot{u}_T + 2\dot{u}_T{}'\dot{x}_T + u_T{}''\dot{x}_T{}^2 + u_T{}'\ddot{x}_T + \ddot{x}_T\right) +$$

$$m_p \ell_P \left(\begin{array}{l} \ddot{\theta}\cos\theta\cos\varphi - \dot{\theta}^2 \sin\theta\cos\varphi - \dot{\theta}\dot{\varphi}\cos\theta\sin\varphi \\ -\ddot{\varphi}\sin\varphi\sin\theta - \dot{\varphi}^2\cos\varphi\sin\theta - \dot{\varphi}\dot{\theta}\sin\varphi\cos\theta \\ +\ddot{\theta}\delta\cos\theta\cos\varphi \big/ \ell_P - \delta\dot{\theta}^2\sin\theta\cos\varphi \big/ \ell_P + 2\dot{\delta}\dot{\theta}\cos\theta\cos\varphi \big/ \ell_P \\ -\ddot{\varphi}\delta\sin\theta\sin\varphi \big/ \ell_P - \delta\dot{\varphi}^2\sin\theta\cos\varphi \big/ \ell_P - 2\dot{\delta}\dot{\theta}\sin\theta\sin\varphi \big/ \ell_P \\ +\ddot{\delta}\sin\theta\cos\varphi \big/ \ell_P - 2\delta\dot{\theta}\dot{\varphi}\cos\theta\sin\varphi \big/ \ell_P \end{array} \right) = 0 \qquad \text{(48a)}$$

Then, the equation of motion associates with the generalized coordinate $q = v_T$ is determined to be of the following form.

$$\frac{d}{dt}\left(\frac{\partial L}{\partial \dot{v}_T}\right) - \frac{\partial L}{\partial v_T} + \frac{\partial F}{\partial \dot{v}_T} = 0$$

Thus,

$$\left(m_T + m_p\right)\left(\ddot{v}_T + 2\dot{v}_T{}'\dot{x}_T + v_T{}''\dot{x}_T{}^2 + v_T{}'\ddot{x}_T\right) +$$

$$m_p \ell_P \left(\begin{array}{l} \ddot{\theta}\sin\theta\cos\varphi + \dot{\theta}^2\cos\theta\cos\varphi - \dot{\theta}\dot{\varphi}\sin\theta\sin\varphi \\ +\ddot{\varphi}\cos\theta\sin\varphi + \dot{\varphi}^2\cos\theta\cos\varphi - \dot{\varphi}\dot{\theta}\sin\theta\sin\varphi \\ +\ddot{\theta}\delta\sin\theta\cos\varphi \big/ \ell_P + \delta\dot{\theta}^2\cos\theta\cos\varphi \big/ \ell_P + 2\dot{\delta}\dot{\theta}\sin\theta\cos\varphi \big/ \ell_P \\ +\ddot{\varphi}\delta\cos\theta\sin\varphi \big/ \ell_P + \delta\dot{\varphi}^2\cos\theta\cos\varphi \big/ \ell_P + 2\dot{\delta}\dot{\varphi}\cos\theta\sin\varphi \big/ \ell_P \\ -\ddot{\delta}\cos\theta\cos\varphi \big/ \ell_P - 2\delta\dot{\theta}\dot{\varphi}\sin\theta\sin\varphi \big/ \ell_P \end{array} \right) + \left(m_T + m_p\right)g = 0 \qquad \text{(48b)}$$

Next, the equation of motion associates with the generalized coordinate $q = w_T$ can be derived and yields Equation (48c).

$$\frac{d}{dt}\left(\frac{\partial L}{\partial \dot{w}_T}\right) - \frac{\partial L}{\partial w_T} + \frac{\partial F}{\partial \dot{w}_T} = 0$$

$$\begin{aligned}&\left(m_T+m_p\right)\left(\ddot{w}_T+2\dot{w}_T{}'\dot{x}_T+w_T{}''\dot{x}_T{}^2+w_T{}'\ddot{x}_T\right)+\\&m_p\ell_P\begin{pmatrix}\ddot{\varphi}\cos\varphi-\dot{\varphi}^2\sin\varphi+\ddot{\delta}\sin\varphi/\ell_P+\ddot{\varphi}\delta\cos\varphi/\ell_P\\-\delta\dot{\varphi}^2\sin\varphi/\ell_P+2\dot{\delta}\dot{\varphi}\cos\varphi/\ell_P\end{pmatrix}=0\end{aligned}\tag{48c}$$

Then, the equation of motion associates with the generalized coordinate $q=x_T$ can be derived as

$$\frac{d}{dt}\left(\frac{\partial L}{\partial\dot{x}_T}\right)-\frac{\partial L}{\partial x_T}+\frac{\partial F}{\partial\dot{x}_T}=f_x$$

Thus,

$$\begin{aligned}&\left(m_T+m_p\right)\left(\ddot{u}_T+2\dot{u}_T{}'\dot{x}_T+u_T{}''\dot{x}_T{}^2+u_T{}'\ddot{x}_T+\ddot{x}_T\right)+\\&m_p\ell_P\begin{pmatrix}\ddot{\theta}\cos\theta\cos\varphi-\dot{\theta}^2\sin\theta\cos\varphi-\dot{\theta}\dot{\varphi}\cos\theta\sin\varphi\\-\ddot{\varphi}\sin\varphi\sin\theta-\dot{\varphi}^2\cos\varphi\sin\theta-\dot{\varphi}\dot{\theta}\sin\varphi\cos\theta\\+\ddot{\theta}\delta\cos\theta\cos\varphi/\ell_P-\delta\dot{\theta}^2\sin\theta\cos\varphi/\ell_P+2\dot{\delta}\dot{\theta}\cos\theta\cos\varphi/\ell_P\\-\ddot{\varphi}\delta\sin\theta\sin\varphi/\ell_P-\delta\dot{\varphi}^2\sin\theta\cos\varphi/\ell_P-2\dot{\delta}\dot{\theta}\sin\theta\sin\varphi/\ell_P\\+\ddot{\delta}\sin\theta\cos\varphi/\ell_P-2\delta\dot{\theta}\dot{\varphi}\cos\theta\sin\varphi/\ell_P\end{pmatrix}=f_x\end{aligned}\tag{48d}$$

Then, the equation of motion associates with the generalized coordinate $q=\theta$:

$$\frac{d}{dt}\left(\frac{\partial L}{\partial\dot{\theta}}\right)-\frac{\partial L}{\partial\theta}+\frac{\partial F}{\partial\dot{\theta}}=0$$

Thus,

$$\begin{pmatrix}\left(\cos\theta\cos\varphi/\ell_P+\delta\cos\theta\cos\varphi/\ell_P{}^2\right)\ddot{x}_T+\left(\cos\theta\cos\varphi/\ell_P+\delta\cos\theta\cos\varphi/\ell_P{}^2\right)\\\left(\ddot{u}_T+2\dot{u}_T{}'\dot{x}_T+u_T{}''\dot{x}_T{}^2+u_T{}'\ddot{x}_T\right)+\left(\sin\theta\cos\varphi/\ell_P+\delta\sin\theta\cos\varphi/\ell_P{}^2\right)\\\left(\ddot{v}_T+2\dot{v}_T{}'\dot{x}_T+v_T{}''\dot{x}_T{}^2+v_T{}'\ddot{x}_T\right)+\left(\cos^2\varphi+2\delta\cos^2\varphi/\ell_P+\delta^2\cos^2\varphi/\ell_P{}^2\right)\ddot{\theta}\\-\left(2\dot{\theta}\dot{\varphi}\sin\varphi\cos\varphi\right)+2\dot{\delta}\dot{\theta}\delta\cos^2\varphi/\ell_P{}^2-2\dot{\varphi}\dot{\theta}\delta^2\cos\varphi\sin\varphi/\ell_P{}^2+2\dot{\delta}\dot{\theta}\cos^2\varphi/\ell_P\\+4\delta\dot{\varphi}\dot{\theta}\sin\varphi\cos\varphi/\ell_P+g\sin\theta\cos\varphi/\ell_P+g\delta\sin\theta\cos\varphi/\ell_P{}^2\end{pmatrix}=0\tag{48e}$$

Next, the equation of motion associates with the generalized coordinate $q = \varphi$ can be derived as follows.

$$\frac{d}{dt}\left(\frac{\partial L}{\partial \dot{\varphi}}\right) - \frac{\partial L}{\partial \varphi} + \frac{\partial F}{\partial \dot{\varphi}} = 0$$

Thus,

$$\begin{pmatrix} \left(-\sin\theta\sin\varphi \big/ \ell_P - \delta\cos\theta\cos\varphi \big/ \ell_P{}^2\right)\ddot{x}_T - \left(\sin\theta\sin\varphi \big/ \ell_P + \delta\sin\theta\sin\varphi \big/ \ell_P{}^2\right) \\ \left(\ddot{u}_T + 2\dot{u}_T{}'\dot{x}_T + u_T{}''\dot{x}_T{}^2 + u_T{}'\ddot{x}_T\right) + \left(\cos\theta\sin\varphi \big/ \ell_P + \delta\cos\theta\sin\varphi \big/ \ell_P{}^2\right) \\ \left(\ddot{v}_T + 2\dot{v}_T{}'\dot{x}_T + v_T{}''\dot{x}_T{}^2 + v_T{}'\ddot{x}_T\right) - \left(\cos\varphi \big/ \ell_P + \delta\cos\varphi \big/ \ell_P{}^2\right) \\ \left(\ddot{w}_T + 2\dot{w}_T{}'\dot{x}_T + w_T{}''\dot{x}_T{}^2 + w_T{}'\ddot{x}_T\right) + \left(1 + 2\delta \big/ \ell_P + \delta^2 \big/ \ell_P{}^2\right)\ddot{\varphi} \\ + 2\dot{\delta}\dot{\varphi} \big/ \ell_P + g\cos\theta\sin\varphi \big/ \ell_P + g\delta\cos\theta\sin\varphi \big/ \ell_P{}^2 \end{pmatrix} = 0 \qquad (48f)$$

Finally, the equation of motion associates with the generalized coordinate $q = \delta$ can be derived as follows.

$$\frac{d}{dt}\left(\frac{\partial L}{\partial \dot{\delta}}\right) - \frac{\partial L}{\partial \delta} + \frac{\partial F}{\partial \dot{\delta}} = 0$$

Thus,

$$\begin{pmatrix} \sin\theta\cos\varphi\ddot{x}_T \big/ \ell_P + \sin\theta\cos\varphi \big/ \ell_P \left(\ddot{u}_T + 2\dot{u}_T{}'\dot{x}_T + u_T{}''\dot{x}_T{}^2 + u_T{}'\ddot{x}_T\right) \\ - \cos\theta\cos\varphi \big/ \ell_P \left(\ddot{v}_T + 2\dot{v}_T{}'\dot{x}_T + v_T{}''\dot{x}_T{}^2 + v_T{}'\ddot{x}_T\right) \\ + \sin\varphi \big/ \ell_P \left(\ddot{w}_T + 2\dot{w}_T{}'\dot{x}_T + w_T{}''\dot{x}_T{}^2 + w_T{}'\ddot{x}_T\right) - \dot{\varphi}^2 - \cos^2\varphi\dot{\theta}^2 \\ + \ddot{\delta} \big/ \ell_P - \delta\dot{\varphi}^2 \big/ \ell_P - \delta\cos^2\varphi\dot{\theta}^2 \big/ \ell_P - g\cos\theta\cos\varphi \big/ \ell_P + k\delta \big/ m_P\ell_P \end{pmatrix} = 0 \qquad (48g)$$

Equations (48a)-(48c) represent external forces vector which cover inertial forces from flexible gantry crane and swing effect of payload to the crane framework at the contact point between trolley and crane framework. It can be written in form:

$$\{f_0(t)\} = (f_{0x}(t))i + (f_{0y}(t))j + (f_{0z}(t))k \tag{49}$$

where f_{0x}, f_{0y} and f_{0z} are the corresponding external force components in the x, y and z direction. The magnitude of these external forces is given by Equations (48a) - (48c) and rewritten as

$$f_{0x} = (m_T + m_p)(\ddot{u}_T + 2\dot{u}_T{}'\dot{x}_T + u_T{}''\dot{x}_T{}^2 + u_T{}'\ddot{x}_T + \ddot{x}_T) + m_p\ell_P \begin{pmatrix} -\ddot{\theta}\cos\theta\cos\varphi\left(1+\delta/\ell_P\right) + \dot{\theta}^2\sin\theta\cos\varphi\left(1+\delta/\ell_P\right) \\ +2\dot{\theta}\dot{\varphi}\cos\theta\sin\varphi\left(1+\delta/\ell_P\right) + \ddot{\varphi}\sin\varphi\sin\theta\left(1+\delta/\ell_P\right) \\ +\dot{\varphi}^2\cos\varphi\sin\theta\left(1+\delta/\ell_P\right) - 2\dot{\delta}\dot{\theta}\cos\theta\cos\varphi/\ell_P \\ +2\dot{\delta}\dot{\theta}\sin\theta\sin\varphi/\ell_P - \ddot{\delta}\sin\theta\cos\varphi/\ell_P \end{pmatrix} \tag{50a}$$

$$f_{0y} = (m_T + m_p)(\ddot{v}_T + 2\dot{v}_T{}'\dot{x}_T + v_T{}''\dot{x}_T{}^2 + v_T{}'\ddot{x}_T) + m_p\ell_P \begin{pmatrix} -\ddot{\theta}\sin\theta\cos\varphi\left(1+\delta/\ell_P\right) - \dot{\theta}^2\cos\theta\cos\varphi\left(1+\delta/\ell_P\right) \\ +2\dot{\theta}\dot{\varphi}\sin\theta\sin\varphi\left(1+\delta/\ell_P\right) - \ddot{\varphi}\cos\theta\sin\varphi\left(1+\delta/\ell_P\right) \\ -\dot{\varphi}^2\cos\theta\cos\varphi\left(1+\delta/\ell_P\right) - 2\dot{\delta}\dot{\theta}\sin\theta\cos\varphi/\ell_P \\ -2\dot{\delta}\dot{\varphi}\cos\theta\sin\varphi/\ell_P + \ddot{\delta}\cos\theta\cos\varphi/\ell_P \end{pmatrix} + (m_T + m_p)g \tag{50b}$$

$$f_{0z} = (m_T + m_p)(\ddot{w}_T + 2\dot{w}_T{}'\dot{x}_T + w_T{}''\dot{x}_T{}^2 + w_T{}'\ddot{x}_T) + m_p\ell_P \begin{pmatrix} \ddot{\varphi}\cos\varphi\left(1+\delta/\ell_P\right) - \dot{\varphi}^2\sin\varphi\left(1+\delta/\ell_P\right) \\ +2\dot{\delta}\dot{\varphi}\cos\varphi/\ell_P + \ddot{\delta}\sin\varphi/\ell_P \end{pmatrix} \tag{50c}$$

As per Equations (41) and (42), external force vector can be written in the following form:

$$\{F_{st}(t)\} = \begin{Bmatrix} \{N_k\}_u{}^T f_{0x} \\ \{N_k\}_v{}^T f_{0y} \\ \{N_k\}_w{}^T f_{0z} \end{Bmatrix} \tag{51}$$

where $\{N_k\}$, $k=1-12$ is shape functions of 3D frame element as per Table 2.4, and $\{N_k\}_u$ $u=k=1,7$, $\{N_k\}_v$ $k=2,6,8,12$ and $\{N_k\}_w$ $w=k=3,5,9,11$ are shape functions associated with translation degree of freedoms in three directions, axial $\{X\}$, vertical $\{Y\}$ and lateral $\{Z\}$ which is compatible with Equation (8).

By combining and manipulating Equations (42) and (51), and referring to Equations (14)-(16), integrated finite element formulation will be generated as follows.

$$\left[[M_{st}]+\begin{bmatrix}0&0&0&0\\0&\overline{M}_{22}&0&0\\0&0&\overline{M}_{33}&0\\0&0&0&\overline{M}_{44}\end{bmatrix}\right]\begin{Bmatrix}\ddot{\Delta}_r\\\ddot{u}_T\\\ddot{v}_T\\\ddot{w}_T\end{Bmatrix}+\left[[C_{st}]+\begin{bmatrix}0&0&0&0\\0&\overline{C}_{22}&0&0\\0&0&\overline{C}_{33}&0\\0&0&0&\overline{C}_{44}\end{bmatrix}\right]\begin{Bmatrix}\dot{\Delta}_r\\\dot{u}_T\\\dot{v}_T\\\dot{w}_T\end{Bmatrix}+\left[[K_{st}]+\begin{bmatrix}0&0&0&0\\0&\overline{K}_{22}&0&0\\0&0&\overline{K}_{33}&0\\0&0&0&\overline{K}_{44}\end{bmatrix}\right]\begin{Bmatrix}\Delta_r\\u_T\\v_T\\w_T\end{Bmatrix}=\begin{Bmatrix}0\\\overline{F}_{21}\\\overline{F}_{31}\\\overline{F}_{41}\end{Bmatrix} \tag{52a}$$

where $\overline{M}_{22},\overline{M}_{33},\overline{M}_{44},\overline{C}_{22},\overline{C}_{33},\overline{C}_{44},\overline{K}_{22},\overline{K}_{33},\overline{K}_{44}$ are given by

$$\begin{aligned}
\overline{M}_{22}&=\left(m_T+m_p\right)\{N_k\}_u{}^T\{N_k\}_u\\
\overline{M}_{33}&=\left(m_T+m_p\right)\{N_k\}_v{}^T\{N_k\}_v\\
\overline{M}_{44}&=\left(m_T+m_p\right)\{N_k\}_w{}^T\{N_k\}_w\\
\\
\overline{C}_{22}&=2\left(m_T+m_p\right)\left(\dot{x}_T+\ddot{x}_T t\right)\{N_k\}_u{}^T\{N_u'\}_u\\
\overline{C}_{33}&=2\left(m_T+m_p\right)\left(\dot{x}_T+\ddot{x}_T\right)\{N_k\}_v{}^T\{N_v'\}_v\\
\overline{C}_{44}&=2\left(m_T+m_p\right)\left(\dot{x}_T+\ddot{x}_T\right)\{N_k\}_w{}^T\{N_w'\}_w\\
\\
\overline{K}_{22}&=\left(m_T+m_p\right)\left(\left(\dot{x}_T+\ddot{x}_T\right)^2\{N_k\}_u{}^T\{N_u''\}_u+\ddot{x}_T\{N_k\}_u{}^T\{N_k'\}_u\right)\\
\overline{K}_{33}&=\left(m_T+m_p\right)\left(\left(\dot{x}_T+\ddot{x}_T\right)^2\{N_k\}_v{}^T\{N_v''\}_v+\ddot{x}_T\{N_k\}_v{}^T\{N_k'\}_v\right)\\
\overline{K}_{44}&=\left(m_T+m_p\right)\left(\left(\dot{x}_T+\ddot{x}_T\right)^2\{N_k\}_w{}^T\{N_w''\}_w+\ddot{x}_T\{N_k\}_w{}^T\{N_k'\}_w\right)
\end{aligned} \tag{52b}$$

$$\overline{F}_{21} = \{N_k\}_u^T \left(-(m_T + m_p)\ddot{x}_T + m_p \ell_P \left(\begin{array}{l} -\ddot{\theta}\cos\theta\cos\varphi\left(1+\delta/\ell_P\right) + \dot{\theta}^2 \sin\theta\cos\varphi\left(1+\delta/\ell_P\right) \\ +2\dot{\theta}\dot{\varphi}\cos\theta\sin\varphi\left(1+\delta/\ell_P\right) + \ddot{\varphi}\sin\varphi\sin\theta\left(1+\delta/\ell_P\right) \\ +\dot{\varphi}^2\cos\varphi\sin\theta\left(1+\delta/\ell_P\right) - 2\dot{\delta}\dot{\theta}\cos\theta\cos\varphi/\ell_P \\ +2\dot{\delta}\dot{\theta}\sin\theta\sin\varphi/\ell_P - \ddot{\delta}\sin\theta\cos\varphi/\ell_P \end{array} \right) \right)$$

$$\overline{F}_{31} = \{N_k\}_v^T \left(m_p \ell_P \left(\begin{array}{l} -\ddot{\theta}\sin\theta\cos\varphi\left(1+\delta/\ell_P\right) - \dot{\theta}^2\cos\theta\cos\varphi\left(1+\delta/\ell_P\right) \\ +2\dot{\theta}\dot{\varphi}\sin\theta\sin\varphi\left(1+\delta/\ell_P\right) - \ddot{\varphi}\cos\theta\sin\varphi\left(1+\delta/\ell_P\right) \\ -\dot{\varphi}^2\cos\theta\cos\varphi\left(1+\delta/\ell_P\right) - 2\dot{\delta}\dot{\theta}\sin\theta\cos\varphi/\ell_P \\ -2\dot{\delta}\dot{\varphi}\cos\theta\sin\varphi/\ell_P + \ddot{\delta}\cos\theta\cos\varphi/\ell_P \end{array} \right) - (m_T + m_p)g \right)$$

$$\overline{F}_{41} = \{N_k\}_w^T \left(m_p \ell_P \left(\ddot{\varphi}\cos\varphi\left(1+\delta/\ell_P\right) - \dot{\varphi}^2\sin\varphi\left(1+\delta/\ell_P\right) + 2\dot{\delta}\dot{\varphi}\cos\varphi/\ell_P + \ddot{\delta}\sin\varphi/\ell_P \right) \right)$$

(52c)

The term $\ddot{x}_T$ in Equation (52) is the acceleration of trolley which appears as the forcing term in payload dynamics, if input force for gantry crane is set up to be zero. It can be observed that at $t = 0$, there is no effect of moving trolley carrying a swinging payload to the crane framework, except the weight of trolley and payload mass $(m_T + m_p)g$ itself as a static force to the crane framework.

Inertial, Coriolis, centrifugal force and gravitational force effects of moving mass to the framework are presented by Equation (52), where notations (u_T, v_T, w_T) and its derivative indicate the nodal displacements, velocities and acceleration, respectively according to the position vector of trolley and payload as per Equation (44c). Vice versa, notation Δ_r and its derivative indicate vectors of displacements, velocities and accelerations for the rest of the degrees of freedom of the crane framework.

Equations (48d)-(48g) are dynamics of gantry crane coupled with dynamics of crane framework and call for some remarks.

1. The term, f_x is input force or driving force for the trolley motion while $(m_T + m_P)$ is mass total from trolley and payload. This term is an equivalent lumped mass which will be effect in the crane framework. Compared than equivalent mass proposed by [10], this term is different. Equivalent mass is denoted as $(m_T + m_P \cos^2\theta)$. This discrepancy occurs because [10] neglected the centrifugal force of the swinging payload. By considering the centrifugal force, it leads to the condition that the magnitude of total mass is not time-dependent, but position of the mass total is still time-variant as reported in [5], [6] and [11].
2. Equations (48d)-(48g) and (52) are equations of motion which represent the coupling between the dynamics of crane framework and gantry crane. Equation (48d) presents dynamics of trolley motion with the input force, while Equations (48e)-(48f) are dynamics of payload. Equation (48g) is dynamics of hoist cable, where appears only when there is flexibility in hoist cable.
3. Trolley acceleration, $(\ddot{x}_T)$ appears as forcing term to the dynamics of gantry crane as shown in Equations (48e)-(48g) if the trolley motion is prescribed.
4. There are contributions of axial, lateral and vertical acceleration of crane framework on the dynamics of gantry crane. These contributions provide flexible moving support for the trolley carrying a swinging payload.
5. There are effects of Coriolis and centrifugal forces in Equation (52) due to $(m_T + m_P)$moves on deformed crane framework.
6. Equations (48d)-(48g) and (52) have led to a system of equations which dynamics of gantry crane are dependent on the dynamics of crane framework and conversely. There is a bidirectional coupling between crane framework and gantry crane, where flexible support of the gantry crane motion offered by vibration of crane framework. This result is also found by [5] and [6].
7. Equation (52) indicates that the overall mass, damping and stiffness matrices of the crane framework are time-variant, where the mass, damping and stiffness matrices of the moving finite element of space frame are given in Equations (14)-(16).

Structural damping matrices in the left side of Equation (52) is assumed proportional to the combination of total mass $[M]$ and stiffness $[K]$ matrices of gantry crane system. Under this assumption, The Rayleigh damping theory is therefore used. The damping matrices can be written as [91]:

$$[C_{st}] = a[M] + b[K] \tag{53}$$

If the damping ratios ζ_m and ζ_n associated with two specific frequencies ω_m, ω_n, the same damping ratio is applied for both control frequencies, ω_1 and ω_2; i.e., $\zeta = \zeta_1 = \zeta_2$. Rayleigh damping factors, a and b can be calculated using the solution of Equation (54), while total damping matrix $[C]$ is calculated based on Equation (52).

$$\begin{Bmatrix} a \\ b \end{Bmatrix} = \frac{2\zeta}{\omega_1 + \omega_2} \begin{Bmatrix} \omega_1 \omega_2 \\ 1 \end{Bmatrix}, \tag{54}$$

Finally, finite element model of crane framework is shown in Figure 4.2 below.

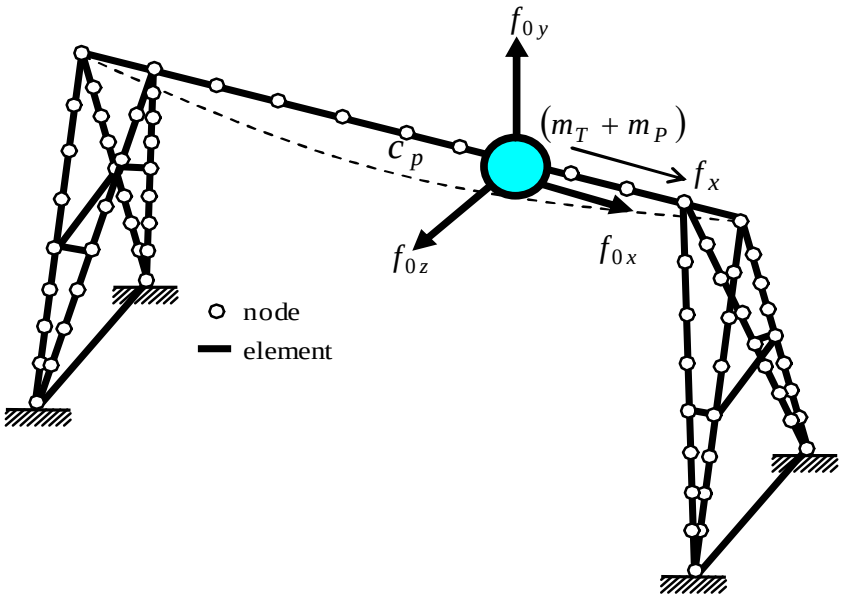

Figure 4.2: Finite element model of the crane framework

4.4 Some Cases on the Equations of Motion

The integrated finite element formulation in Equations (48d)-(48g) and (52) contain the motion of trolley ($\ddot{x}_T$ and its derivatives), the motion of payload (φ, θ and their derivatives), the motion of hoist cable (δ and its derivative) and the motion of flexible crane framework. Those equations reflect three loading cases on gantry crane system as depicted in Figure 4.3 below.

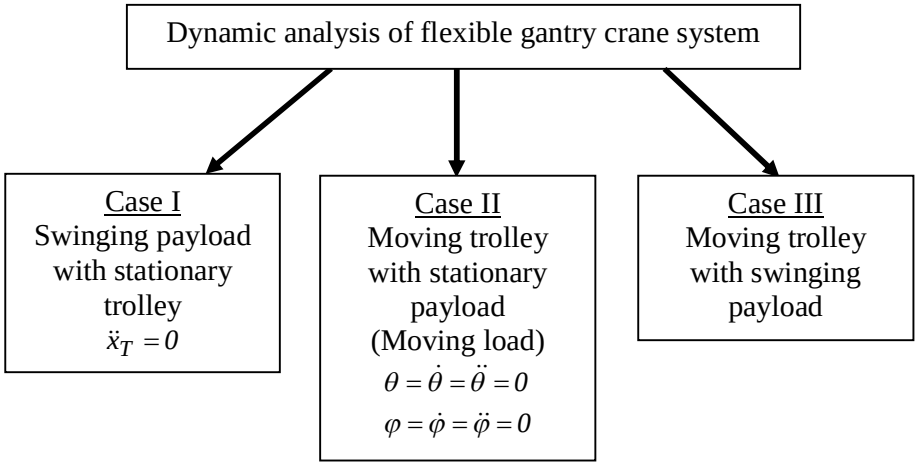

Figure 4.3: Three loading cases on flexible gantry crane system

For each case, the equations of motion can be written:

Case I

Trolley locates at the central point c_P of the top beam of crane framework, while the payload swings freely with initial condition. Equations of motion of the system will be under swinging motion of payload as case I.

$$\begin{pmatrix} -\left(\sin\theta\sin\varphi/\ell_P + \delta\sin\theta\sin\varphi/\ell_P{}^2\right)\ddot{u}_T + \left(\cos\theta\sin\varphi/\ell_P + \delta\cos\theta\sin\varphi/\ell_P{}^2\right)\ddot{v}_T \\ -\left(\cos\varphi/\ell_P + \delta\cos\varphi/\ell_P{}^2\right)\ddot{w}_T + \left(1 + 2\delta/\ell_P + \delta^2/\ell_P{}^2\right)\ddot{\varphi} \\ + 2\dot{\delta}\dot{\varphi}/\ell_P + g\cos\theta\sin\varphi/\ell_P + g\delta\cos\theta\sin\varphi/\ell_P{}^2 \end{pmatrix} = 0 \quad (55a)$$

$$\begin{pmatrix} \sin\theta\cos\varphi/\ell_P\,\ddot{u}_T - \cos\theta\cos\varphi/\ell_P\,\ddot{v}_T + \sin\varphi/\ell_P\,\ddot{w}_T - \dot{\varphi}^2 - \cos^2\varphi\dot{\theta}^2 \\ + \ddot{\delta}/\ell_P - \delta\dot{\varphi}^2/\ell_P - \delta\cos^2\varphi\dot{\theta}^2/\ell_P - g\cos\theta\cos\varphi/\ell_P + k\delta/m_P\ell_P \end{pmatrix} = 0 \qquad (55b)$$

$$\begin{pmatrix} \left(\cos\theta\cos\varphi/\ell_P + \delta\cos\theta\cos\varphi/\ell_P^2\right)\ddot{u}_T \\ + \left(\sin\theta\cos\varphi/\ell_P + \delta\sin\theta\cos\varphi/\ell_P^2\right)\ddot{v}_T + \left(\cos^2\varphi + 2\delta\cos^2\varphi/\ell_P + \delta^2\cos^2\varphi/\ell_P^2\right)\ddot{\theta} \\ -\left(2\dot{\theta}\dot{\varphi}\sin\varphi\cos\varphi\right) + 2\dot{\delta}\dot{\theta}\delta\cos^2\varphi/\ell_P^2 - 2\dot{\varphi}\dot{\theta}\delta^2\cos\varphi\sin\varphi/\ell_P^2 + 2\dot{\delta}\dot{\theta}\cos^2\varphi/\ell_P + 2\delta\dot{\varphi}\dot{\theta}\sin\varphi\cos\varphi/\ell_P \\ + g\sin\theta\cos\varphi/\ell_P + g\delta\sin\theta\cos\varphi/\ell_P^2 \end{pmatrix} = 0 \qquad (55c)$$

$$\left[M_{st}\right] + \begin{bmatrix} 0 & 0 & 0 & 0 \\ 0 & \left(m_T + m_p\right) & 0 & 0 \\ 0 & 0 & \left(m_T + m_p\right) & 0 \\ 0 & 0 & 0 & \left(m_T + m_p\right) \end{bmatrix} \begin{Bmatrix} \ddot{\Delta}_r \\ \ddot{u}_T \\ \ddot{v}_T \\ \ddot{w}_T \end{Bmatrix} + \left[C_{st}\right]\{\dot{q}_{st}\} + \left[K_{st}\right]\{q_{st}\}$$

$$= \begin{Bmatrix} 0 \\ m_p\ell_P\begin{pmatrix} -\ddot{\theta}\cos\theta\cos\varphi\left(1+\delta/\ell_P\right) + \dot{\theta}^2\sin\theta\cos\varphi\left(1+\delta/\ell_P\right) + 2\dot{\theta}\dot{\varphi}\cos\theta\sin\varphi\left(1+\delta/\ell_P\right) \\ + \ddot{\varphi}\sin\varphi\sin\theta\left(1+\delta/\ell_P\right) + \dot{\varphi}^2\cos\varphi\sin\theta\left(1+\delta/\ell_P\right) - 2\dot{\delta}\dot{\theta}\cos\theta\cos\varphi/\ell_P \\ + 2\dot{\delta}\dot{\theta}\sin\theta\sin\varphi/\ell_P - \ddot{\delta}\sin\theta\cos\varphi/\ell_P \end{pmatrix} \\ m_p\ell_P\begin{pmatrix} -\ddot{\theta}\sin\theta\cos\varphi\left(1+\delta/\ell_P\right) - \dot{\theta}^2\cos\theta\cos\varphi\left(1+\delta/\ell_P\right) + 2\dot{\theta}\dot{\varphi}\sin\theta\sin\varphi\left(1+\delta/\ell_P\right) \\ -\ddot{\varphi}\cos\theta\sin\varphi\left(1+\delta/\ell_P\right) - \dot{\varphi}^2\cos\theta\cos\varphi\left(1+\delta/\ell_P\right) - 2\dot{\delta}\dot{\theta}\sin\theta\cos\varphi/\ell_P \\ -2\dot{\delta}\dot{\varphi}\cos\theta\sin\varphi/\ell_P + \ddot{\delta}\cos\theta\cos\varphi/\ell_P \end{pmatrix} - \left(m_T + m_p\right)g \\ m_p\ell_P\left(\ddot{\varphi}\cos\varphi\left(1+\delta/\ell_P\right) - \dot{\varphi}^2\sin\varphi\left(1+\delta/\ell_P\right) + 2\dot{\delta}\dot{\varphi}\cos\varphi/\ell_P + \ddot{\delta}\sin\varphi/\ell_P\right) \end{Bmatrix} \qquad (55d)$$

Under the assumptions that the crane framework and hoist cable are to be rigid, vibration of the crane framework and hoist cable vanish in the Equations (55a)-(55d). Equations of motion of the system can be reduced into classical pendulum system with fixed support or called rigid model for case I.

$$\ddot{\theta}\cos^2\varphi - 2\dot{\theta}\dot{\varphi}\sin\varphi\cos\varphi + \frac{g}{\ell_P}\sin\theta\cos\varphi = 0 \tag{56a}$$

$$\ddot{\varphi} + \cos\varphi\sin\varphi\dot{\theta}^2 + \frac{g}{\ell_P}\cos\theta\sin\varphi = 0 \tag{56b}$$

Case II

If there is no swinging motion of payload, equations of motion of the system in Equation (52) will be moving load case as case II. Equations (57a) and (57b) indicate that the trolley and payload is taken as moving mass, its inertial effect is considered. Vice versa, if inertia effect is negligible, then it will be taken as moving force where $f_{0x} = 0$ and the only external force which subjected to crane framework is vertical force $f_{0y} = (m_T + m_P)g$.

$$\left[[M_{st}] + \begin{bmatrix} 0 & 0 & 0 & 0 \\ 0 & \overline{M}_{22} & 0 & 0 \\ 0 & 0 & \overline{M}_{33} & 0 \\ 0 & 0 & 0 & \overline{M}_{44} \end{bmatrix}\right]\begin{Bmatrix} \ddot{\Delta}_r \\ \ddot{u}_T \\ \ddot{v}_T \\ \ddot{w}_T \end{Bmatrix} + \left[[C_{st}] + \begin{bmatrix} 0 & 0 & 0 & 0 \\ 0 & \overline{C}_{22} & 0 & 0 \\ 0 & 0 & \overline{C}_{33} & 0 \\ 0 & 0 & 0 & \overline{C}_{44} \end{bmatrix}\right]\begin{Bmatrix} \dot{\Delta}_r \\ \dot{u}_T \\ \dot{v}_T \\ \dot{w}_T \end{Bmatrix} + \left[[K_{st}] + \begin{bmatrix} 0 & 0 & 0 & 0 \\ 0 & \overline{K}_{22} & 0 & 0 \\ 0 & 0 & \overline{K}_{33} & 0 \\ 0 & 0 & 0 & \overline{K}_{44} \end{bmatrix}\right]\begin{Bmatrix} \Delta_r \\ u_T \\ v_T \\ w_T \end{Bmatrix}$$
$$= \begin{Bmatrix} 0 \\ -\{N_k\}_u^T (m_T + m_p)\ddot{x}_T \\ -\{N_k\}_v^T (m_T + m_p)g \\ 0 \end{Bmatrix} \tag{57a}$$

$$(m_T + m_p)\left(\ddot{u}_T + 2\dot{u}_T'\dot{x}_T + u_T''\dot{x}_T^2 + u_T'\ddot{x}_T + \ddot{x}_T\right) = f_x \tag{57b}$$

Case III

This is the case where the flexible gantry crane moves on flexible crane framework based on Equations (48d)-(48g) and (52). Similar with case I, under the assumptions that the crane framework and hoist cable are to be rigid, vibration of the crane framework vanishes in those equations. Equations of motion of the system can be reduced greatly and the results are the same with Newton's motion law for classical pendulum system with moving support or called in this thesis as rigid model for case III.

$$\left(m_T + m_p\right)\ddot{x}_T + m_p \ell_P \begin{pmatrix} \ddot{\theta}\cos\theta\cos\varphi - \dot{\theta}^2 \sin\theta\cos\varphi - \dot{\theta}\dot{\varphi}\cos\theta\sin\varphi \\ -\ddot{\varphi}\sin\varphi\sin\theta - \dot{\varphi}^2\cos\varphi\sin\theta - \dot{\varphi}\dot{\theta}\sin\varphi\cos\theta \end{pmatrix} = f_x \tag{58}$$

$$\frac{\ddot{x}_T}{\ell_P}\cos\theta\cos\varphi + \ddot{\theta}\cos^2\varphi - 2\dot{\theta}\dot{\varphi}\sin\varphi\cos\varphi + \frac{g}{\ell_P}\sin\theta\cos\varphi = 0 \tag{59a}$$

4.5 Numerical Approach

The computational scheme for solving Equations (48d)-(48g) and (52) is based on Newmark-β and fourth-order Runge-Kutta method simultaneously. The crane framework responses are calculated by Newmark-β method of direct integration. The two parameters are selected as β=0.25 and γ=0.5, which implies a constant average acceleration with unconditional numerical stability. Gantry crane responses are calculated by fourth-order Runge-Kutta method. For each integration step, Newmark-β and fourth-order Runge-Kutta method are combined to obtain the responses of crane framework and crane system.

The computational procedures with a time interval of Δt that performs the direct numerical integration can be summarized as follows.

1. Set initial condition for velocity and acceleration.

$$\{q\}_0 = \{q(t=0)\} \text{ and } \{\dot{q}\}_0 = \{\dot{q}(t=0)\} \tag{60}$$

2. The initial external force vector $\{F\}_0 = \{F(t=0)\}$ is calculated using the terms on the right side of Equation (52) by using initial conditions ($\theta, \dot{\theta}, \ddot{\theta}$, $\varphi, \dot{\varphi}, \ddot{\varphi}$ and $\delta, \dot{\delta}, \ddot{\delta}$) of payload.
3. The initial acceleration vector is then calculated as:

$$\{\ddot{q}\}_0 = [M_{st}]^{-1}\{\{F\}_0 - [C_{st}]\{\dot{q}\}_0 - [K_{st}]\{q\}_0\} \tag{61}$$

4. Evaluation of constants from a_0 to a_7 .The parameters a_i are shown in Table 4.1.

Table 4.1: Newmark's parameters

$a_0 = \frac{1}{\beta \Delta t^2}$	$a_1 = \frac{\gamma}{\beta \Delta t}$	$a_2 = \frac{1}{\beta \Delta t}$	$a_3 = \frac{1}{2\beta} - 1$
$a_4 = \frac{\gamma}{\beta} - 1$	$a_5 = \frac{\Delta t}{2}\left(\frac{\gamma}{\beta} - 2\right)$	$a_6 = \Delta t(1-\gamma)$	$a_7 = \gamma \Delta t$

5. For each time step:
   - Generate the overall mass matrix $[M]$ and overall stiffness matrix $[K]$ of the system by using Equation (52).
   - Calculation of the first and second natural frequencies (ω_1 and ω_2) of the overall crane framework. The overall damping matrix $[C]$ is calculated using Equations (52) and (53).
   - Equations (48d)-(48g) are solved to obtain $\theta, \dot{\theta}, \ddot{\theta}$, $\varphi, \dot{\varphi}, \ddot{\varphi}$ and $\delta, \dot{\delta}, \ddot{\delta}$ using fourth-order Runge-Kutta and external force vector $\{F\}_{t+\Delta t}$ is then updated. The force vector $\{F\}_{t+\Delta t}$ denotes the external loads of the system at time $t + \Delta t$.
   - Equation of motion of the system is represented as below.

$$[\overline{K}]_{t+\Delta t}\{q\}_{t+\Delta t} = \{\overline{F}\}_{t+\Delta t} \tag{62}$$

The effective stiffness matrix $\{\overline{K}\}$ and the effective load vector $\{\overline{F}\}$ are defined as follows.

$$\{\overline{K}\}_{t+\Delta t} = [K]_t + a_0[M]_t + a_1[C]_t \tag{63}$$

$$\{\overline{F}\}_{t+\Delta t} = \{F\}_{t+\Delta t} + [M]_t\left(a_0\{q\}_t + a_2\{\dot{q}\}_t + a_3\{\ddot{q}\}_t\right) \tag{64}$$

where $[M]_t, [C]_t, [K]_t$ are, respectively, the stiffness, mass and damping matrix of the system evaluated at time t.

   - The displacement, velocity and acceleration responses are computed with satisfying Equations (65) – (67).

$$\{q\}_{t+\Delta t} = \left[\overline{K}\right]_{t+\Delta t}^{-1} \{\overline{F}\}_{t+\Delta t} \tag{65}$$

$$\{\ddot{q}\}_{t+\Delta t} = a_0 \left(\{q\}_{t+\Delta t} - \{q\}_t\right) - a_2 \{\dot{q}\}_t - a_3 \{\ddot{q}\}_t \tag{66}$$

$$\{\dot{q}\}_{t+\Delta t} = \{\dot{q}\}_t + a_6 \{\ddot{q}\}_t + a_7 \{\ddot{q}\}_{t+\Delta t} \tag{67}$$

4.6 Summary

Equations of motion of flexible gantry crane system are derived using Lagrange's equations in conjunction with moving finite element and finite element method. The equations of motion represent the coupling between the dynamics of crane framework and gantry crane, namely dynamics of trolley motion with the input force, dynamics of payload, dynamics of hoist cable and dynamics of crane framework.

The system equations describe that gantry crane behaves as an elastic pendulum with moving flexible support which undergoes accelerations in three directions due to the vibration of crane framework. These accelerations are provided by the flexibility of crane framework and affected by the flexibility of hoist cable. The derived system equations are coupled differential equations with nonlinear exciting forces. Some cases are stated in Section 4.4, where the equations of motion reflect three loading cases on gantry crane system, namely swinging motion of payload as case I, moving load as case II and moving trolley carrying a swinging payload as case III. By assuming the crane framework and hoist cable are rigid, the generated governing equations correctly simplified to nonlinear equations, which exactly fulfill Newton's of motion for classical pendulum system either with fixed support or moving support.

The equations of motion for dynamics of gantry crane system with flexibility in crane framework and hoist cable are then solved numerically by two kinds of numerical integration method simultaneously, namely Newmark-β and fourth-order Runge-Kutta method simultaneously. These methods are utilized to obtain the dynamic responses of crane framework and gantry crane, either small or large swing angles of payload.

CHAPTER 5

DYNAMIC RESPONSES AND ANALYSIS

5.1 Introduction

Dynamic analysis of gantry crane system covers three types of loading condition. Firstly, it is induced by swinging payload with stationary trolley as case I. The analysis is then extended to moving trolley with stationary payload (moving load) traverse on skeletal structures as case II, and finally under moving trolley with swinging payload as case III. The cross-sections of crane framework are uniform, isotropic and homogeneous material properties. The gravitational acceleration is $g = 9.81$ m/s^2 and time interval is $\Delta t = 0.005$ s. The issue of total number of elements and nodes will not be treated as a parameter that will be varied in the simulations.

5.2 Free Vibration of Gantry Crane Framework

Free vibration analysis is firstly conducted. The model and the dimensions for crane framework are taken from [89] and file data is put in Appendix B. The first three mode shapes of crane framework, which is the most pertinent of crane framework corresponding to the crane framework to vibrate in axial (X), vertical (Y) and lateral (Z) are shown in Figure 5.1.

It can be observed that the first mode shape with natural frequency $f_1 = 6.56\ Hz$ is dominated by axial deformation of crane framework. The second is dominated by lateral deformation of the top beam of crane framework with natural frequency $f_2 = 6.65\ Hz$. Vertical deformation of the top beam of crane framework is found in the third mode shape with natural frequency $f_3 = 6.78\ Hz$.

For verification of natural frequencies generated by present computer code, ANSYS is used as comparison and presented in Table 5.1 and also verified with analytical method in free vibration of the simply supported beam (see Appendix C). It is seen that the first five natural frequencies obtained in ANSYS and present code are almost identical and reliable for the next dynamic analysis of gantry crane system.

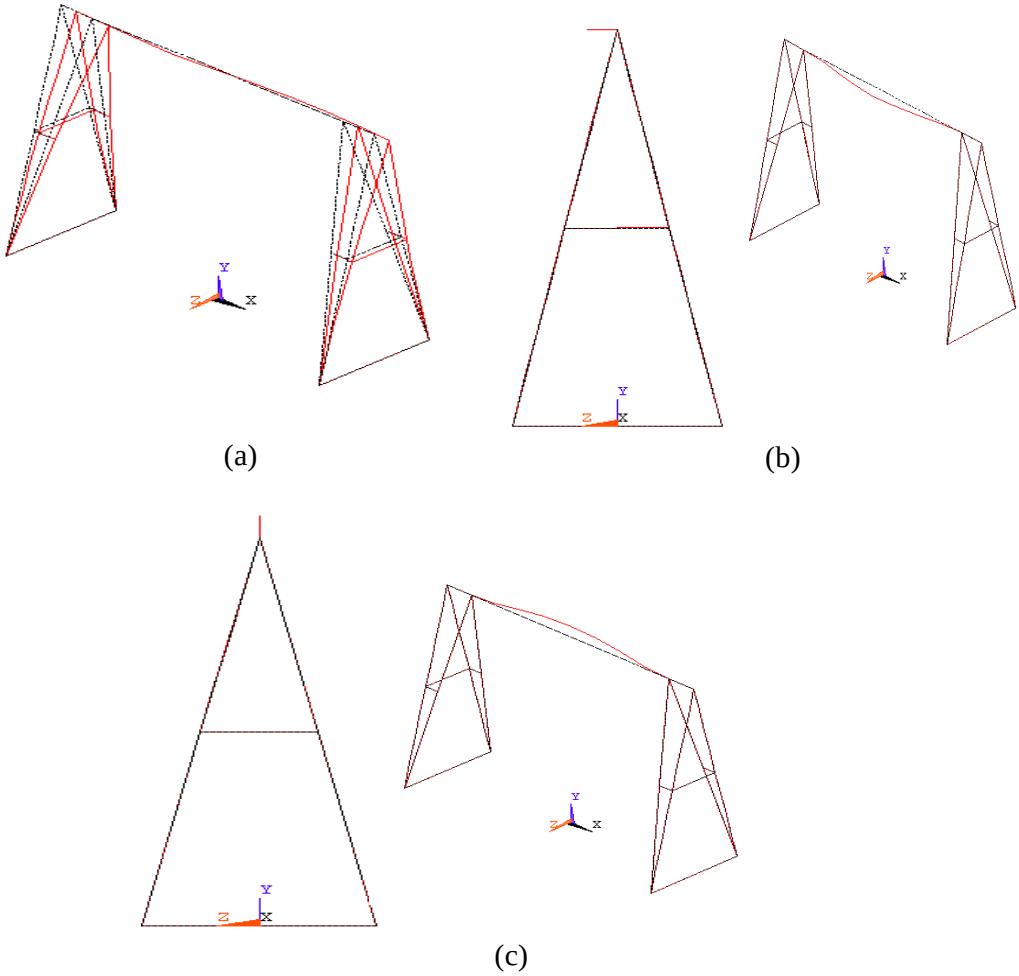

Figure 5.1: Corresponding mode shapes of crane framework, (a) 1st mode shape, 6.56 Hz (b) 2nd mode shape, 6.65Hz (c) 3rd mode shape, 6.78Hz

Table 5.1: Verification of natural frequency and mode shape

Natural frequency (Hz)	Mode number		
	1st	2nd	3rd
ANSYS	6.55	6.64	6.77
Present code	6.56	6.65	6.78

5.3 Simple Case of a Coupled Dynamic System

Before proceeding into dynamic analysis of gantry crane system, the developed computer program must be verified first by solving a simple coupled dynamic model. The model and its equations of motion are taken from [88], who studied the dynamic sub-structuring technique to a simple nonlinear system consist of pendulum attached to a mass-spring-damper (MSD). The configuration of the system is depicted in Figure 5.2. The parameters of the system are shown in Table 5.2.

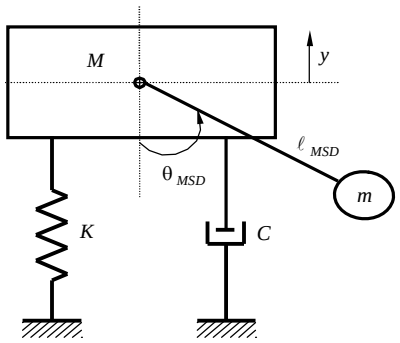

Figure 5.2: Pendulum attached to a MSD system

Table 5.2: Pendulum Attached to a MSD parameters

Parameters	
Mass of MSD, M	$4kg$
Damping of MSD, C	$20kg/s$
Stiffness of MSD, K	$5000N/m$
Pendulum mass, m_{MSD}	$0.9kg$
Pendulum length, ℓ_{MSD}	$0.5m$
Initial swing angle, $\theta_o, \dot{\theta}_0, \ddot{\theta}_0$	$5^o, 0, 0$
Initial vertical displacement, $y_o, \dot{y}_o, \ddot{y}_o$	$10^{-3}mm, 0, 0$

5.3.1 Pendulum Attached to a MSD under the Action of Pendulum Motion

Under the action of pendulum motion, the equations of motion are solved by developed Newmark-β-Runge-Kutta and state space approach for linear model and Newmark-β-Runge-Kutta and ODE-45 for nonlinear model. The displacements of linear model are shown in Figures 5.3 and 5.4, and very good agreement between the solutions offered by both methods.

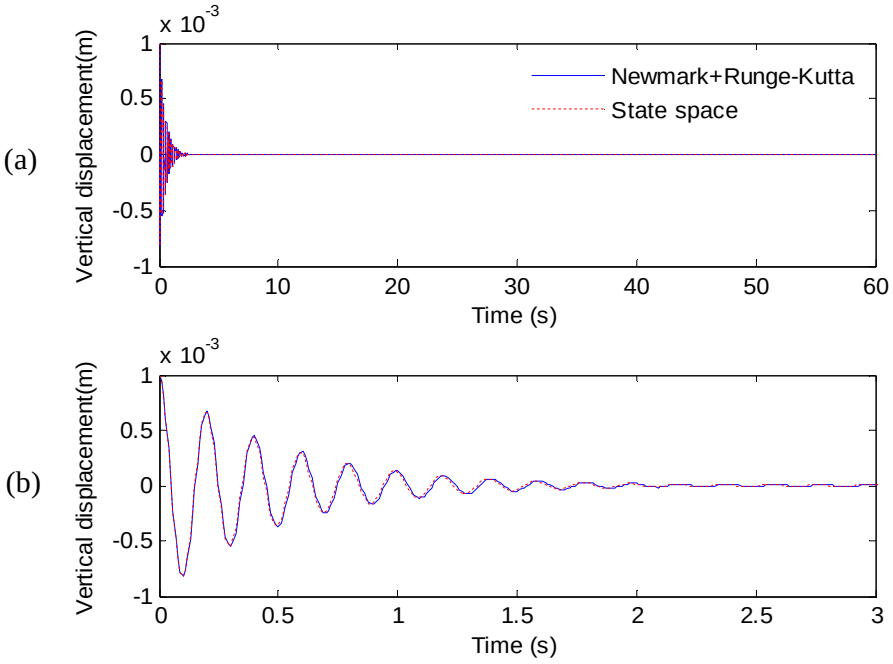

Figure 5.3: Vertical displacement responses (a) Time window for 60 s (b) Time window for 3 s

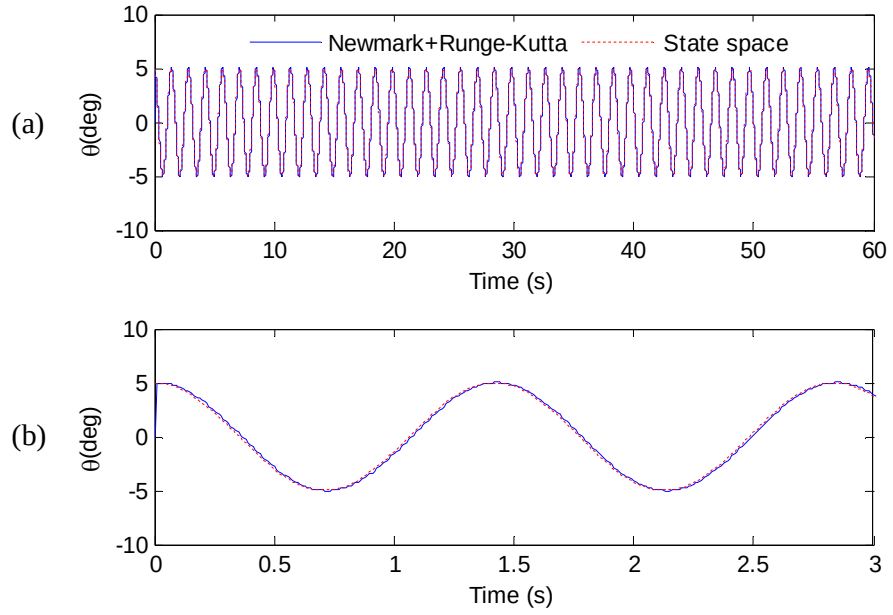

Figure 5.4: Angular displacement responses (a) Time window for 60 s (b) Time window for 3 s

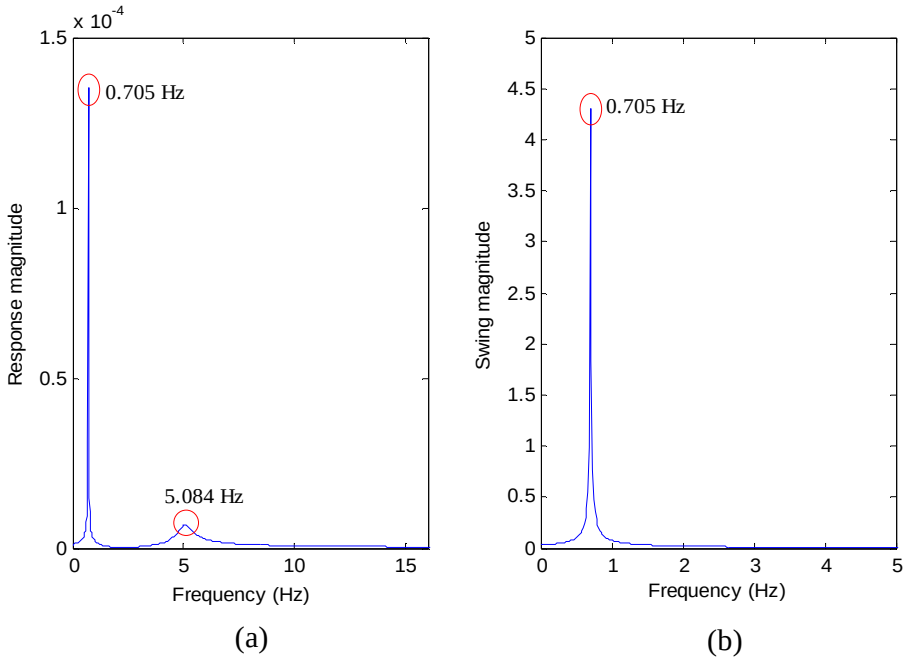

Figure 5.5: FFT analyses for linear model (a) Vertical response (b) Angular response

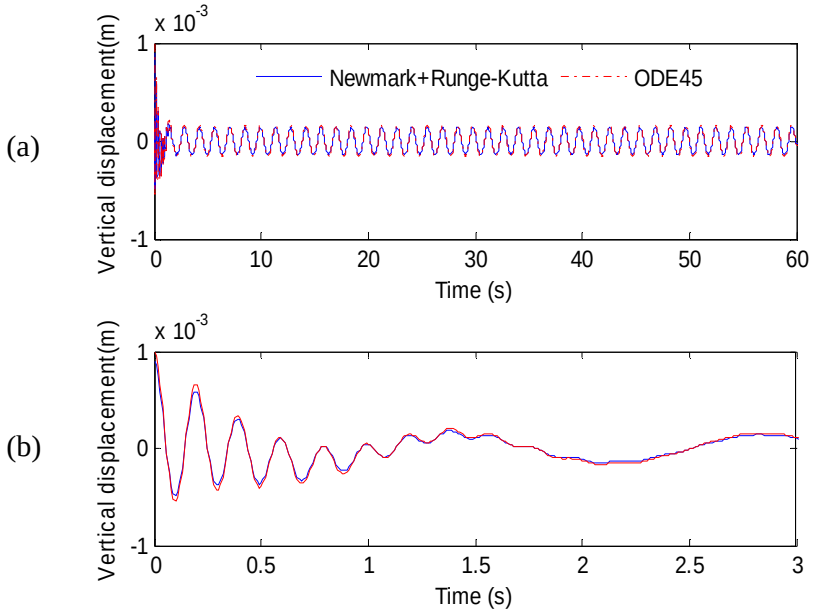

Figure 5.6: Vertical displacement responses with nonlinear model (a) Time window for 60 s (b) Time window for 3 s

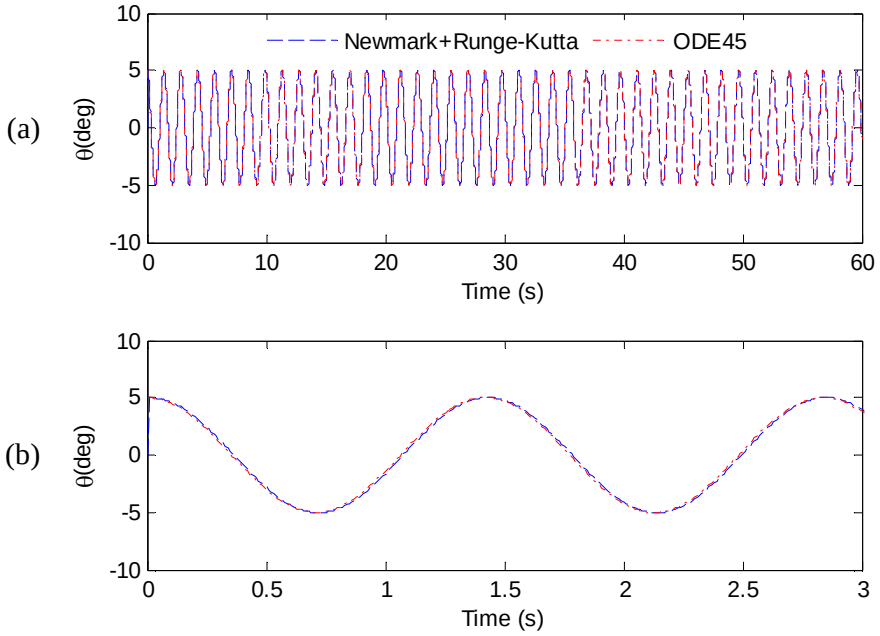

Figure 5.7: Angular displacement responses with nonlinear model
(a) Time window for 60 s (b) Time window for 3 s

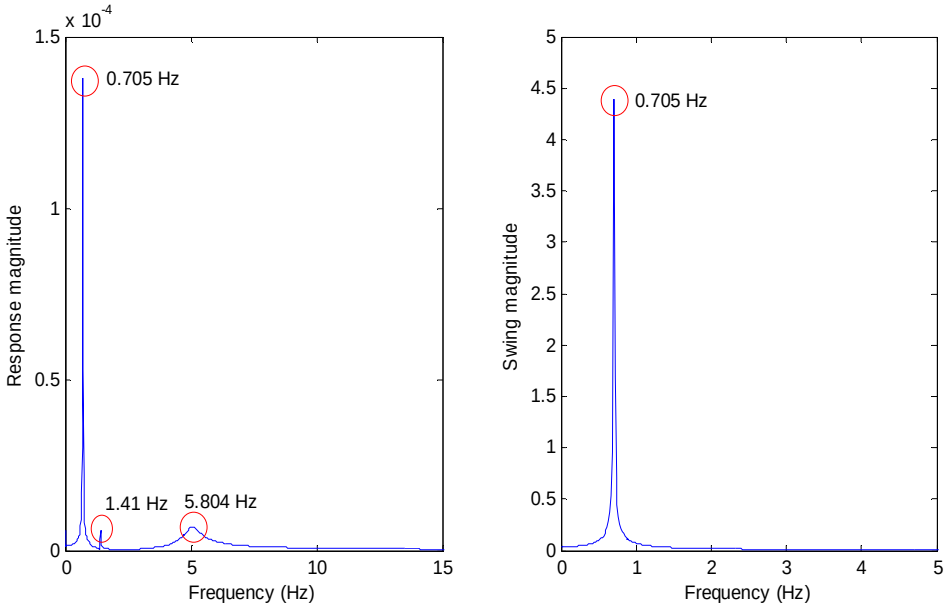

(a) (b)

Figure 5.8: FFT analysis for nonlinear model
(a) Vertical response (b) Angular response

Furthermore, both displacements from nonlinear model are also in good agreement as shown in Figures 5.6 and 5.7. Frequency contents of vertical response in Figures 5.5 and 5.8 are estimated using FFT analysis. There are two peak points at the FFT result in Figure 5.5, namely 0.705 Hz and 5.804 Hz. The first peak frequency, 0.705 Hz is the natural frequency of the pendulum given by $f_p = \frac{1}{2\pi}\sqrt{\frac{g}{\ell_{MSD}}} \left(\approx 0.705\, Hz\right)$. The second peak frequency, 5.804 Hz given by $f_{MSD} = \frac{1}{2\pi}\sqrt{\frac{K}{(M+m)}} \left(\approx 5.804\, Hz\right)$ corresponds to the natural frequency of MSD system. Interesting features are found in Figure 5.8, where it shows the appearance of second harmonic of the natural frequency of the pendulum due to nonlinear model of the coupled MSD system with the pendulum motion. This phenomenon is also found by Ju *et al*. [18].

5.3.2 Pendulum Attached to a MSD under the Action of Driving Force

Similar with Subsection 5.3.1, the system is excited by sinusoidal input force shown in Figure 5.9. This simulation is conducted with parameters listed in Tables 5.2, except initial vertical displacement is $y_0 = 0$. It is noted that the nonlinear model is used in this sub-section. The displacements are shown in Figures 5.10-5.11, and good agreement between the two numerical methods is found. It is proved that the developed computer programs are reliable and can tackle coupled dynamic model such as MSD-pendulum system. It can be used for further study in solving coupled dynamic system in this thesis.

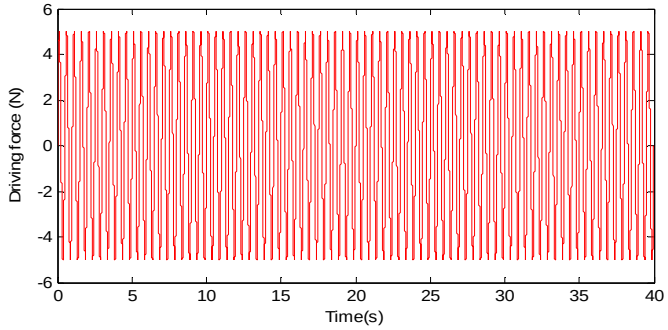

Figure 5.9: Driving force for pendulum attached to a MSD system

(a)

(b)

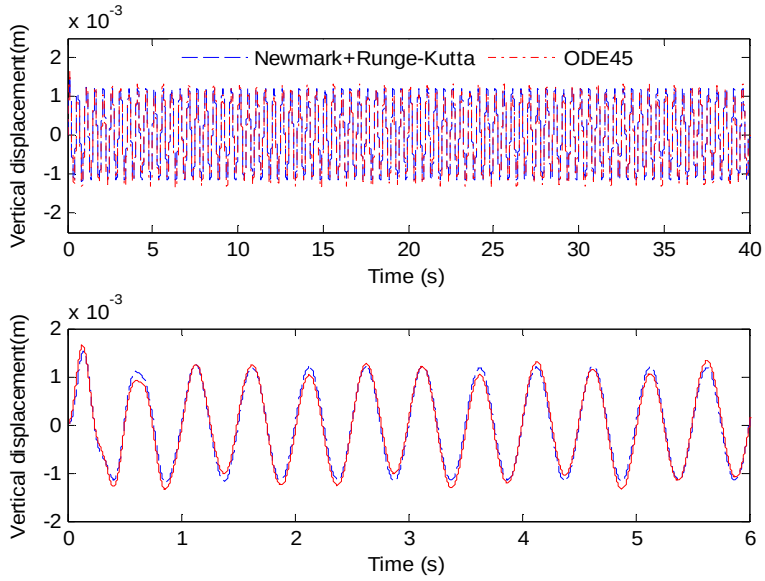

Figure 5.10: Vertical displacement responses
(a) Time window for 40 s (b) Time window for 6 s

(a)

(b)

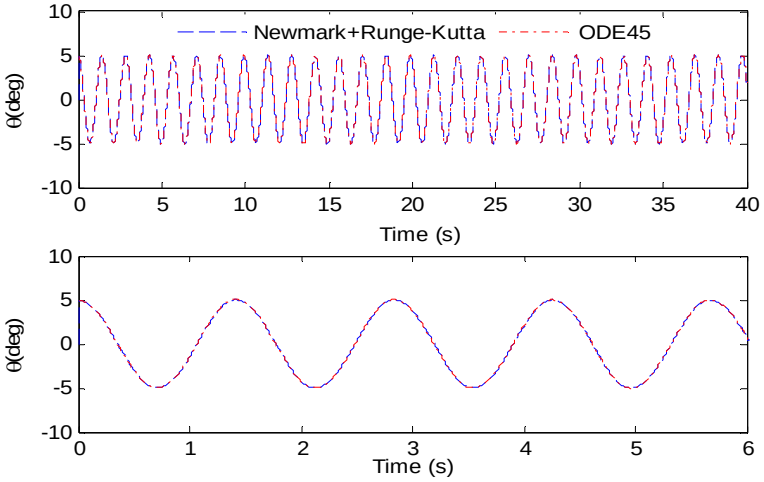

Figure 5.11: Angular displacement responses
(a) Time window for 40 s (b) Time window for 6 s

5.4 Gantry Crane System under Swinging Payload with Stationary Trolley (Case I)

In this subsection, dynamic response of gantry crane system subjected to swinging motion of payload is studied. The payload experiences planar and space swinging motion simultaneously as shown in Figure 5.12. As a benchmark, rigid model of

gantry crane is used. Rigid model means that the members of crane framework and hoist cable are rigid and equivalent with classical pendulum with static pivot point.

The equations of motion of rigid model are based on Equations (46a)-(46b). It is noted that that there is no damping either in dynamics of crane framework or payload, unless particularly stated. This is expected to avoid the effect of structural damping in dynamics of payload and make it as a direct comparison with the pendulum model.

5.4.1 Swinging Payload with Stationary Trolley under Three Kinds of Flexibility

In this subsection, swinging payload with stationary trolley on flexible gantry crane system is investigated using Equations (45a)-(45d). The parameters for gantry cranes are shown in Table 5.3, while the properties of crane framework are shown in Table 5.4. Crane framework is discretized into 58 elements and 82 nodes as shown in Figure 5.12.

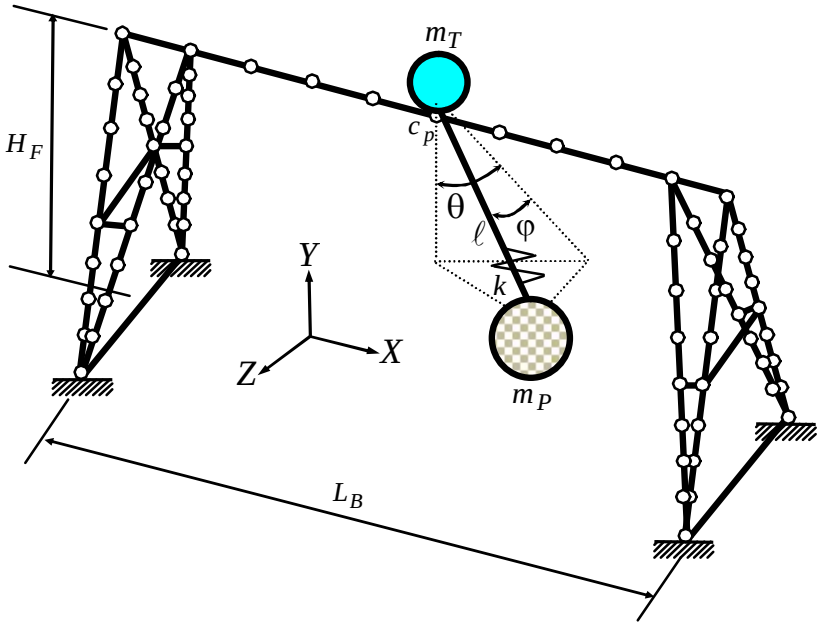

Figure 5.12: Finite element model of flexible gantry crane system under case I

Table 5.3: Gantry crane parameters

Parameters	
Trolley mass, m_T	50 kg
Payload mass, m_p	1200 kg
Cable length, ℓ_P	1 m
Cable stiffness, k	$2.5 \cdot 10^5\ N/m$
Initial swing angle, $\theta_o, \dot{\theta}_0, \ddot{\theta}_0$	5^o,0,0
Initial swing angle, $\varphi_o, \dot{\varphi}_o, \ddot{\varphi}_o$	5^o,0,0
Initial hoist cable displacement, $\delta_o, \dot{\delta}_o, \ddot{\delta}_o$	*static*,0,0

Table 5.4: Crane framework properties

Properties		
	Top beam Support (Right and Left)	Top beam
Material	Steel	
Young's modulus, E	2.10e11 kg/m^2	
Density, ρ	7860 kg/m^3	
Cross-section area, A	3.45e-02 m^2	1.516e-02 m^2
Inertia, I_{xx}	3.139e-03 m^4	8.741e-04 m^4
I_{yy}	2.7e-03 m^4	1.76e-05 m^4
Span of framework, L_B	12 m	
Height of framework, H_F	10.6 m	

The dynamic responses of payload swing angles with the rigid and flexible gantry crane for time duration 20 s are illustrated in Figures 5.13 – 5.14. Flexible gantry crane covers flexibility in hoist cable, members of crane framework and hoist cable-crane framework. The rigid and flexible model deviation are $\Delta\theta$ and $\Delta\varphi$ where $\Delta\theta = \theta_{flexible} - \theta_{rigid}$, $\Delta\varphi = \varphi_{flexible} - \varphi_{rigid}$, respectively. By observing Figures 5.13 – 5.14, it can be seen that all the flexible models have longer periods or lower frequencies than the rigid model. The deviation between the rigid assumption and the flexible model results is clearly observed.

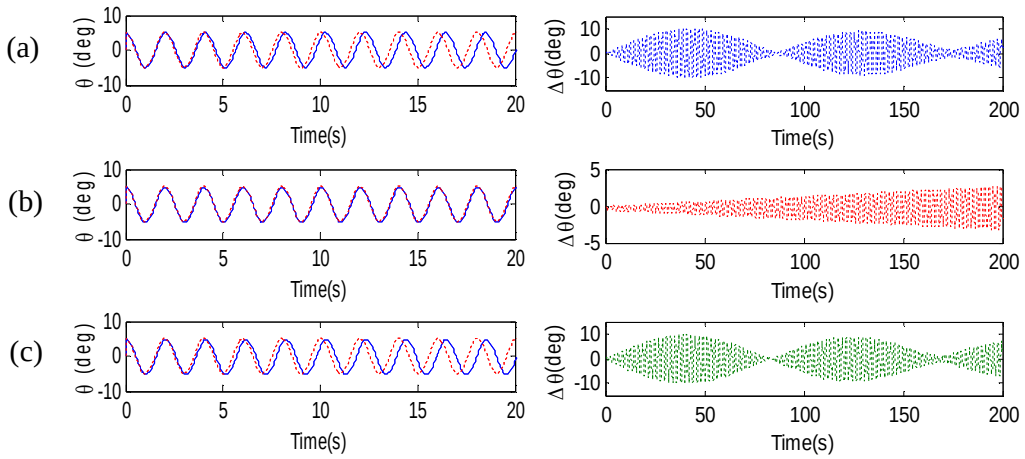

Figure 5.13: Time history of θ and Δθ (—) flexible model; (- - -) rigid model; (-.-.-) Δθ (a) Flexible hoist cable (b) Flexible crane framework (c) Flexible hoist cable-crane framework

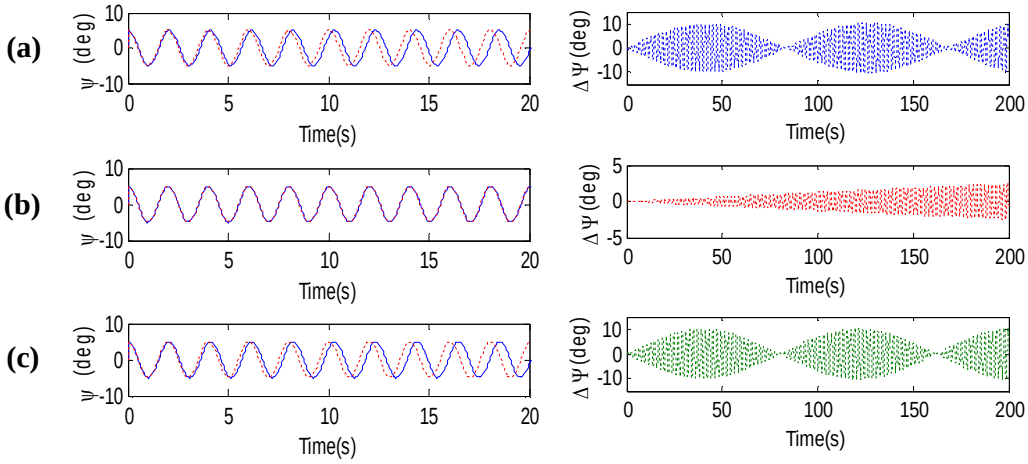

Figure 5.14: Time history of φ and Δφ (—) flexible model; (- - -) rigid model; (-.-.-) Δφ (a) Flexible hoist cable (b) Flexible crane framework (c) Flexible hoist cable -crane framework

Table 5.5: FFT results for three kinds of flexibility

Flexibility	Dominant frequency of rigid model (Hz)		Dominant frequency of flexible model (Hz)	
	θ	φ	θ	φ
Cable hoist	0.4985	0.4985	0.49	0.49
Crane framework	0.4985	0.4985	0.495	0.495
Hoist cable -crane framework	0.4985	0.4985	0.485	0.485

The FFT results as shown in Table 5.5 reveal that swing angles frequency with flexible model is lower than that of the rigid model. This is expected since the rigid model of crane is stiffer than the flexible crane, that is why the stiffer model vibrates at a higher frequency. It is noted that the natural frequency for both swing angles of rigid model are consistent with the frequency obtained from Equations (46a) and (46b).

The finding results in Figures 5.13-4.14 and Table 5.5 show that the gantry crane system with flexible hoist cable-crane framework produces greater amplitudes in frequency θ,φ which is confirmed by the time histories of $\Delta\theta,\Delta\varphi$. It has the lowest swing angles frequency compared to the gantry crane system with flexible hoist cable or crane framework only with respect to rigid model. It will be used for further investigation hereafter.

The dynamic responses of crane framework with flexible hoist cable-crane framework and hoist cable for time window 20 s are presented in Figure 5.15. Static displacements, denoted by dashed line (----) show that the value of static displacements in axial (X) and lateral (Z) are very small compared to vertical (Y) displacement. That is because the crane framework is imposed by static load $(m_T + m_P)$ at the central point c_p of the top beam of crane framework in vertical direction and the crane framework is weaker at that direction.

This result is also found in tower crane as reported by Ju *et al.* [18]. When the crane framework is subjected to swinging motion of payload at the central point c_p of the top beam, the dynamic displacements in axial (X) and lateral (Z) are significantly affected. The maximum amplitude of dynamic displacements over their corresponding static displacements becomes very large.

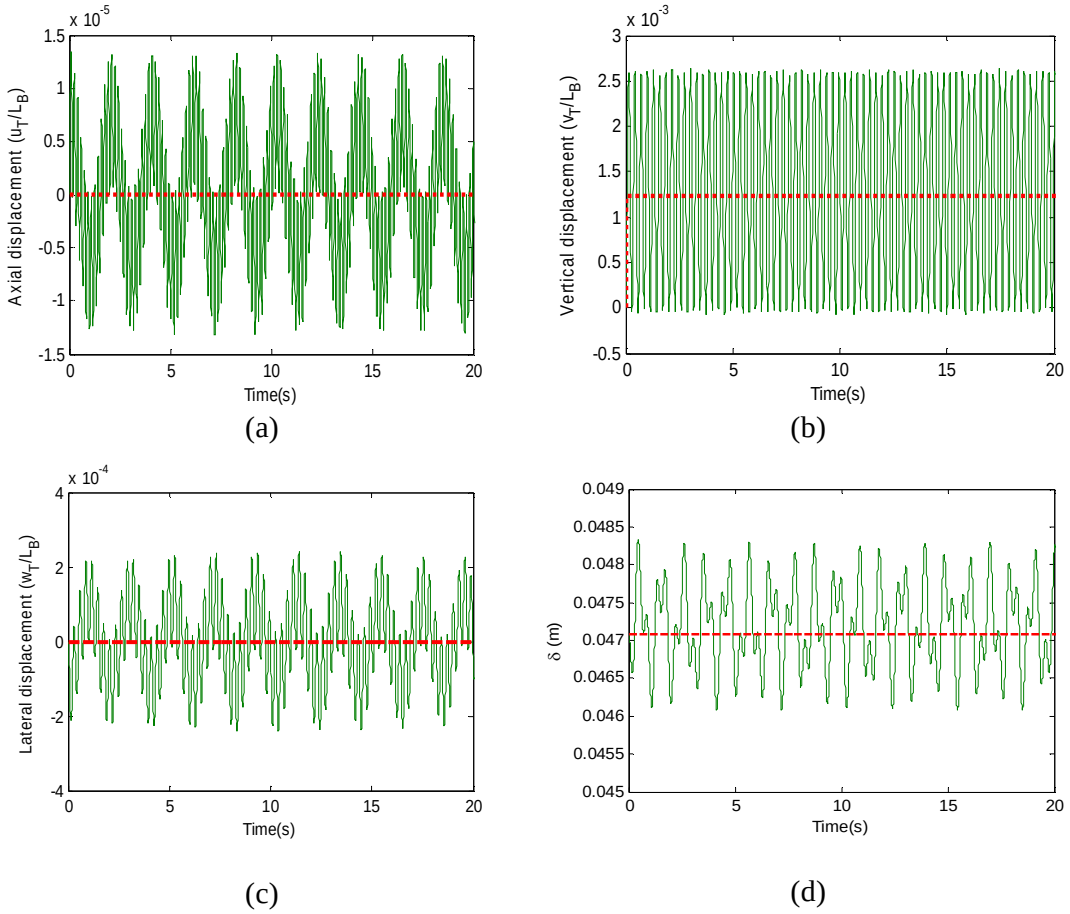

Figure 5.15: Crane framework and hoist cable response (—) corresponding dynamic displacements; (- - -) corresponding static displacements (a) axial (b) vertical (c) lateral (d) hoist cable

It is noted that all the responses are normalized displacements of crane framework and hoist cable to the span length of top beam and cable length of payload. By using FFT analysis, the frequency content of crane framework response can be estimated and depicted in Figure 5.16.

There are four peak points at the power density spectrum of vertical response, which are located, respectively at 0.49 Hz, 0.99 Hz, 2.29 Hz and 6.78 Hz. Those four frequencies can be explained as follows. The first peak frequency, 0.49 Hz is the natural frequency of the payload given by $f_p = \frac{1}{2\pi}\sqrt{\frac{g}{\ell_P}} \left(\approx 0.49\ Hz\right)$. The second peak point, 0.99 Hz is appearance of second harmonic of the natural frequency of the payload. This phenomenon is also reported by Ju *et al.* [18]. The third peak point,

2.29 Hz is given by $f_{cable} = 1/2\pi\sqrt{k/(m_T + m_P)} (\approx 2.29\ Hz)$ corresponds to the natural frequency of hoist cable. The last frequency is the third natural frequency of crane framework as shown by Figure 5.1(c). By knowing the frequency content of crane framework response, it can be found out that the dynamic response of crane framework is dominated by the third mode shape which is vertical deformation of the top beam of crane framework.

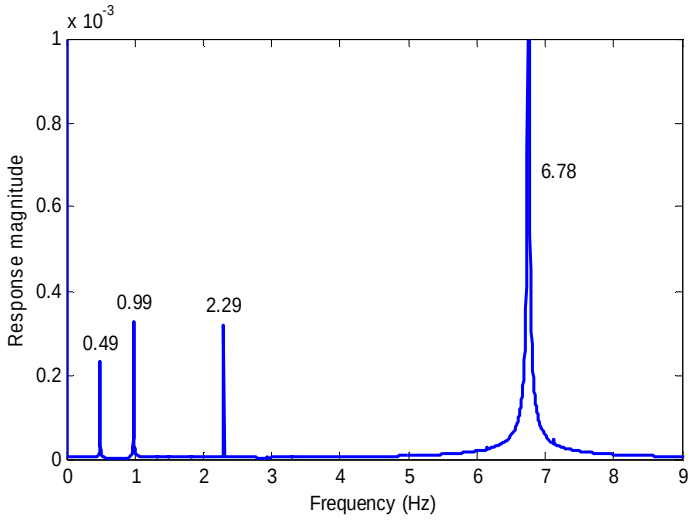

Figure 5.16: FFT analyses of vertical displacement of crane framework under case I

Further, Figures 5.13c and 5.14c show a beating phenomenon either in the time histories of $\Delta\theta$ or $\Delta\varphi$. The beating phenomenon that appears in $\Delta\theta$ and $\Delta\varphi$ plots because of the superimposed plot of the rigid and flexible response, which can be explained by sampling the time history of θ during $86\,s$, approximately 43 cycles as shown by Figure 5.17. The figure depicts that $\theta_{flexible}$ and θ_{rigid} produces a phase shift after a half cycle as shown in Figure 5.18a. This phase shift accumulates over the cycles and maximum into approximately cycle 20 or $35 \le t \le 45\,s$ as presented by Figure 5.18b.

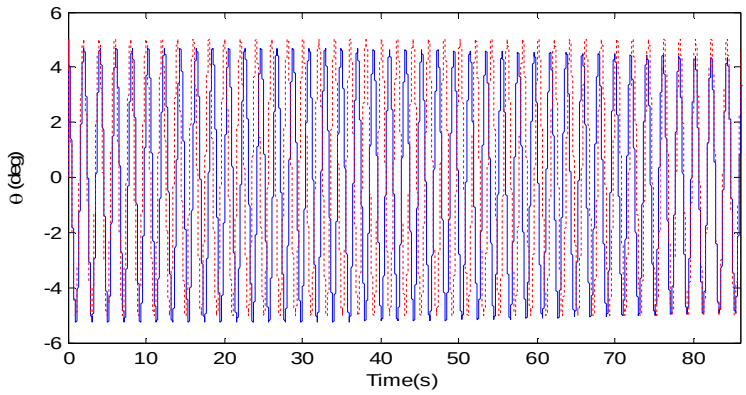

Figure 5.17: Payload swing response of θ for time window 86 s
(—) flexible model, (….) rigid model

In the subsequent cycles, the accumulated phase shift decreases until approaching cycle 42 or $80 \le t \le 86\,s$ as shown in Figure 5.18c. This behavior will repeat until prescribed time duration and so do the time history of φ. The phase shift must be caused by contribution of flexibility of the crane framework and hoist cable as shown in Equations (45a) - (45c). From those equations, it may be seen that θ couples to $\ddot{u}_T$ and $\ddot{v}_T$, φ couples with $\ddot{u}_T, \ddot{v}_T$, $\ddot{w}_T$ while flexibility of hoist cable in term of δ are existed in both swing angles.

The flexibility of crane framework in terms $\ddot{u}_T, \ddot{v}_T, \ddot{w}_T$ provides acceleration in three directions to the pivot point of payload. This condition creates bidirectional dynamic interaction between dynamics of crane framework and pendulum-like swinging motion of payload if large swing angles are allowed as also found out by [6].

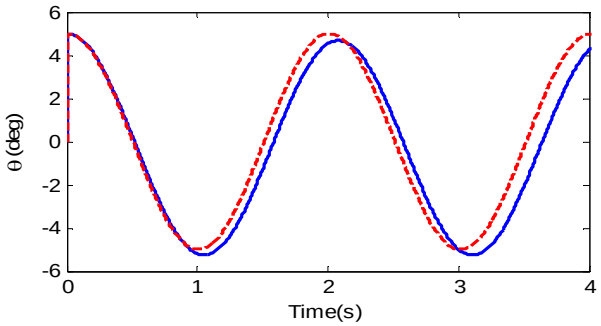

(a)

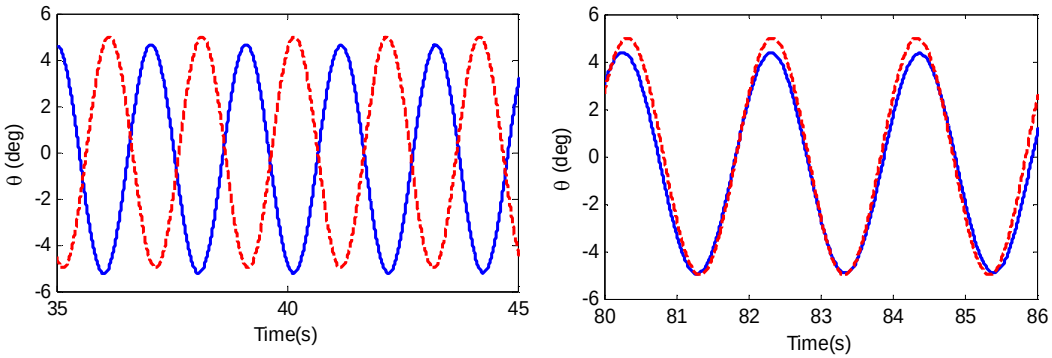

Figure 5.18: Rigid and flexible model responses of θ
(a) Time window $0 \le t \le 4\ s$ (b) $35 \le t \le 45\ s$ (c) $80 \le t \le 86\ s$

Phase portrait of $\theta_{flexible}$ and θ_{rigid} for one cycle is presented. After one cycle has been completed, the free end of $\theta_{flexible}$ noted by $A^{'}$ in phase portrait of Figure 5.19 does not return to its original location, which is contrary with free end of θ_{rigid}, noted by $B^{'}$. From those figures, it can be seen that the flexibilities significantly affects the swinging motion of payload. The effects in terms of $\ddot{u}_T, \ddot{v}_T, \ddot{w}_T$ and $\delta, \dot{\delta}, \ddot{\delta}$ create difference in amplitude, frequency and phase between rigid and flexible model along the periodicity of θ and φ. It may be observed also that magnitude of swing angle for crane with flexible model is smaller than the rigid one, which is similar with work in Reference [8].

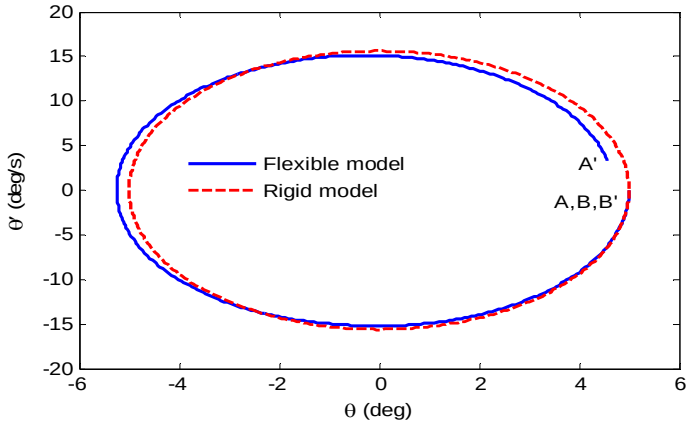

Figure 5.19: Phase portrait of rigid and flexible model of θ for one cycle

5.4.2 Effect of Structural Damping

For the present subsection, the simulation is conducted with parameters listed Table 5.3 and 5.4. The damping ratios are taken to be $\xi_1 = \xi_2 = 0.000, 0.001, 0.003 \text{and} 0.005$. The time histories of swing angles θ and φ, including with their corresponding $\Delta\theta$ and $\Delta\varphi$ are demonstrated in Figures 5.20 and 5.21. It is observed that the frequencies of payload swing angles are lower for the flexible gantry crane system compared to the rigid model. These differences will decrease with the increase of structural damping as shown by $\Delta\theta$ and $\Delta\varphi$. Compared to significant change in frequency, minimal change in amplitudes is observed in both payload swing angles. It may be explained by considering Figure 5.22 that the structural damping has the effect of reducing the axial, vertical and lateral displacements of crane framework. The increase in structural dynamic displacements offers lower flexibility in the pivot point of payload.

The increase in structural dynamic displacements offers higher flexibility in the pivot point of payload. That is because the vibration of crane framework is contributed into the dynamics of payload at the contact point between trolley and the top beam of crane framework as it can be seen from Equations (45a)-(45c). Figure 5.22 shows the elastic displacements of the central point c_p of the top beam and hoist cable under structural damping variation, respectively.

It can be seen from those figures that the structural damping significantly influences the dynamic responses of crane framework, especially for vertical (Y) responses. At the beginning of time duration, the vibration amplitude is higher, and then they vibrate as sinusoidal curve with a spatial decay about its corresponding static displacement until the end of process. Due to structural damping, the vibration converges slower and slower as time goes on. However, it will take long time to converge into its static displacement due to weakly damped [7]. Further, structural damping has no discernable effect for the hoist cable response as shown by Figure 5.19d.

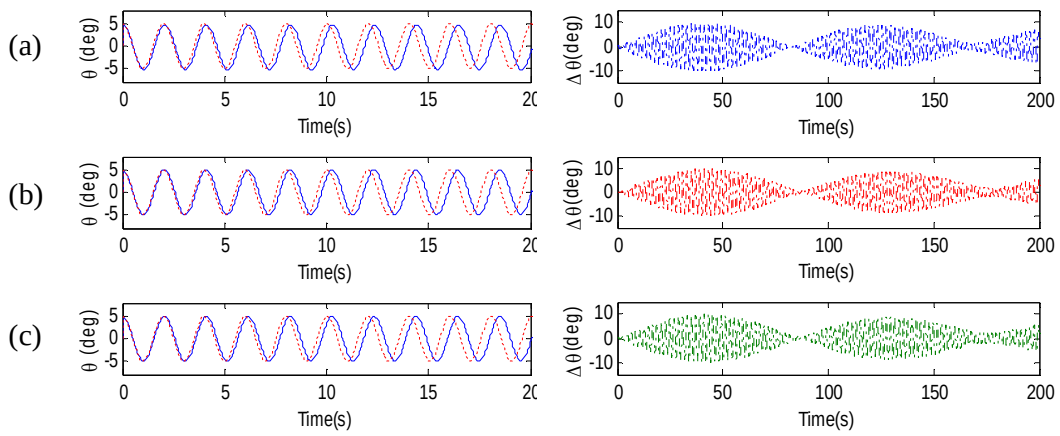

Figure 5.20: Time history of θ and $\Delta\theta$ under case I: (—) flexible model; (- - -) rigid model; (-.-.-) $\Delta\theta$ (a) $\xi_1 = \xi_2 = 0.000$ (b) $\xi_1 = \xi_2 = 0.001$ (c) $\xi_1 = \xi_2 = 0.005$

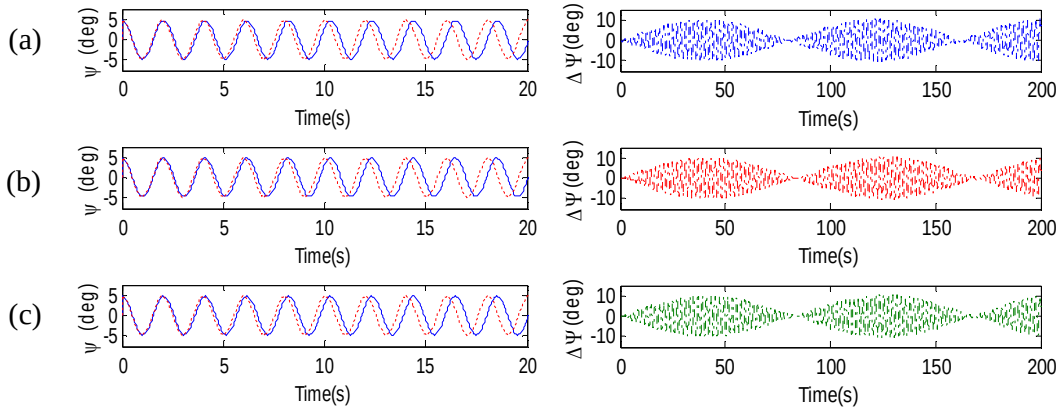

Figure 5.21: Time history of φ and $\Delta\varphi$ under case I: (—) flexible model; (- - -) rigid model; (-.-.-) $\Delta\varphi$ (a) $\xi_1 = \xi_2 = 0.000$ (b) $\xi_1 = \xi_2 = 0.001$ (c) $\xi_1 = \xi_2 = 0.005$

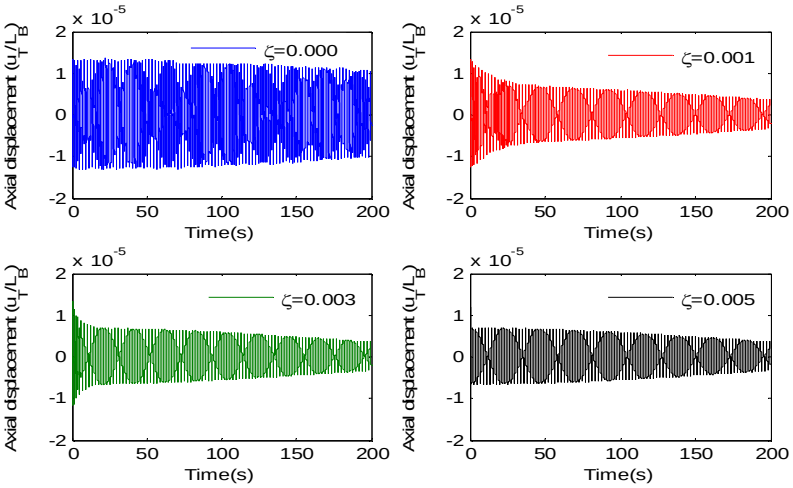
x 10^-5
Axial displacement (u/L_B)
ζ=0.000
ζ=0.001
ζ=0.003
ζ=0.005
Time(s)

(a)

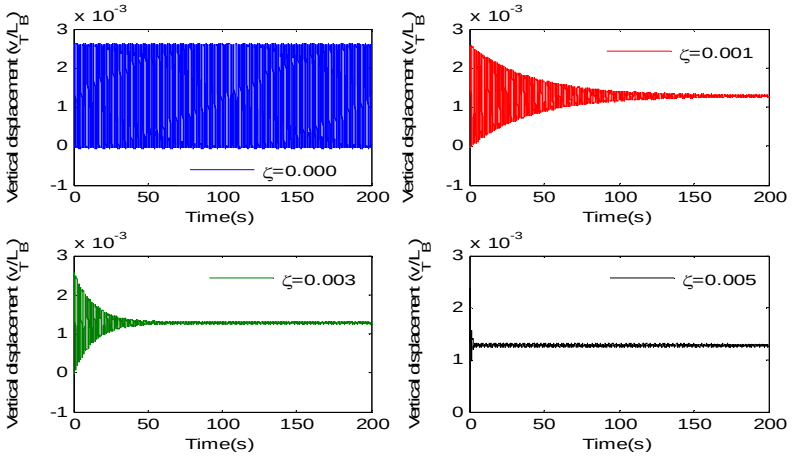
x 10^-3
Vertical displacement (v/L_B)
ζ=0.000
ζ=0.001
ζ=0.003
ζ=0.005
Time(s)

(b)

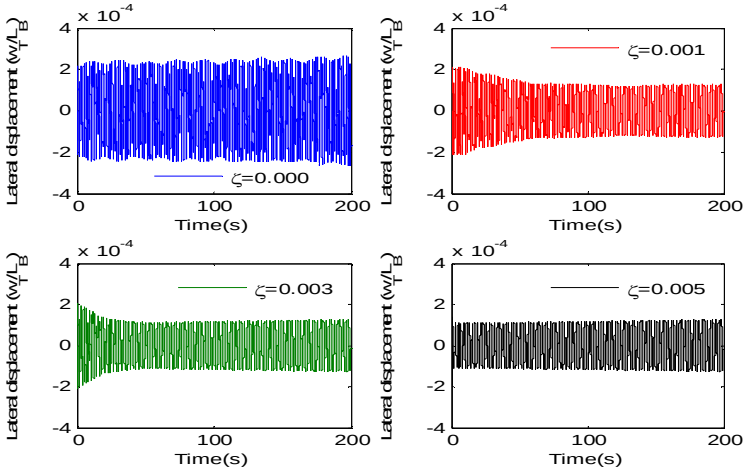
x 10^-4
Lateral displacement (w/L_B)
ζ=0.000
ζ=0.001
ζ=0.003
ζ=0.005
Time(s)

(c)

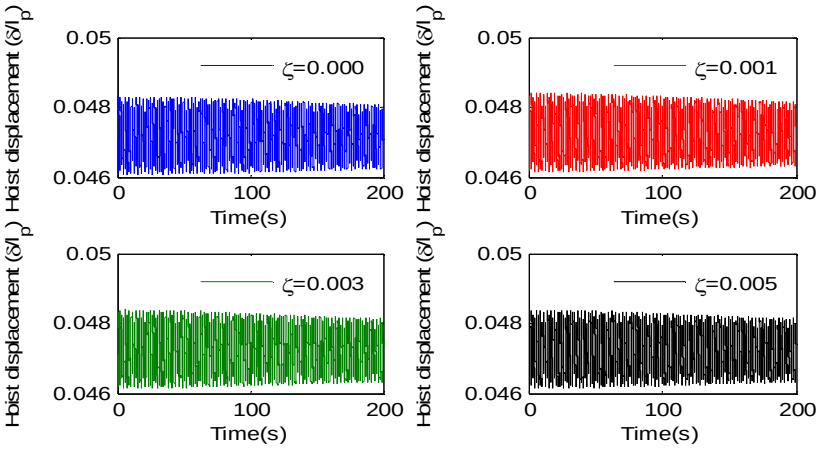

(d)

Figure 5.22: Damping effect on crane framework and hoist cable responses (a) axial (b) lateral (c) vertical (d) hoist cable displacements

5.4.3 Effect of Initial Payload Swing Angle

In this subsection, initial swing angle θ_0 is varied while $\varphi_0 = 5^o$ is fixed to see its effect on the dynamics of payload and crane framework. It is found in Figures 5.23-5.24 that the increase of initial payload swing angle significantly affects the swing amplitude and frequency of payload. The increase of initial swing angle θ_0 causes the amplitudes of θ increase, as confirmed by time histories of $\Delta\theta$. However, change in amplitude is dominant compared to change in frequency for both swing angles.

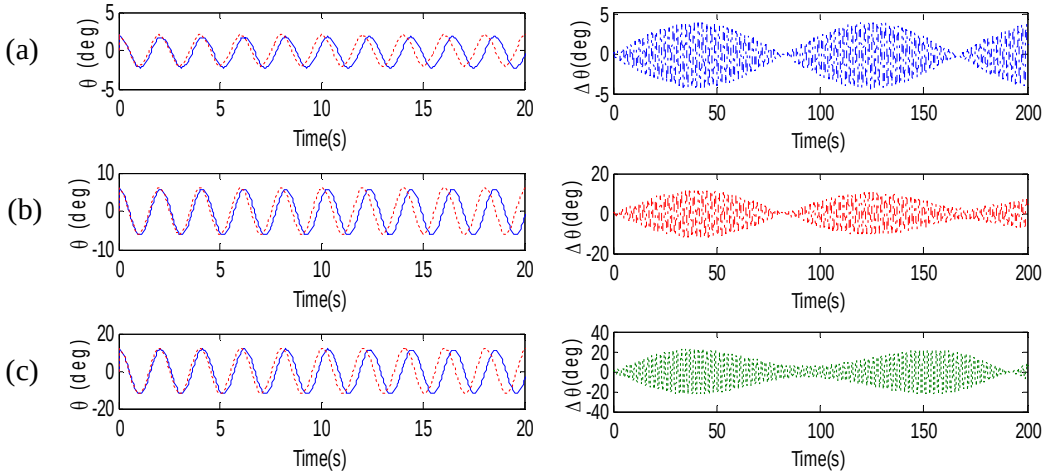

Figure 5.23: Time history of θ and $\Delta\theta$ under case I: (—) flexible model; (- - -) rigid model; (-.-.-) $\Delta\theta$ (a) $\theta_0 = 2^o$ (b) $\theta_0 = 6^o$ (c) $\theta_0 = 12^o$

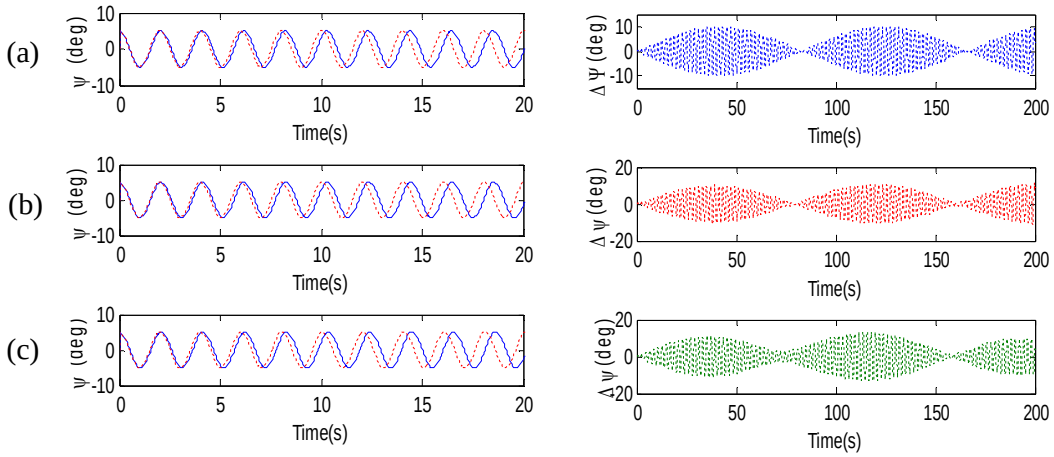

Figure 5.24: Time history of φ and $\Delta\varphi$ under case I: (—) flexible model; (- - -) rigid model; (-.-.-) $\Delta\varphi$ (a) $\theta_0 = 2^o$ (b) $\theta_0 = 6^o$ (c) $\theta_0 = 12^o$

Figure 5.24 also depicts that the responses of $\varphi_{flexible}$ noted by solid line (—) have discernable difference with φ_{rigid} which is noted by dashed line (- - -). It can be found out that the contribution of flexibility in crane framework and hoist cable into the dynamics of payload only changes the frequency of φ by fixing the value of $\varphi_0 = 5^o$. It should be noted that the variation of φ_0 while setting value of θ_0 to the fixed value generates the same trend as θ_0 is varied. It is quite representative to only display the effect of θ_0 variation in this thesis.

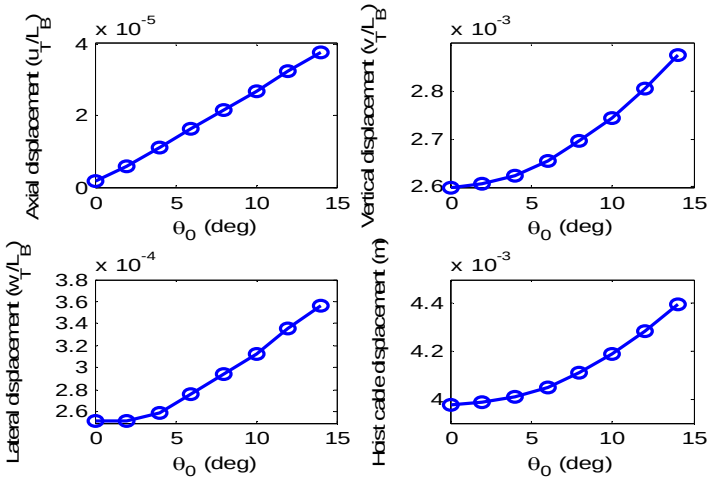

Figure 5.25: Maximum dynamic responses of crane framework under initial payload swing angle variation for case I

The maximum axial (X), vertical (Y) and lateral (Z) displacements of the central point c_p of the top beam of crane framework and hoist cable under θ_0 variation are depicted in Figure 5.25. It is observed that all the displacements increase with the increase of θ_0. This is to be expected since the larger swing angles magnitude, the larger exciting forces in the right side of Equation (45d). The increases are slightly nonlinear for vertical, lateral and hoist cable displacements, but slightly linear for axial displacement.

5.4.4 Effect of Payload Mass Variation for Case I

Except the payload mass, this simulation is conducted with parameters listed in Tables 5.3 and 5.4. By means of Equations (46a)-(46b), mass of payload has no effect on dynamics of payload. The condition will be different if the flexibility of crane framework and the hoist cable are introduced in Equations (45a)-(45c).

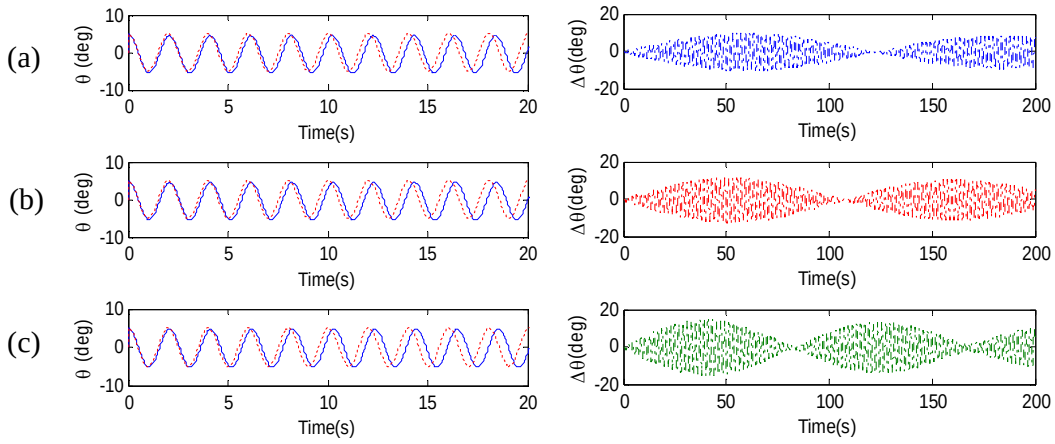

Figure 5.26: Time history of θ and $\Delta\theta$ under case I: (—) flexible model; (- - -) rigid model; (-.-.-) $\Delta\theta$ (a) $m_P = 700\ kg$ (b) $m_P = 900kg$ (c) $m_P = 1200\ kg$

The increase of payload mass has discernable effect on the payload swings, where the frequencies and amplitudes of the payload swing increase by the increasing of payload mass for both swing angles for time duration 20 s as shown in Figures 5.26-5.27. This is a reasonable result, since the displacements of crane framework and cable hoist depends on the magnitude of payload mass. The higher the payload mass, the higher the exciting force in the right side of Equation (45d), which in turn increasing the displacements.

The larger vibration amplitudes of crane framework offer higher flexibility to pivot point of the swinging payload. This is also confirmed by FFT results for θ and φ in Table 5.6, where the frequency associated with the larger masses is getting lower than the rigid model.

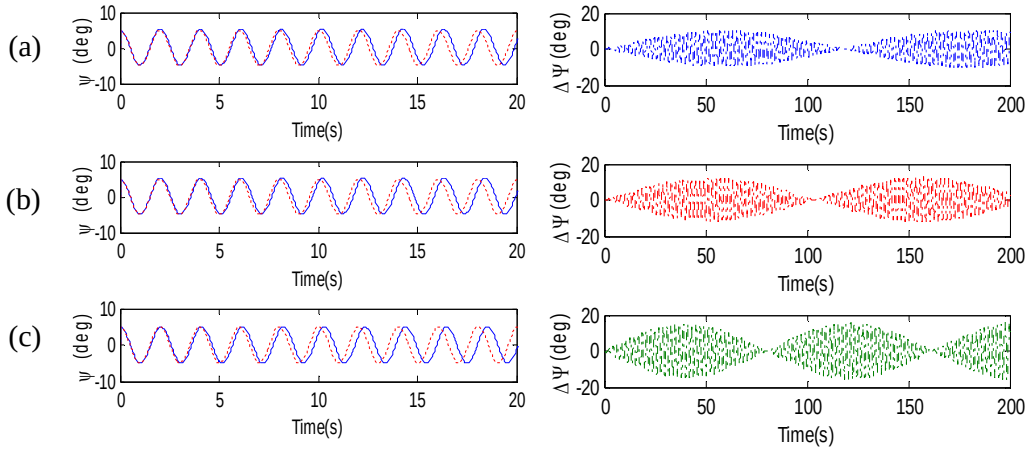

Figure 5.27: Time history of φ and Δφ under case I: (—) flexible model; (- - -) rigid model; (-.-.-) Δφ (a) $m_P = 700\ kg$ (b) $m_P = 900 kg$ (c) $m_P = 1200\ kg$

Table 5.6: FFT results under payload mass variation

Payload mass m_P (kg)	Dominant frequency of rigid model (Hz)		Dominant frequency of flexible model (Hz)	
	θ	φ	θ	φ
700	0.4985	0.4985	0.495	0.495
900	0.4985	0.4985	0.49	0.49
1200	0.4985	0.4985	0.485	0.485

The maximum axial (X), vertical (Y) and lateral (Z) displacements of the central point c_p of the top beam and cable hoist are depicted in Figure 5.28. It is seen that, all the displacements increase with the increase of m_P. The increases are slightly linear for axial, vertical, lateral and hoist cable displacements.

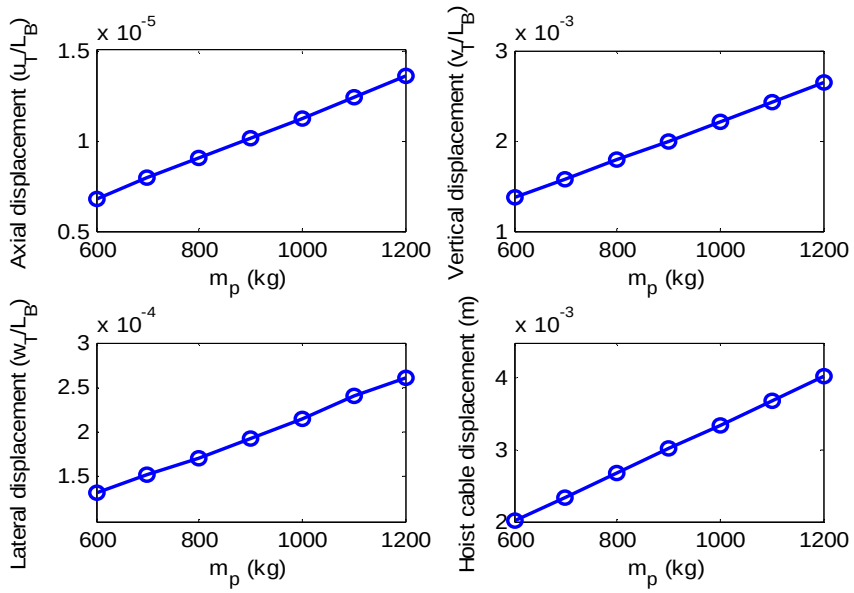

Figure 5.28: Maximum dynamic responses of crane framework under payload mass variation for case I

5.4.5 Effect of Cable Length Variation for Case I

Further, the cable length is varied in order to see its effect on the payload swing angles, hoist cable and crane framework. Except the cable length, other parameters are identical with Table 5.3 and 5.4.

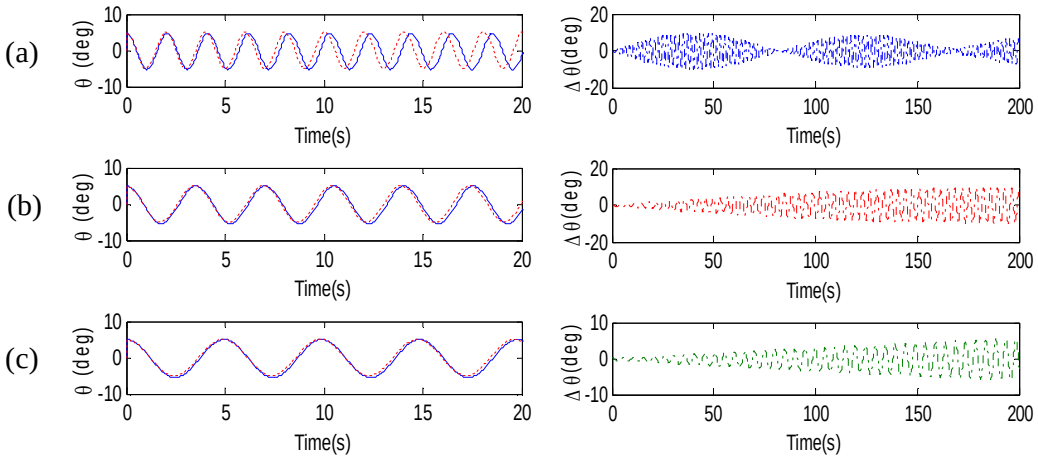

Figure 5.29: Time history of θ and $\Delta\theta$ under case I: (—) flexible model; (- - -) rigid model; (-.-.-) $\Delta\theta$ (a) $\ell_P = 1\,m$ (b) $\ell_P = 3m$ (c) $\ell_P = 6\,m$

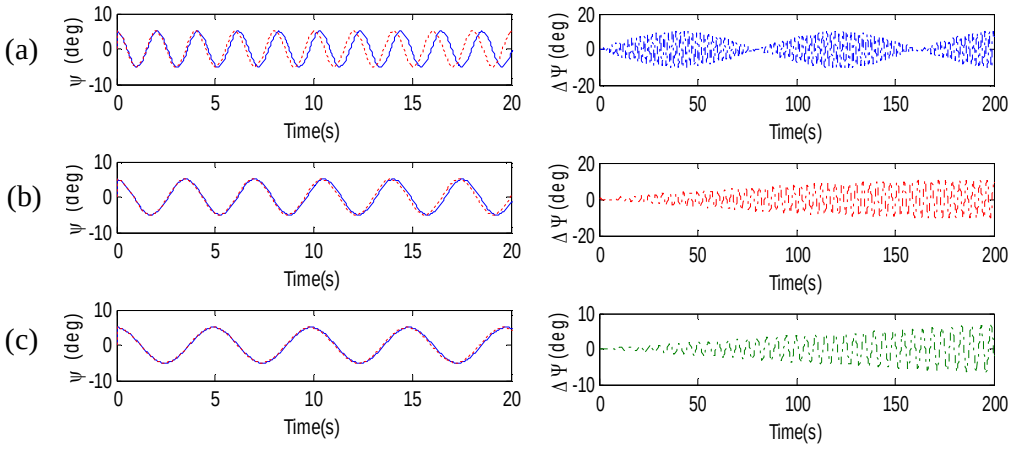

Figure 5.30: Time history of φ and $\Delta\varphi$ under case I: (—) flexible model; (- - -) rigid model; (-.-.-) $\Delta\varphi$ (a) $\ell_P = 1\,m$ (b) $\ell_P = 3\,m$ (c) $\ell_P = 6\,m$

Figures 5.29 - 5.30 depict that the amplitudes and frequencies of θ and φ are dependent on the cable length of payload. The time history results of $\Delta\theta$ and $\Delta\varphi$ show that the amplitudes and frequencies in the payload swing responses decrease with increasing length of payload cable. The corresponding dominant frequency contents of θ and φ to the cable length is displayed in Table 5.7 and confirm the results shown in Figures 5.29-5.30.

Table 5.7: FFT results under cable length variation

Cable length ℓ_P (m)	Dominant frequency of rigid model (Hz)		Dominant frequency of Flexible model (Hz)	
	θ	φ	θ	φ
1	0.4985	0.4985	0.485	0.485
3	0.287	0.287	0.285	0.285
6	0.2035	0.2035	0.202	0.202

The trend of the maximum axial (X), vertical (Y) and lateral (Z) displacements of the central point c_p of the top beam and hoist cable under cable length variation is different with payload mass variation as depicted in Figure 5.31. It may be seen that all the displacements decrease with the increase of ℓ_P. It can be explained by observing Figures 5.29 - 5.30, where the longer cable length will contributes smaller amplitudes of payload swing angles to the dynamics of crane framework.

This contribution, which in turn producing smaller exciting forces for the crane framework as it can be seen in the right side of Equation (55d). The result is also found by the author in Reference [12].

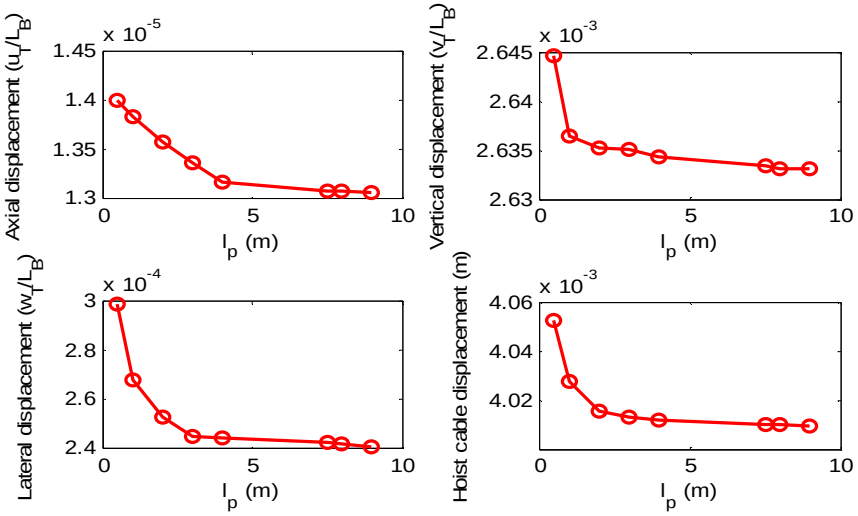

Figure 5.31: Maximum dynamic responses of crane framework under cable length variation for case I

5.4.6 Effect of Hoist Cable Stiffness for Case I

To find out the effect of cable stiffness on the responses of payload swings, crane framework and the hoist cable, the value of cable stiffness is varied, while other parameters are listed in Tables 5.3 and 5.4. Here, the cable stiffness is axial cable stiffness due to the cable is assumed to be in tension as explained in Section 4.4. Under the use of same material and hoist cable length, axial cable stiffness depends on cross-section area only. However, direct value of axial cable stiffness k is varied in this thesis. Another range of cable stiffness value may be selected, but the main purpose is to show the trend of dynamic response of payload and crane framework under cable stiffness variation.

Three cable stiffness values are only selected to be depicted in Figures 5.32-5.33, namely: $k_1 = 2.5 \cdot 10^4\ N/m$, $k_2 = 2.5 \cdot 10^5\ N/m$ and $k_3 = 2.5 \cdot 10^6\ N/m$. From those figures, the increase of cable stiffness tends to decrease the amplitude and frequency of θ and φ. The trend is confirmed with time histories of $\Delta\theta, \Delta\varphi$ and FFT analysis in Table 5.8. It is strongly presumed that if the cable stiffness is getting

larger, the responses of both swing angles θ and φ will approach the responses of flexible gantry crane system with flexible in crane framework only.

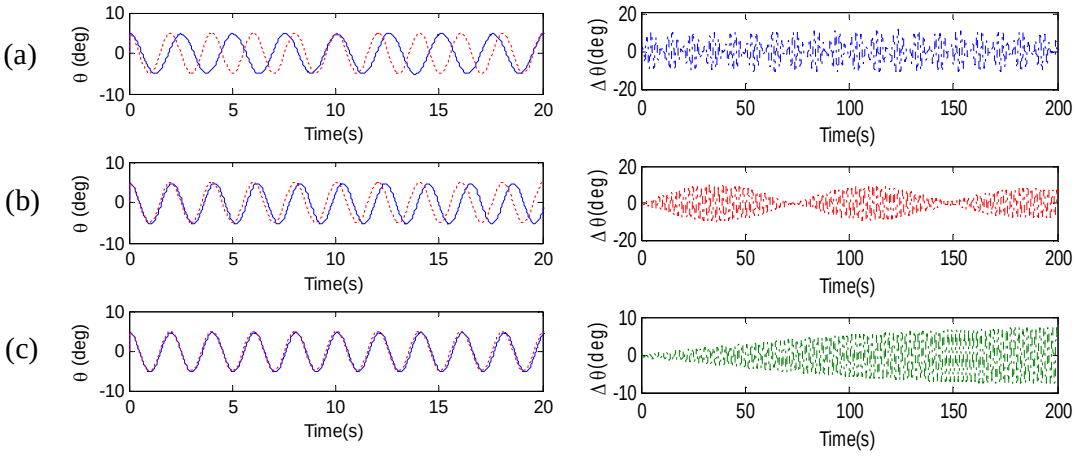

Figure 5.32: Time history of θ and $\Delta\theta$ under case I: (—) flexible model; (- - -) rigid model; (-.-.-) $\Delta\theta$ (a) k_1 (b) k_2 (c) k_3

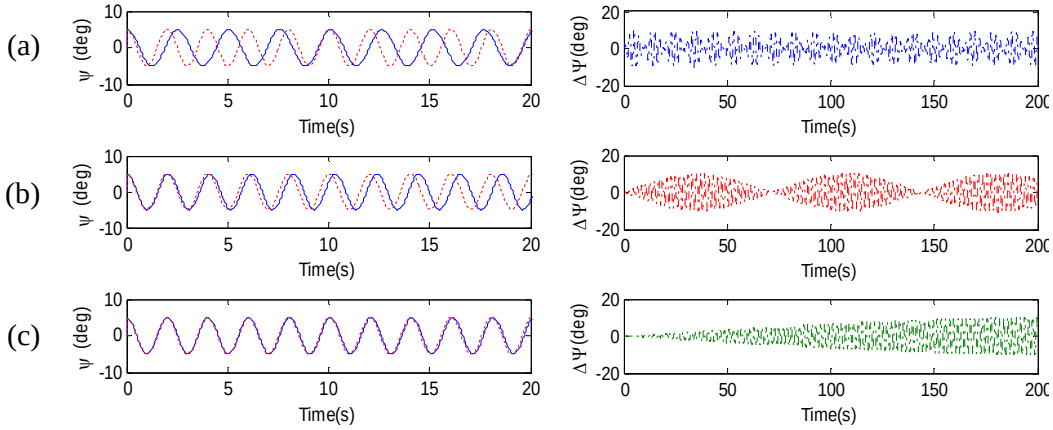

Figure 5.33: Time history of φ and $\Delta\varphi$ under case I: (—) flexible model; (- - -) rigid model; (-.-.-) $\Delta\varphi$ (a) k_1 (b) k_2 (c) k_3

Table 5.8: FFT results under cable stiffness variation

Cable stiffness k (N/m)	Dominant frequency of rigid model (Hz)		Dominant frequency of flexible model (Hz)	
	θ	φ	θ	φ
$2.5\cdot10^4$	0.4985	0.4985	0.445	0.445
$2.5\cdot10^5$	0.4985	0.4985	0.485	0.485
$2.5\cdot10^6$	0.4985	0.4985	0.495	0.495

The cable stiffness significantly affects the responses of crane framework and cable hoist as shown by Figure 5.34. The more rigid hoist cable, the smaller displacements of crane framework and hoist cable will be. This trend can be explained by considering the right side of Equation (45d) where the dynamics of hoist cable, $\delta,\dot{\delta},\ddot{\delta}$ influences the external force, the axial (X) force component f_{0x}, the lateral (Y) force component f_{0y} and (Z) force component f_{0z}. Since the lower cable stiffness produces the higher dynamic displacement of hoist cable, which in turn increasing the magnitude of exciting forces. This is the reason for the trend shown by Figure 5.34. This effect is contributed into the dynamics of payload, due to dynamics of gantry crane and crane framework is coupled system. This is also the reason for the trend shown by Figures 5.32-5.33.

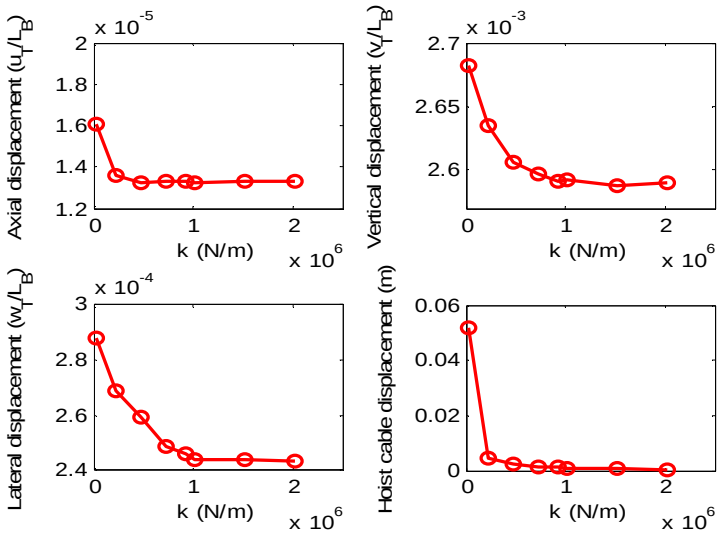

Figure 5.34: Maximum dynamic responses of crane framework under cable stiffness variation for case I

5.4.7 Effect of Crane Framework flexibility for Case I

Crane framework flexibility can be determined by cross-sectional area, material properties and geometric of crane framework i.e., height of crane framework/span of the top beam, H_F/L_B. Here, cross-sectional dimensions of crane framework's members are varied to investigate their effects on dynamics of payload and crane framework. Except for member's cross-sectional properties, other parameters are identical with Table 5.3 and 5.4.

The time histories of swing angles responses showed in Figures 5.35-5.36 use three cross-sections, namely cross-section 1, cross-section 2 and cross-section 3. As reference, cross-section 2 is taken from Table 5.4 meaning that all the properties of cross-section 2 are referred to Table 5.4. If the dimensions of cross-section 2 are reduced into 0.5 times or 50 % from original dimensions, then it is named as cross-section 1. Dimensions of cross-section 3 are increment about 3 time or 300 % from original dimensions of cross-section 2. It is clear that the increment or decrement of cross-sectional dimensions will change the cross-sectional properties, such as cross-sectional area (A), inertia (I_{xx}, I_{yy}, I_{zz}) of respective cross-section, respectively.

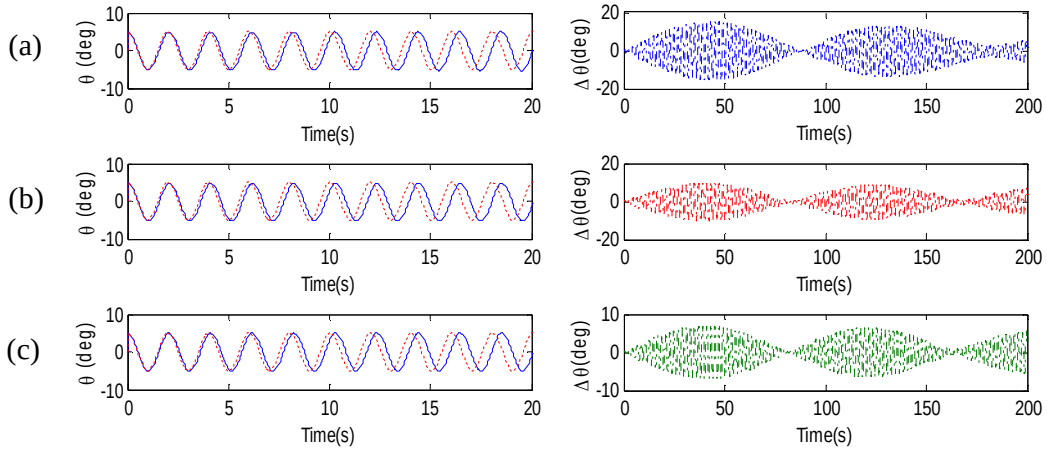

Figure 5.35: Time history of θ and $\Delta\theta$ under case I: (—) flexible model; (- - -) rigid model; (-.-.-) $\Delta\theta$ (a) cross-section1 (b) cross-section 2 (c) cross-section 3

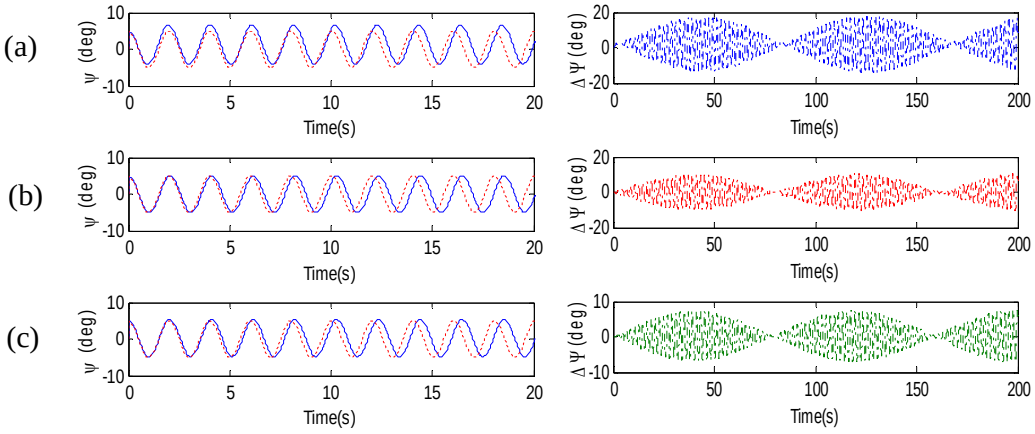

Figure 5.36: Time history of φ and $\Delta\varphi$ under case I: (—) flexible model; (- - -) rigid model; (-.-.-) $\Delta\varphi$ (a) cross-section 1 (b) cross-section 2 (c) cross-section 3

By changing the cross-sectional dimension of crane framework, it is evident that the amplitudes and frequencies of θ and φ are significantly affected as confirmed by time histories of $\Delta\theta$ and $\Delta\varphi$ and Table 5.9. The lowest cross-sectional properties among the three cross-sections exhibit more differences with the rigid model. Simulations strongly presume that the larger cross-sectional properties, the smaller differences, $\Delta\theta$ and $\Delta\varphi$ between flexible and rigid model. However, it certainly calls further study in structural optimization due to the size and geometric of overall crane framework must be considered with respect to load capacity of gantry crane.

This is to be expected since the increase of cross-sectional dimension of beam will reduce the flexibility of overall crane framework. It will be stiffness modulator in gantry crane dynamics. The results show that the flexibility of crane framework affects the dynamic responses of gantry crane.

Table 5.9: FFT results under crane framework flexibility

Cross-section	Dominant frequency of rigid model (Hz)		Dominant frequency of flexible model (Hz)	
	θ	φ	θ	φ
1	0.4985	0.4985	0.485	0.485
2	0.4985	0.4985	0.49	0.49
3	0.4985	0.4985	0.495	0.495

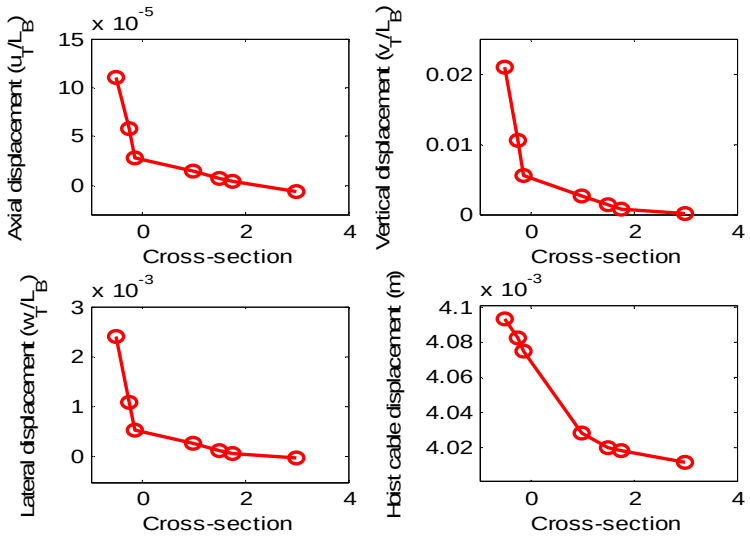

Figure 5.37: Maximum dynamic responses of crane framework under framework flexibility for case I

Similar with cable stiffness, the cross-sectional properties of structural's members of crane framework have significant effect on the responses of crane framework as shown by Figure 5.37. The increase of cross-sectional properties make the maximum dynamic displacements of crane framework will decrease. This trend is also followed by maximum dynamic displacement of the hoist cable. It is a reasonable result since the more rigid the crane framework, the more rigid the support of the hoist cable to vibrate due to swinging motion of payload.

5.5 Crane Framework under Moving Trolley with Stationary Payload (Case II)

In this subsection, structural dynamic analysis of the crane framework induced by moving load, either moving force or moving mass is studied. Besides that, beam and portal frame are studied as well. It is noted that the effects of payload swing, namely θ and φ are not considered as per Equations (47). Verification is conducted by generating some extended subroutine in ANSYS in order to get confidence about the correctness of developed computer programs for the moving load case.

5.5.1 Beam Structure

Undamped beam structure in Figure 5.38 comprises 21 nodes and 20 elements, with the length of each beam element being 0.05 m with cross-section $A = b \times h$ = 0.015 m $\times$ 0.015 m. The beam is excited to a load m = 10 kg moving from the left end to the right end of the beam with a constant speed V = 0.75 m/s.

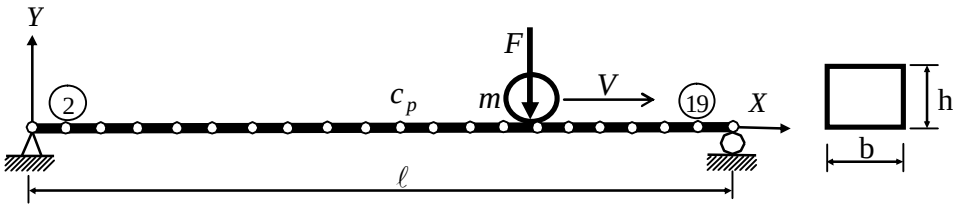

Figure 5.38: Simply supported beam induced by a moving mass and moving force

The time histories for vertical (Y) displacements of the central point c_P of the beam in node 11 under the moving load when inertial effects are considered and when inertial effects are ignored are shown in Figure 5.39.

The fluctuating features between moving mass and moving force are similar. The results obtained from present code under Matlab® agree well with the results obtained from ANSYS as shown in Figure 5.39.

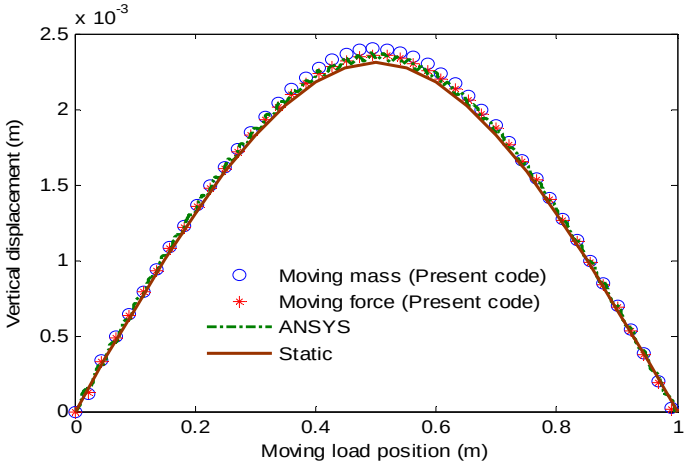

Figure 5.39: Displacements of node 11 of the beam due to moving load

5.5.2 Portal Frame

A portal frame is studied in this subsection. It is composed of 20 beam elements: 10 elements for the top beam, the left side-beam have 2 members with 10 identical elements and so do the right-side beam as depicted in Figure 5.40. The dimensions of and material properties of the portal frame are identical with Table 5.4.

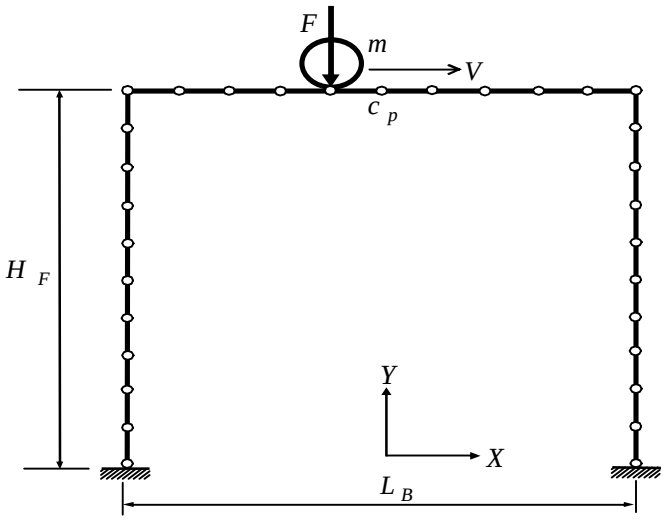

Figure 5.40 Portal frame induced by a moving mass and moving force

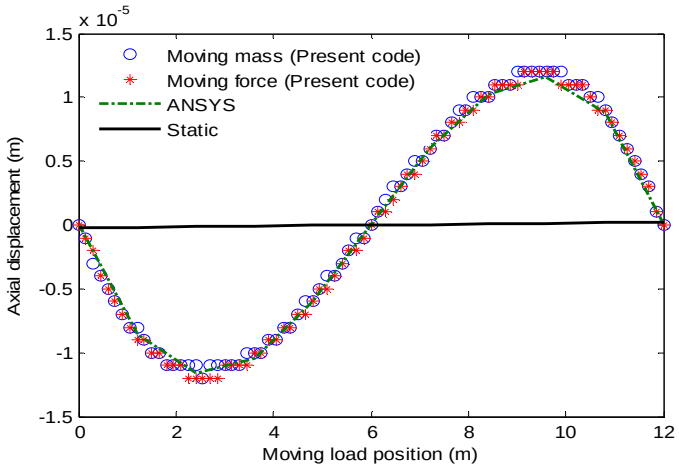

Figure 5.41 Axial displacements of the central point c_p the top beam

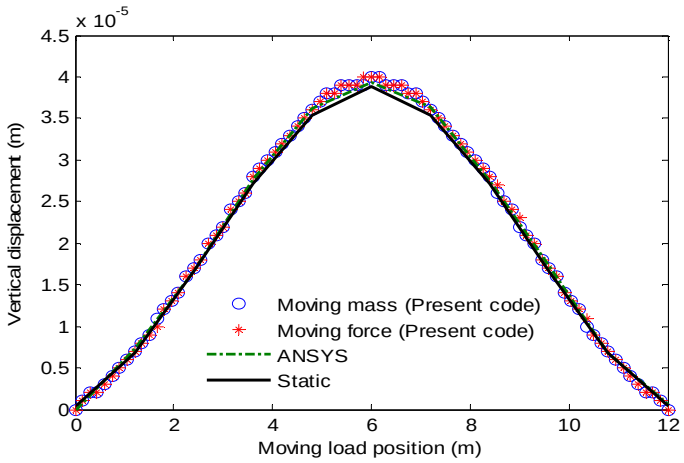

Figure 5.42 Vertical displacements of the central point c_p of the top beam

The portal is subjected to a load moving from the left end to the right end of the top beam with constant velocity V = 0.75 m/s, $m = 60\ kg$ without structural damping $\xi_1 = \xi_2 = 0$. The axial and vertical displacement of the central point c_p of the top beam can be seen in Figures 5.41 and 5.42. Agreement in fluctuating features of the associated curve among moving mass, moving force obtained from present code under Matlab® and ANSYS are found.

5.5.3 Crane Framework

A three crane framework is shown in Figure 5.43. The dimensions and material properties of the crane framework are identical with Table 5.4.

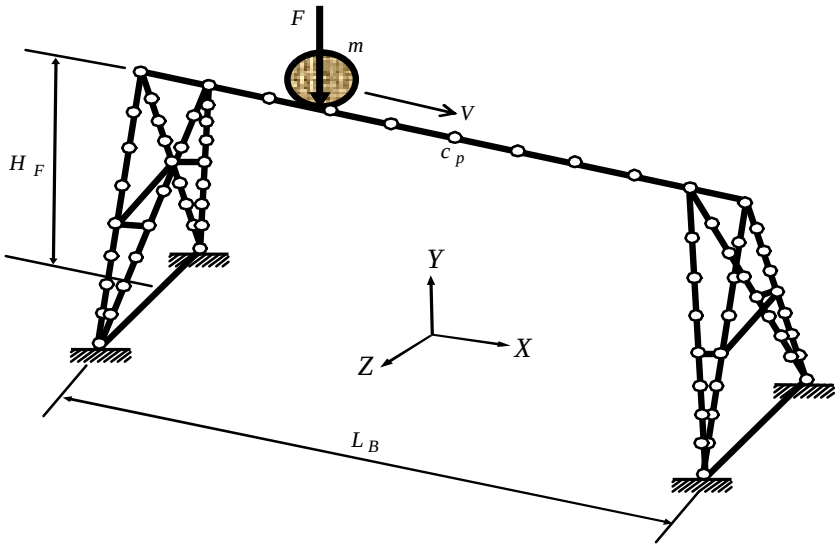

Figure 5.43: Crane framework induced by a moving mass and moving force

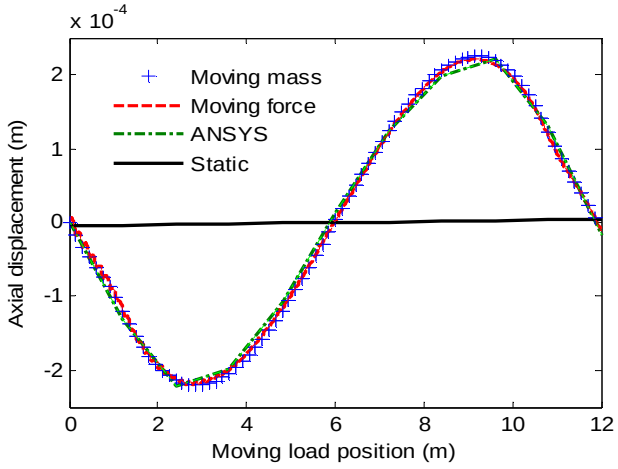

(a)

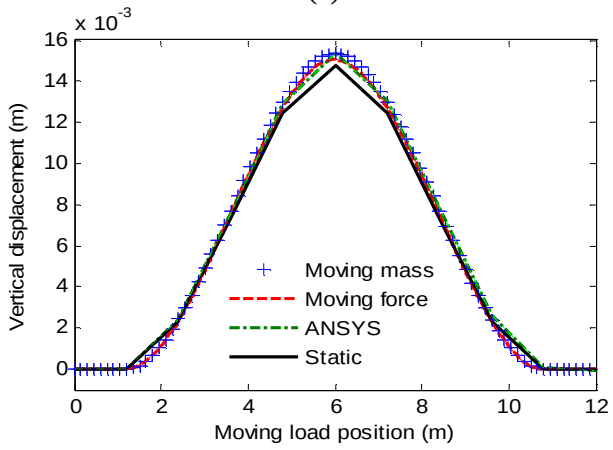

(b)

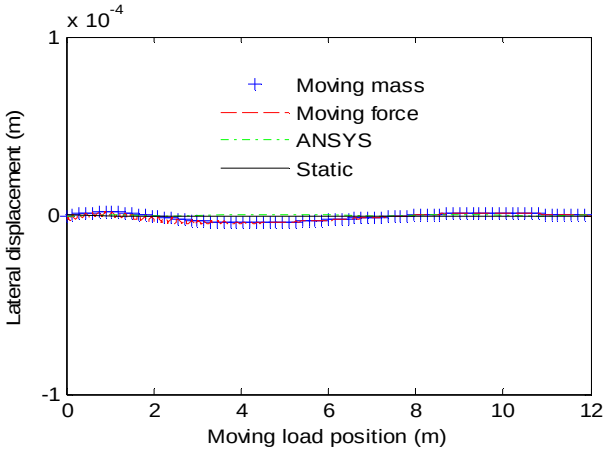

(c)

Figure 5.44: Dynamic displacements of crane framework (a) axial (b) vertical (c) lateral

Moving loads move with constant velocity V = 1 m/s, mass m = 1200 kg on the top beam of undamped crane framework. The axial (X), vertical (Y), lateral (Z) displacements are shown in Figure 5.44. The figures show that the value of static displacements in axial (X) and lateral (Z) are very small compared to vertical (Y) displacement. The deformation of crane framework is dominant in vertical direction, since it is weaker at that direction. It is also seen that besides the vertical responses, moving loads have significant effect in axial and lateral responses compared than their corresponding static responses. From the simulations, dynamic responses among moving force, moving mass and ANSYS agree well.

5.5.3.1 Effect of Moving Load Magnitude on Crane Framework

Mass is moved from the left hand side of the top beam using trajectory profile in Figure 5.45, but stops in the middle of the top beam. The mass is accelerated at a rate 1 m/s^2 to a maximum velocity of 1 m/s. The mass coasted at this velocity for 5 s. After 6 s from the beginning maneuver, the trolley is decelerated at a rate 1 m/s^2 for 1 s. In the end, the trolley has moved 6 m in 7 s and rest in 40 s.

The axial, vertical and lateral displacements of the central point c_p of the top beam due to moving mass magnitude variation, m_1 = 600 kg, m_2 = 900 kg and

m_3 =1200 kg under structural damping $\xi_1 = \xi_1$ = 0.005 are shown in Figures 5.46-5.50.

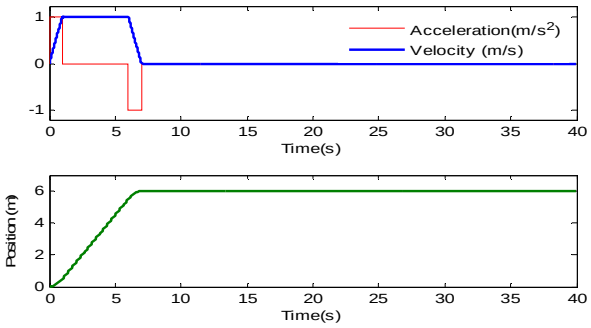

Figure 5.45 Moving mass trajectories

It can be seen that the vibration amplitudes increase by the increase of moving mass magnitudes, where there is no change in vibration frequency at all moving load magnitude range as shown in Figure 5.48 and 5.52. It is also interesting to note that all the dynamic responses damp to their corresponding static displacements due to effect of structural damping.

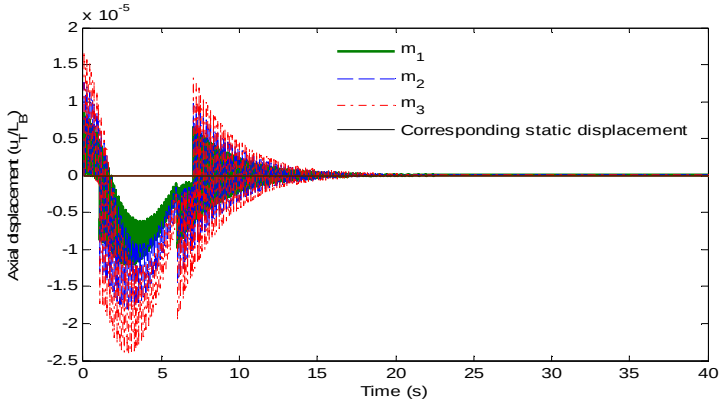

Figure 5.46 Axial displacements of the central point c_p of the top beam under moving mass magnitude variation for case II

When axial displacements in Figure 5.46 at time 0-7 s is zoomed as shown by Figure 5.47 it is clearly seen that the vibration amplitudes in the acceleration phase (a = 1 m/s during t = 0-1 s) or deceleration phase (a = 1 m/s during t = 6-7 s) are clearly visible than the corresponding ones in the constant speed phase (a = 0. during t = 1-6 s). This dynamic phenomenon is also found by Wu [10] in portal frame.

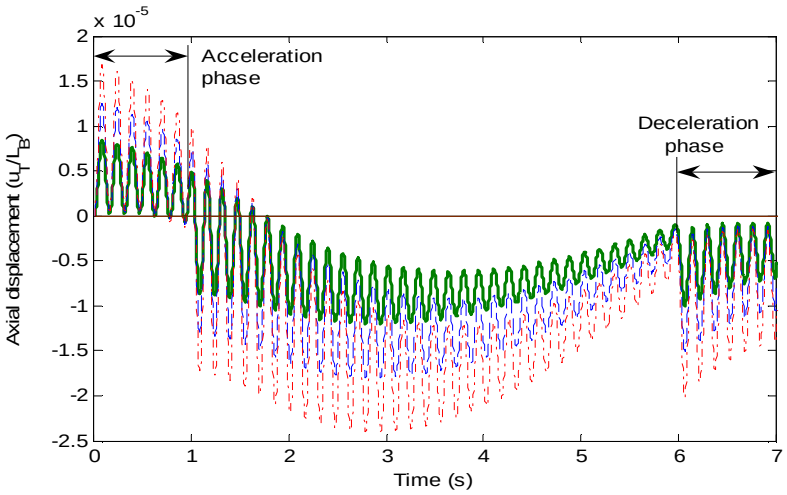

Figure 5.47: Zoom of figure 5.46 during time 0-7 s

This is expected since during those phases, external forces as forcing term is generated in axial direction due to inertial force of moving mass motion, while in constant velocity phase is zero. The inertial force in axial direction is proportional to moving mass magnitude as it can be observed from Equations (47).

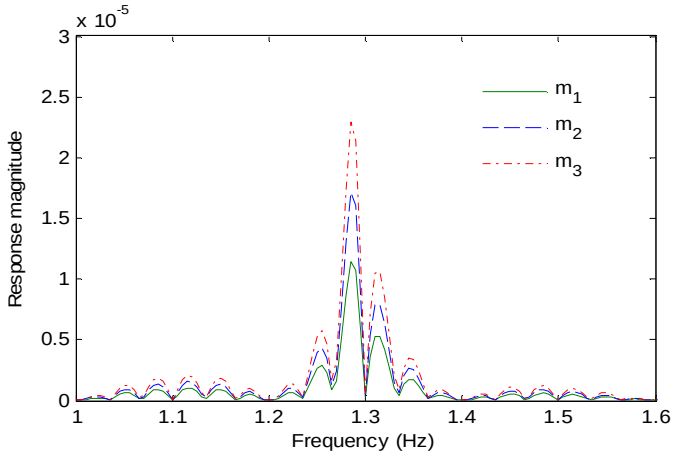

Figure 5.48: FFT analysis of axial displacement of crane framework under moving mass magnitude variation for case II

Time histories for the vertical displacement of the central point c_p of the top beam are shown in Figure 5.49. It is interesting to note that the dynamic responses converge to a displacement which is greater than the corresponding static displacement. The difference between the static and the final dynamic displacement increase by increasing moving mass magnitude.

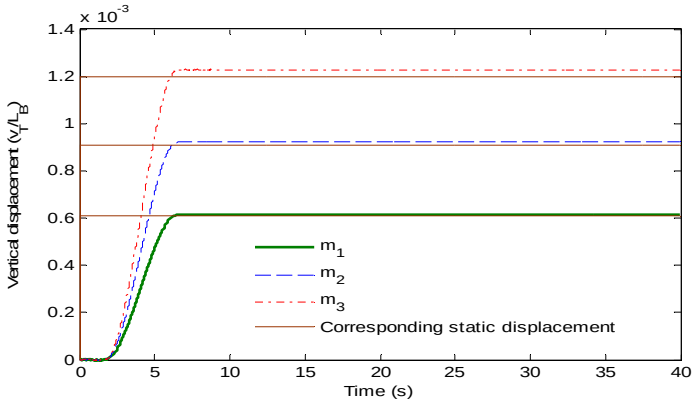

Figure 5.49: Vertical displacements of the central point c_p of the top beam under moving mass magnitude variation for case II

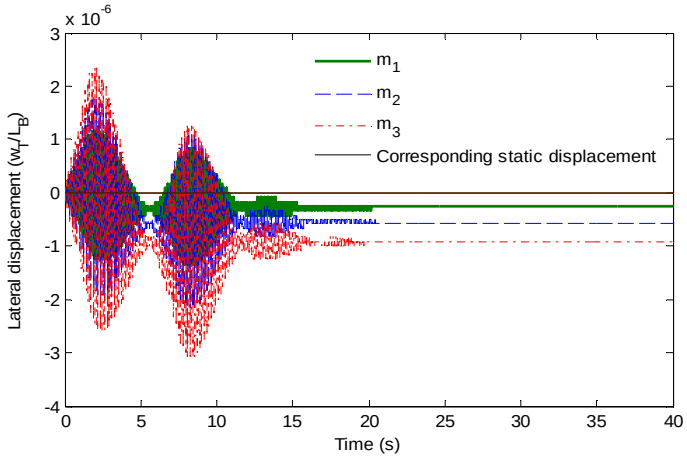

Figure 5.50: Lateral displacements of the central point c_p of the top beam under moving mass magnitude variation for case II

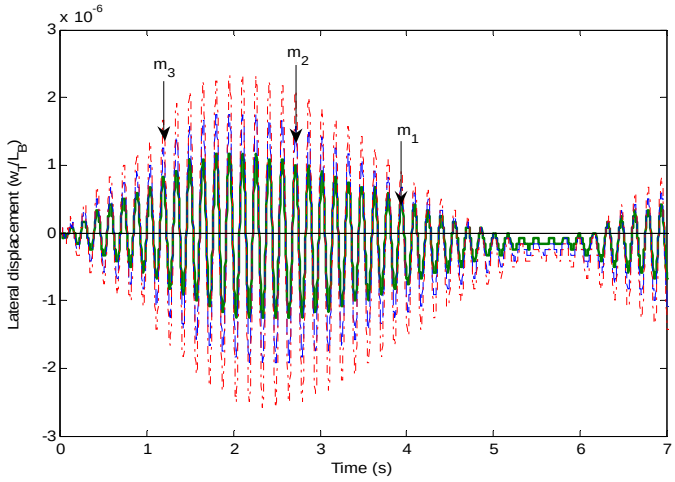

Figure 5.51: Zoom of figure 5.50 during time 0-7 s

Further, the lateral responses, measured at the central point c_p of the top beam exhibit the clear beating behavior as illustrated in Figures 5.50-5.51, where they decay due to structural damping.

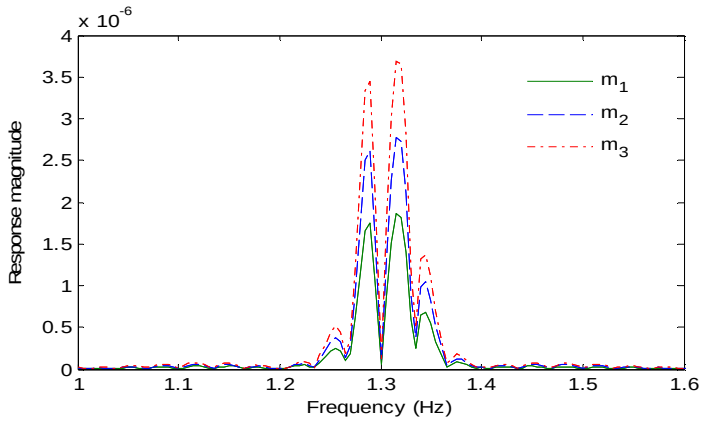

Figure 5.52: FFT analysis of analysis lateral displacement of crane framework under moving mass magnitude variation for case II

5.5.3.2 Effect of Moving Load Velocity on Crane Framework

To study the effect of moving mass speed to both axial and vertical displacements, the velocity $V_1(t)$, $V_2(t)$ and $V_3(t)$ are applied to moving mass as given in Figure 5.53 but still stops in the middle of the top beam.

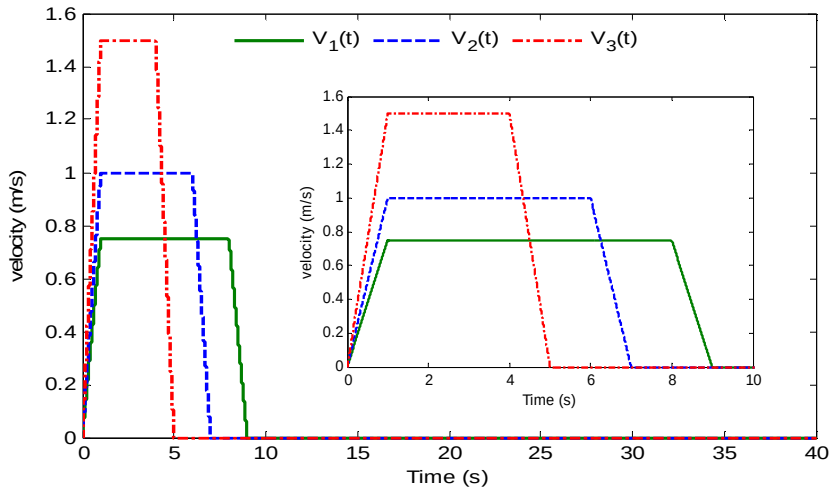

Figure 5.53: Variation of moving mass velocity histories

The velocity histories are defined in Table 5.10, m = 900 kg and $\xi_1 = \xi_1$ = 0.005. It is noted that other forms of velocities history could have been chosen, but here an arbitrary profiles were chosen to primarily illustrate the effect of moving load velocity on the dynamic response of crane framework.

Table 5.10: Velocity history of moving mass

Velocity History	Time phase (s)				
	Stationary	Acceleration	Constant velocity	Deceleration	Stationary
$V_1(t)$	0	0-1	1-8	8-9	9-40
$V_2(t)$	0	0-1	1-6	6-7	7-40
$V_3(t)$	0	0-1	1-4	4-5	5-40

Axial (X), vertical (Y) and lateral (Z) displacements of crane framework under velocity variation are given in Figures 5.54, 5.57 and 5.59. Zoom of axial displacements in Figure 5.54 as shown in Figure 5.55 depict that the increase of moving mass speed will increase vibration amplitudes. The change of vibration frequency in axial displacements is evident at all velocity histories as shown in Figure 5.56 and 5.58. For the larger velocity history, moving mass propagates along the top beam faster than the others. It reveals that the velocity of moving load has significant effect on vibration frequency and maximum displacement of axial displacement. This trend is similar for lateral responses as shown by Figure 5.57.

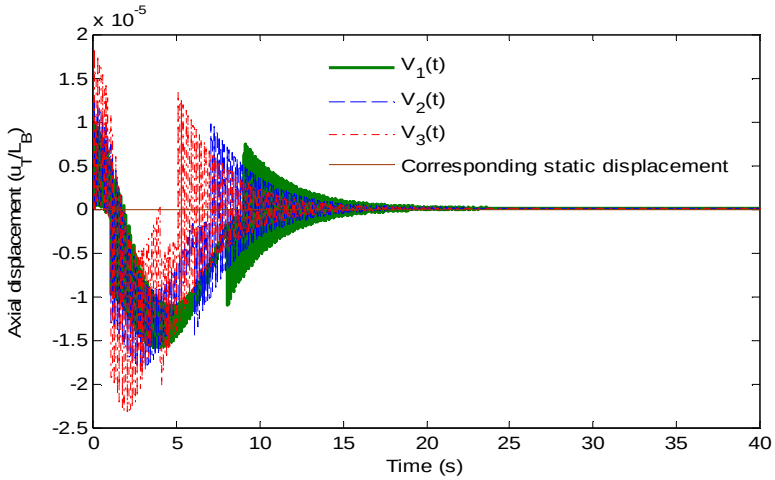

Figure 5.54: Axial displacements of the central point c_p of the top beam under moving mass velocity variation for case II

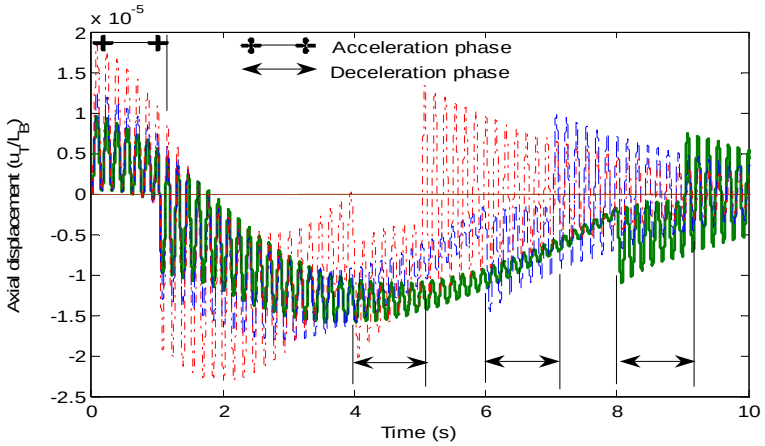

Figure 5.55: Zoom of figure 5.54 during time 0-10 s

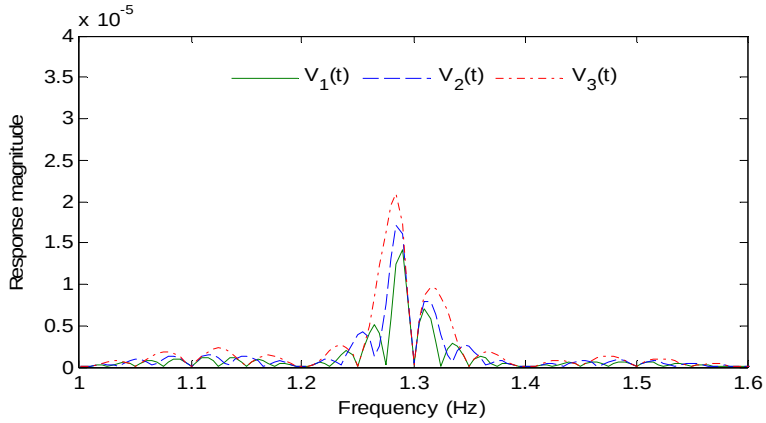

Figure 5.56: FFT analysis of axial displacement of crane framework under moving mass velocity variation for case II

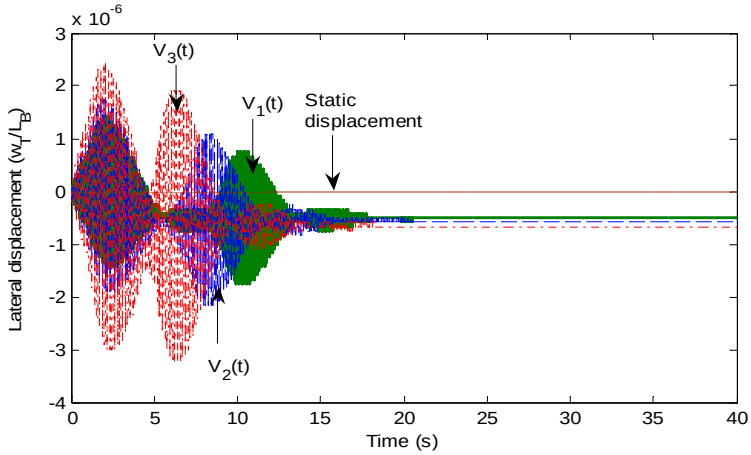

Figure 5.57: Lateral displacements of the central point c_p of the top beam under moving mass velocity variation for case II

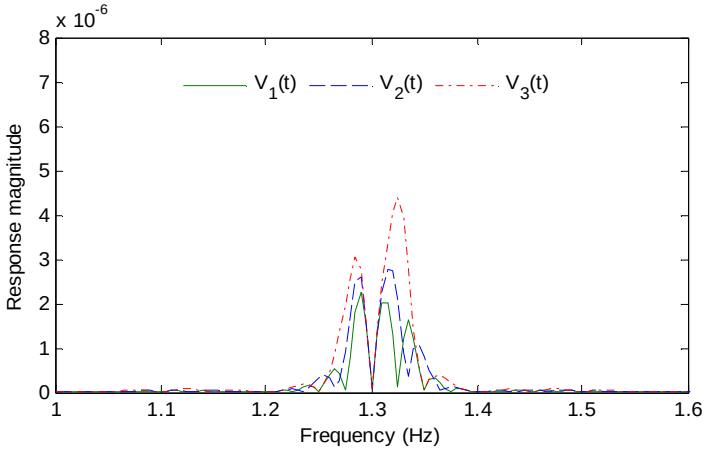

Figure 5.58: FFT analysis of analysis lateral displacement of crane framework under moving mass velocity variation for case II

Effects of acceleration and deceleration phase induce slighter vertical displacements for all the velocity histories as shown by Figure 5.59.

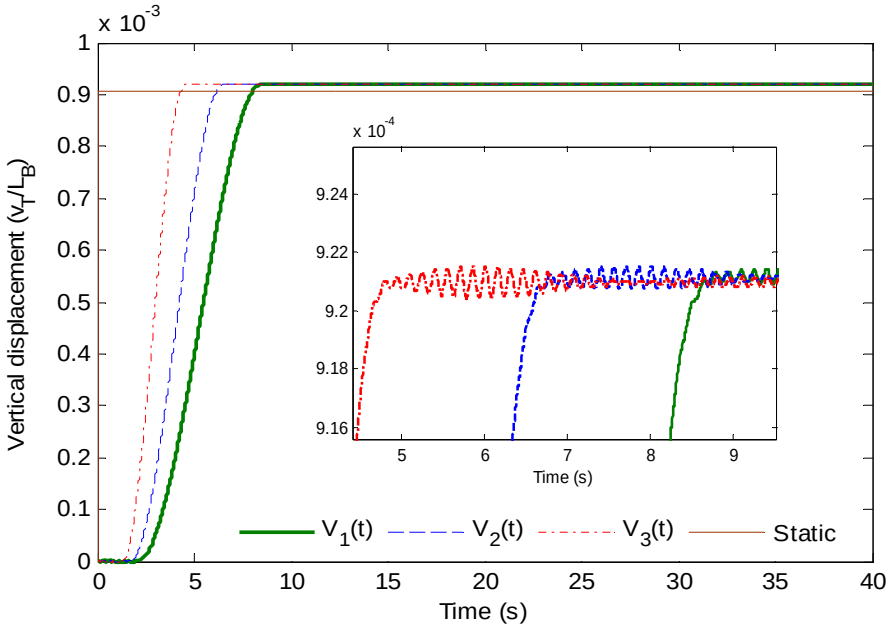

Figure 5.59: Vertical displacements of the central point c_p of the top beam under moving mass velocity variation for case II

5.6 Gantry Crane System under Moving Trolley with Swinging Payload (Case III)

The dimensions of the framework of the crane in this sub-section are exactly the same as those in the Table 5.4. A moving trolley m_T carrying a swinging payload m_P moves from the left end to the right end with trolley driving force $F(t)$ on the top beam of the stationary crane framework. Basically, case III is combination between case I and case II, where the swinging motion of payload is moving along the top beam of flexible crane framework due to trolley motion. The developed computer codes are then combination from both cases.

As a benchmark, similar with case I, the implemented code are verified by comparing analysis results with those obtained using the well-known classical pendulum with moving pivot or called as rigid model of crane system as shown in Figure 5.60. The equations of motion of rigid model are presented by Equations (49a)-(49b).

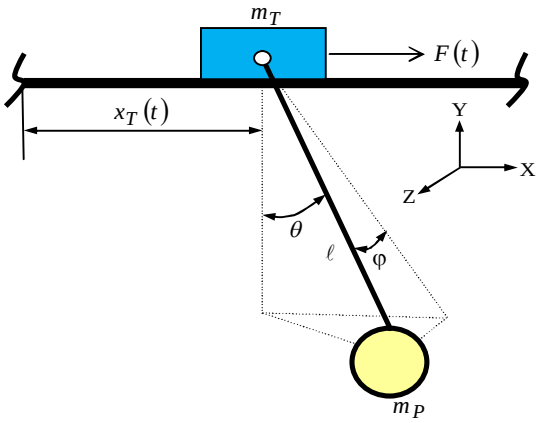

Figure 5.60: Simple pendulum system with moving pivot

To investigate the influence of moving trolley carrying a swinging payload on flexible crane framework and vice versa, the parametric studies are conducted. Time histories are presented as functions of a limited set of parameters for quite simple but representative for gantry crane system.

5.6.1 Open-Loop Responses

The finite element model of flexible gantry crane system under case III is shown in Figure 5.61.

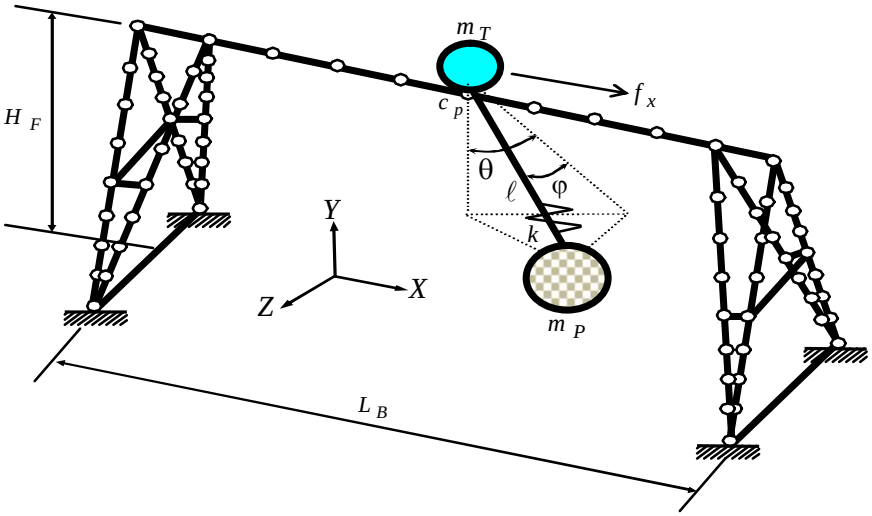

Figure 5.61: Finite element model of flexible gantry crane under case III

In this subsection, as a test for the dynamic model in Equations (48d)-(48g) and (52), open-loop responses are performed under two types of driving force f_x, namely bang-bang input force and harmonic input force. It is noted that that other forms of driving force could have been chosen, but here an arbitrary form is chosen to primarily attempt to model the real driving force situation for the actual crane system.

5.6.1.1 Responses under Bang-bang Input Force

The simulation is performed where bang-bang input force is applied to move the trolley of gantry crane. Magnitude of bang-bang input force is varied in order such that the trolley reaches 3m, 6m and 12 m from the left end of the top beam of crane framework as depicted in Figure 5.62.

It can be observed in Figure 5.63, and confirmed by Figure 5.67 that accelerations and decelerations phases can be clearly seen in swing angle θ, due to the profile of bang-bang input force. Swing amplitudes in the periods of accelerations and decelerations are greater than in the constant-speed phases.

When the trolley accelerates, payload swings behind the trolley. Vice versa, the payload swings ahead of trolley when trolley decelerates. The swing angles are identical when the trolley speed is constant or the trolley stops.

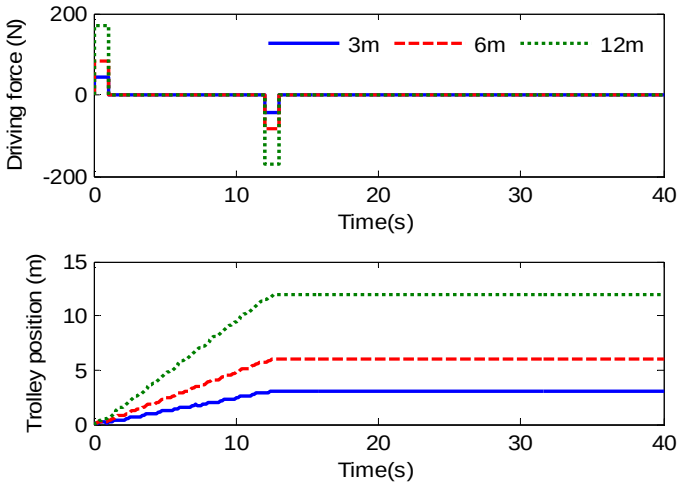

Figure 5.62: Bang-bang input forces and trolley positions

The payload will continue swing although the force is taken after 13s. This is due to the dynamics of payload is without damping as it can be seen from Equations (49a)-(49b). This characteristic does not appear in swing angle φ, as it is noticed from Figure 5.64.

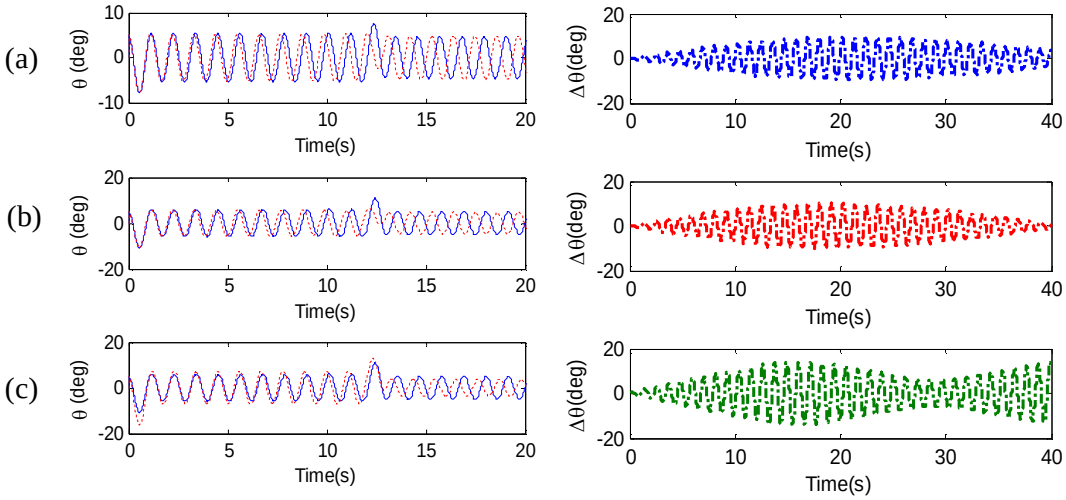

Figure 5.63: Time history of θ and $\Delta\theta$ under bang-bang input force: (—) flexible model; (- - -) rigid model; (-.-.-) $\Delta\theta$ (a) 3m (b) 6m (c) 12m

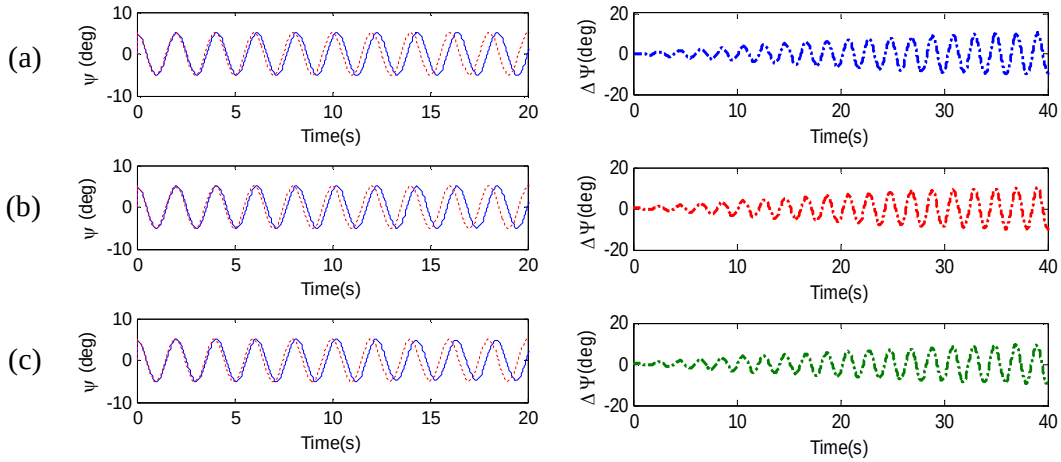

Figure 5.64: Time history of φ and Δφ under bang-bang input force: (—) flexible model; (- - -) rigid model; (-.-.-) Δφ (a) 3m (b) 6m (c) 12m

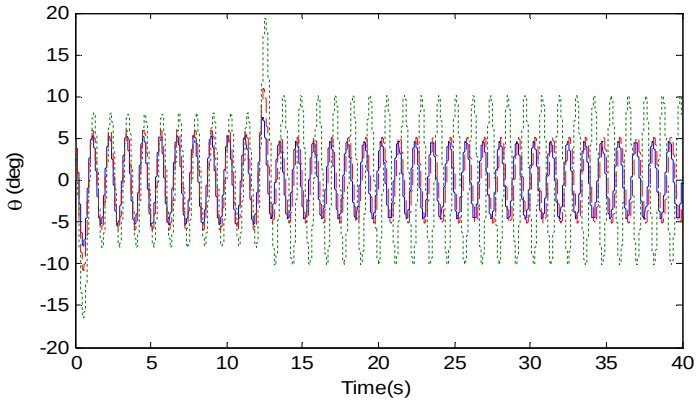

(a)

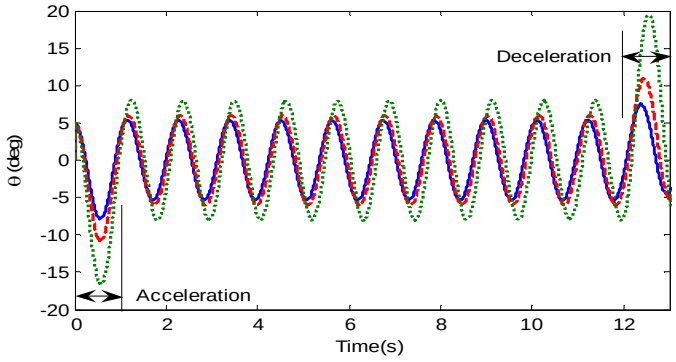

(b)

Figure 5.65: Flexible model responses of θ under bang-bang input force
(a) Time window for 40 s (b) Time window for 13 s

That is because the horizontal (X) inertia force induced by moving trolley carrying a swinging payload significantly affects the payload swing in planar motion than that in space motion due to input force is applied in the horizontal direction. Further, amplitudes and frequencies of $\Delta\theta$ are about 2 times when trolley moves to 12 m (final position) than 3m and 4m. There is no discernable effect in $\Delta\varphi$ observed in Figures 5.63 and 5.64, respectively.

From Figure 5.66(b), it can be found that the vertical displacements at the central point c_p of the top beam of crane framework damps to zero when the trolley stops at the right side of beam for position 12m and to corresponding static displacements for position 3m and 6m. It is interesting to note that the dynamic response converges to a displacement which is greater than the corresponding static response in Figure 5.66(b), Figure 5.66(c) and Figure 5.67, respectively. The difference between the static and the final dynamic response increase by decreasing the position of trolley. The definition for Dynamic Amplification Factor (DAF) in this study is the ratio between the absolute maximum dynamic displacement to the absolute maximum static displacement [44]. DAF for axial displacements are 1.21 when trolley moves to 3 m, while 1.12 for 6 m. DAF for vertical displacements are almost the same for all trolley position, it is about 1.37, while lateral displacements have very large DAF because the crane framework is more rigid when it is loaded with static load compared to loaded with moving trolley with swinging payload.

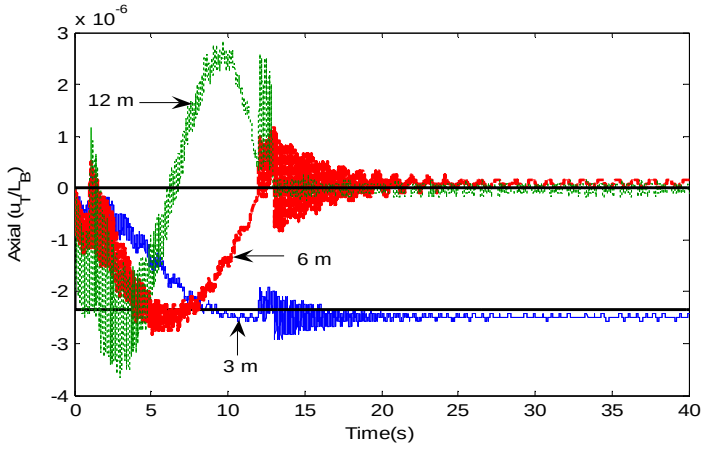

(a)

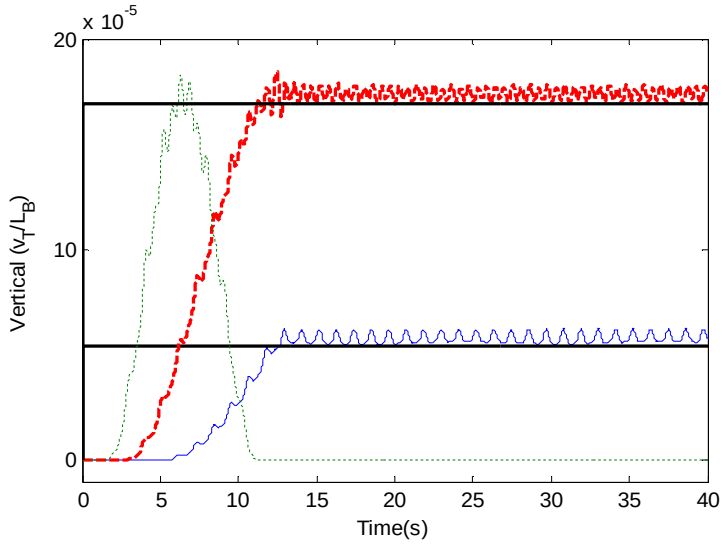

(b)

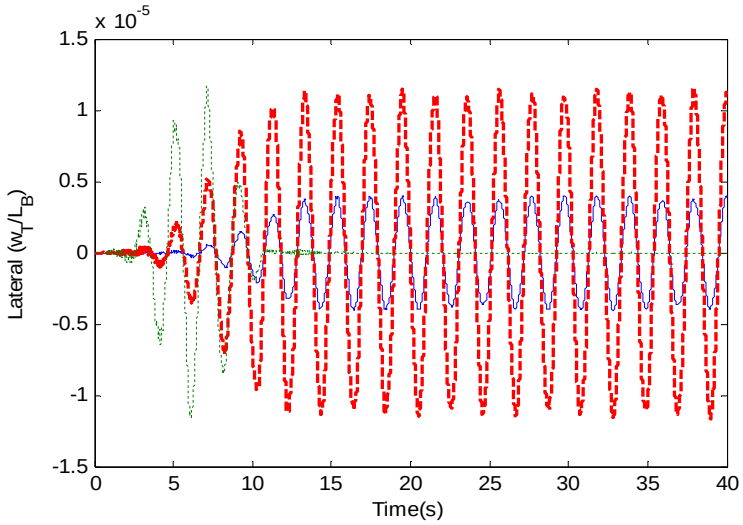

(c)

Figure 5.66: Dynamic responses of crane framework under bang-bang input force: (—) 3m; (- - -) 6m; (….) 12m (**—**) corresponding static displacements (a) axial (b) vertical (c) lateral displacements

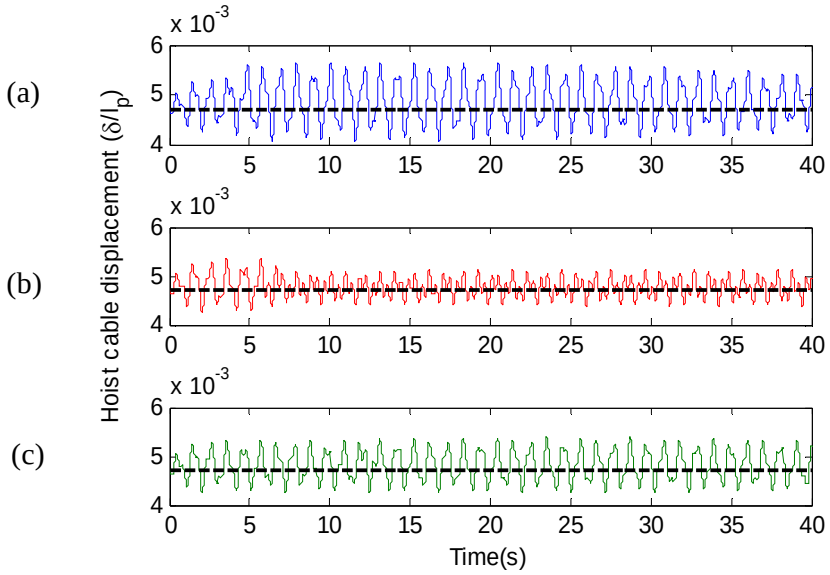

Figure 5.67: Dynamic responses of hoist cable under
Bang-bang input force (—) dynamic (- - -) static (a) 3m (b) 6m (c) 12m

5.6.1.2 Responses under Harmonic Input Force

The effect of different harmonic input force frequencies on the responses of payload swings and crane framework is investigated. The parameters are identical with Table 5.3 and 5.4. The harmonic input force frequencies are $0.1\omega_n$, $0.95\omega_n$ and $1.5\omega_n$ as presented in Figure 5.68.

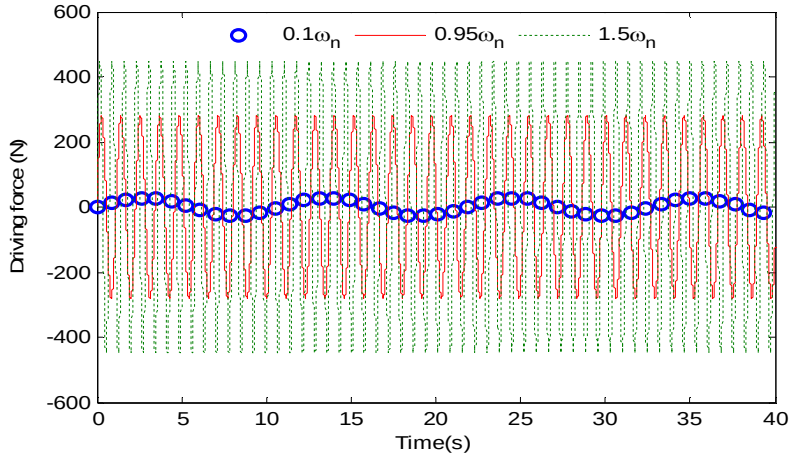

Figure 5.68: Harmonic input forces

Term ω_n corresponds to natural frequency of payload with hoist cable length, ℓ_P =1m. The dynamic responses of payload swings and difference with rigid model are shown in Figures 5.69-5.70. The results show that θ and φ depend on the harmonic frequency. As the harmonic frequency approaches the natural frequency of payload, the amplitudes of swing angles increase erratically. It is seen also that swing angle, θ is larger than φ.

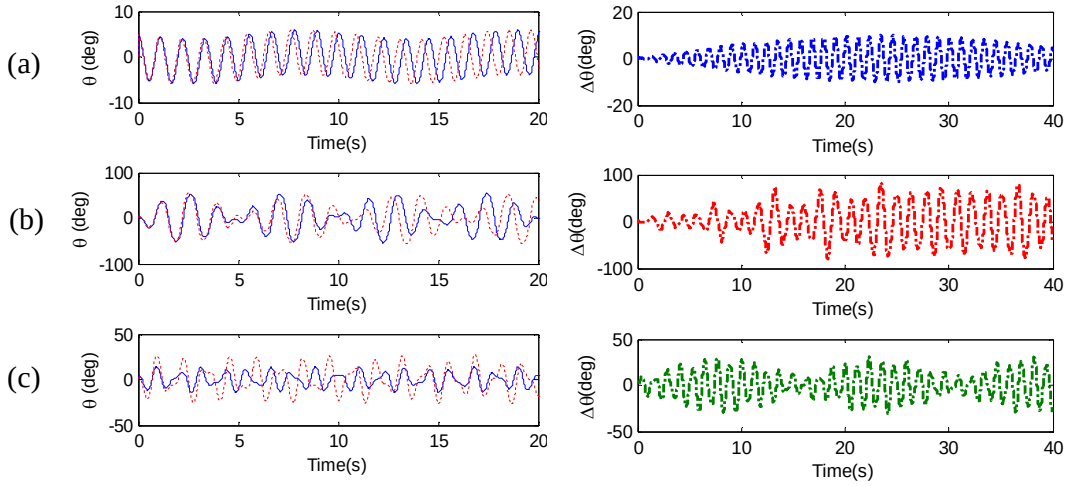

Figure 5.69: Time history of θ and $\Delta\theta$ under harmonic input force: (—) flexible model; (- - -) rigid model; (-.-.-) $\Delta\theta$ (a) $0.1\omega_n$ (b) $0.95\omega_n$ (c) $1.5\omega_n$

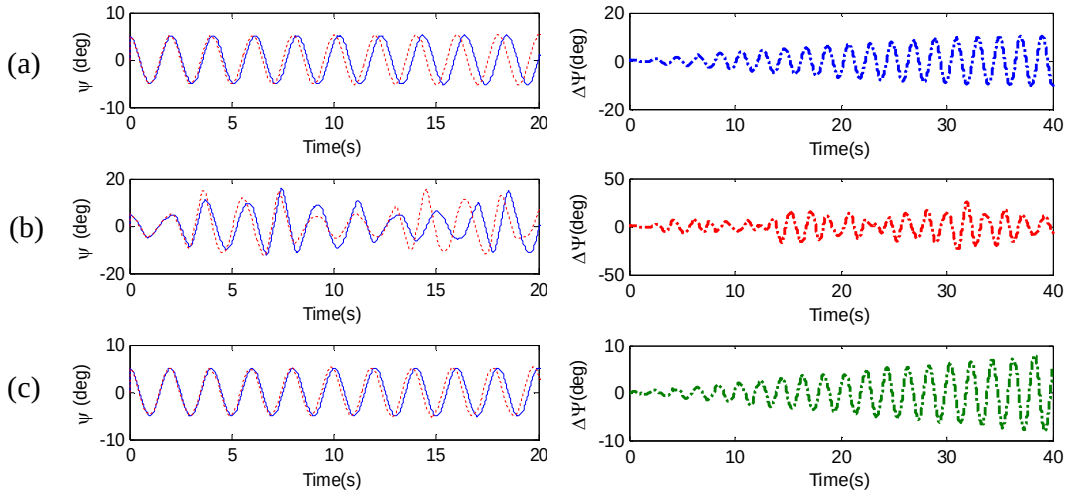

Figure 5.70: Time history of φ and $\Delta\varphi$ under harmonic input force: (—) flexible model; (- - -) rigid model; (-.-.-) $\Delta\theta$ (a) $0.1\omega_n$ (b) $0.95\omega_n$ (c) $1.5\omega_n$

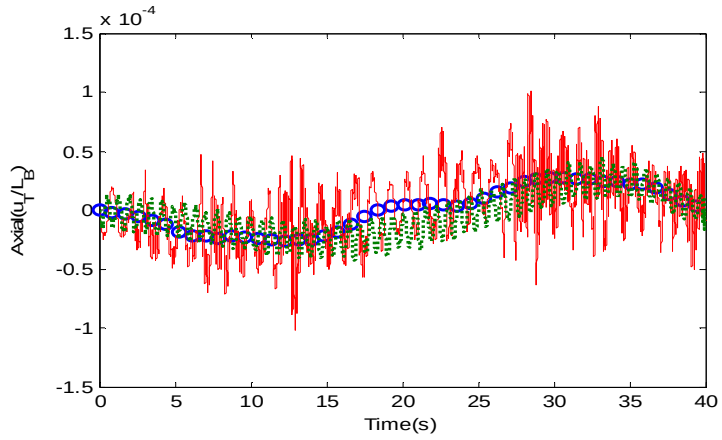

(a)

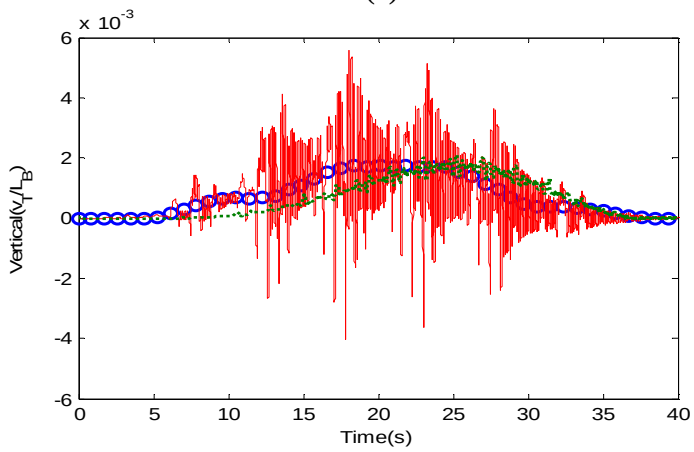

(b)

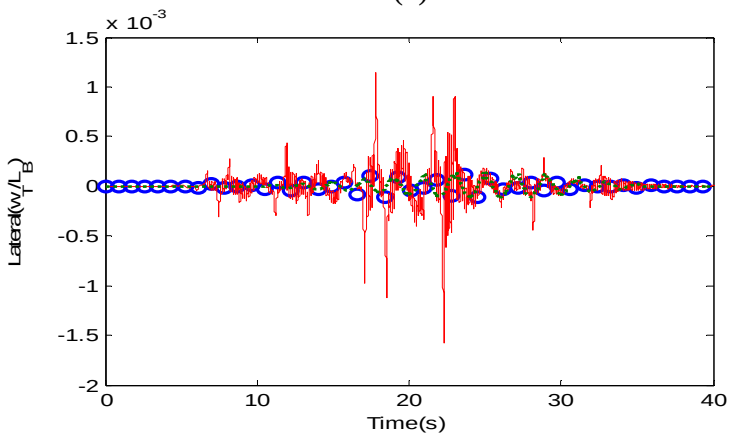

(c)

Figure 5.71: Dynamic responses of crane framework under harmonic force input (ooo) $0.1\omega_n$; (—) $0.95\omega_n$; (- - -) $1.5\omega_n$ (a) axial (b) vertical (c) lateral displacements

The amplitudes of swing angles increase almost 10 times below and 5 times above the harmonic frequency. Elastic displacements of the central point c_P of the top beam under variation of harmonic force input are shown in Figure 5.71. It is observed that when the harmonic frequency of input force approaches the natural frequency of payload, DAF for axial displacement is about 32.614; while for vertical displacement is about 4.54. Similar with bang-bang input force, lateral displacement produces very large DAF.

5.6.2 Effect of Structural Flexibility for Case III

All the parameters for the gantry crane and crane framework in this subsection are identical with Table 5.3 and 5.4, unless particularly stated. The gantry crane is traversed by prescribed trolley trajectory as shown in Figure 5.72.

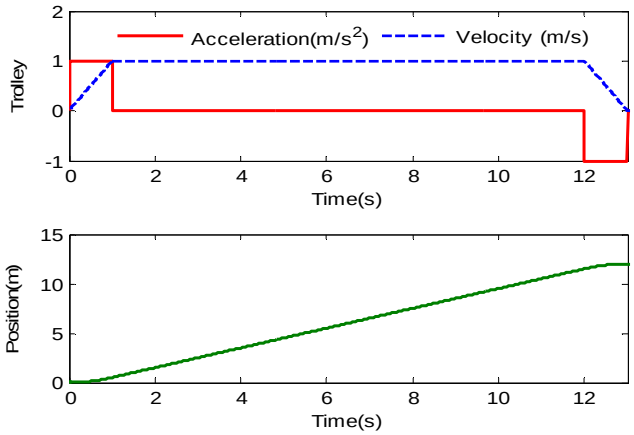

Figure 5.72: Trolley trajectory for case III

5.6.2.1 Effect of Hoist Cable Stiffness

Figures 5.73-5.74 show that the frequencies of θ and φ increase with the decrease of the hoist cable stiffness with respect to their rigid model. The amplitudes of $\theta_{flexible}$ increase with the increase of hoist cable stiffness approaching θ_{rigid}, while minimal changes are found in amplitude of $\varphi_{flexible}$. Compared to case I, minimal changes in frequency and greater changes in amplitude of $\Delta\theta$ and $\Delta\varphi$ are observed.

That is because the contributions of trolley velocity and acceleration, $\dot{x}_T, \ddot{x}_T$ in the payload dynamics in Equations (48d)-(48g).

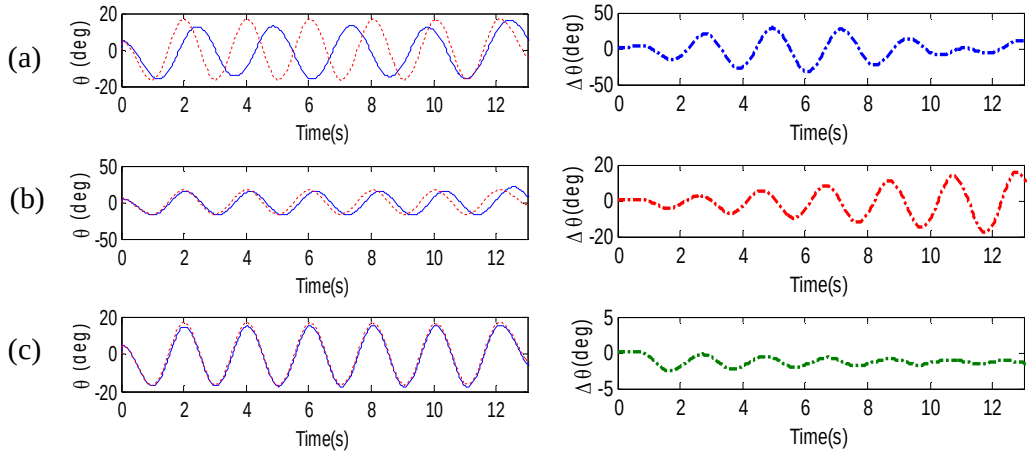

Figure 5.73: Time history of θ and $\Delta\theta$ under case III: (—) flexible model; (- - -) rigid model; (-.-.-) $\Delta\theta$ k_1 (b) k_2 (c) k_3

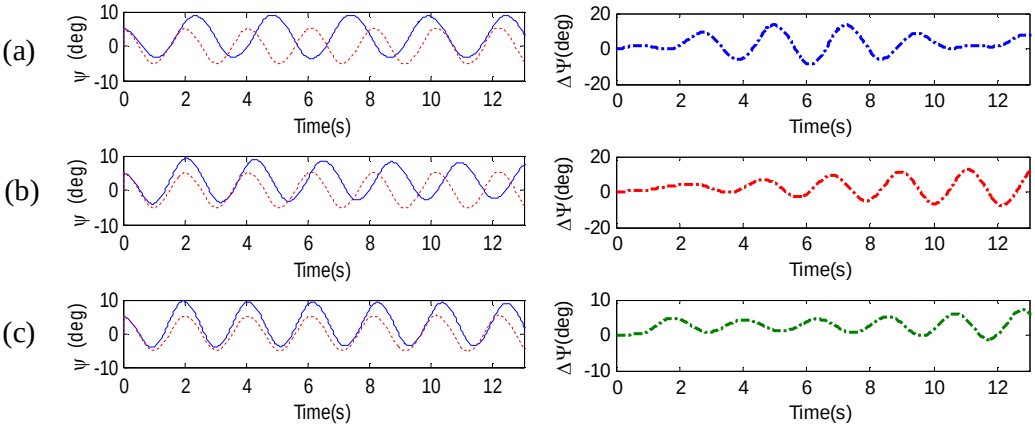

Figure 5.74: Time history of φ and $\Delta\varphi$ under case III: (—) flexible model; (- - -) rigid model; (-.-.-) $\Delta\varphi$ k_1 (b) k_2 (c) k_3

One interesting characteristic can be seen that the values of $\Delta\theta$ and $\Delta\varphi$ are bigger than θ and φ for the lowest hoist cable stiffness, $k_1 = 2.5 \cdot 10^4 \ N/m$ for both swing angles. That is because the contribution of flexibility of hoist cable makes the time history of $\theta_{flexible}$ and $\varphi_{flexible}$ with frequency $0.36Hz$ produces the different phase about $t = 1.7s$ compared than their corresponding rigid model with frequency $0.4985Hz$.

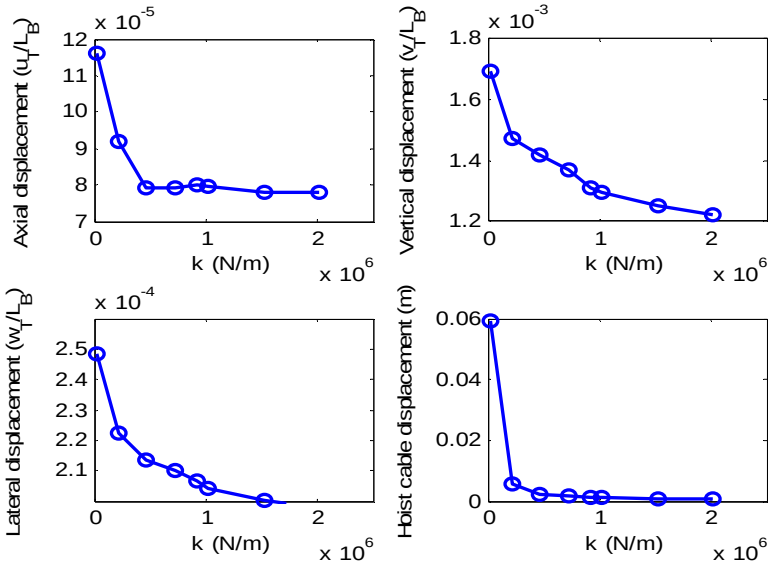

Figure 5.75: Maximum dynamic responses of crane framework under cable stiffness variation for case III

As the stiffness of hoist cable increases, this difference phase will decrease and the value of $\Delta\theta$ become negative due to the magnitude of $\theta_{rigid} > \theta_{flexible}$, while the value of $\Delta\varphi$ become positive due to the magnitude of $\varphi_{rigid} < \varphi_{flexible}$. However, the swing frequency of flexible model is still lower than the rigid model.

The maximum axial (X), vertical (Y) and lateral (Z) displacements of the central point c_p of the top beam of crane framework and hoist cable under variation of cable stiffness are shown in Figure 5.75. The trend is similar with case I, where the higher cable stiffness, the lower dynamic displacement of crane framework and hoist cable will be.

5.6.2.2 Effect of Crane Framework Flexibility for Case III

Dynamic behavior of gantry crane and crane framework for this case is almost similar with case I. The increase of cross-section dimensions of crane framework will make the time history of θ and φ are getting close into the rigid model as depicted by Figures 5.76 and 5.77. Unlike case I, the contributions of trolley velocity and acceleration $\dot{x}_T, \ddot{x}_T$ are significantly demonstrated by the lowest cross-sectional

properties among the others. The trend for all the maximum displacements of crane framework and hoist cable is similar with case I as depicted in Figures 5.78.

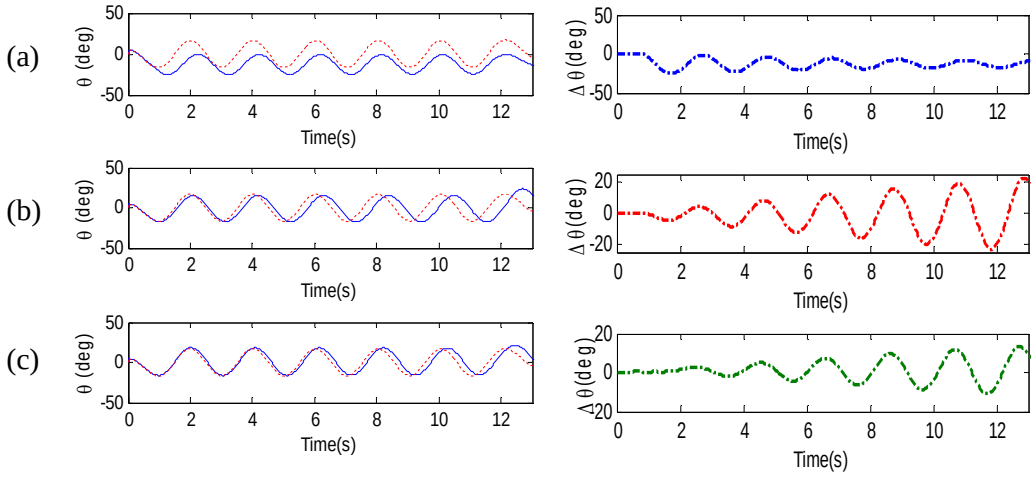

Figure 5.76: Time history of θ and $\Delta\theta$ under case III: (—) flexible model; (- - -) rigid model; (-.-.-) $\Delta\theta$ (a) cross-section 1 (b) cross-section 2 (c) cross-section 3

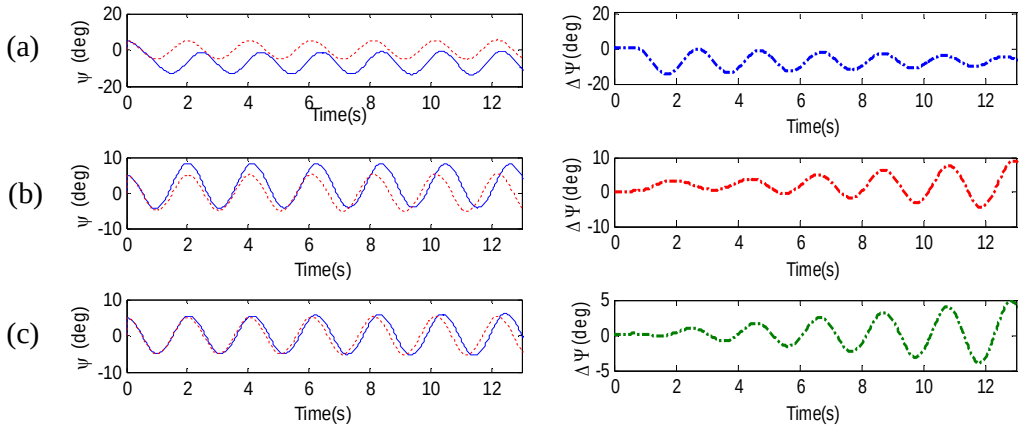

Figure 5.77: Time history of φ and $\Delta\varphi$ under case III: (—) flexible model; (- - -) rigid model; (-.-.-) $\Delta\varphi$ (a) cross-section 1 (b) cross-section 2 (c) cross-section 3

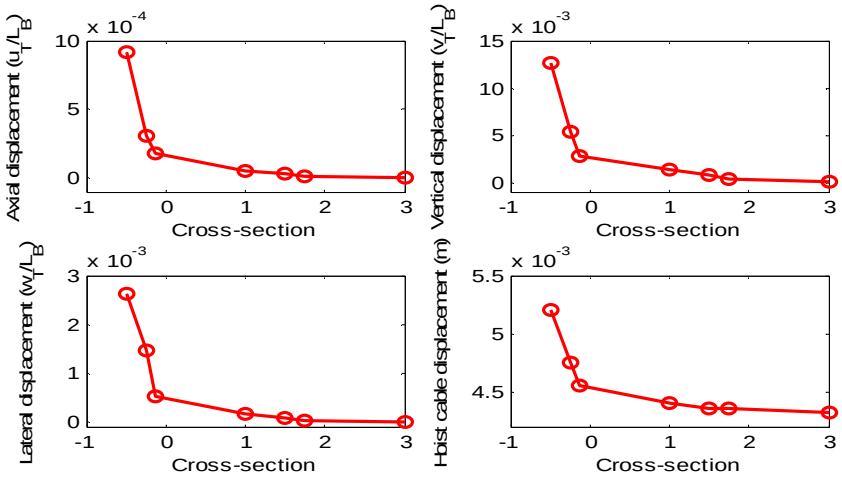

Figure 5.78: Maximum dynamic responses of crane framework under crane framework flexibility variation for case III

5.6.3 Gantry Crane Parametric Studies

5.6.3.1 Effect of Cable Length Variation for case III

Similar with case I under cable length variation, a definite change in amplitudes and frequencies are clearly observed. This to be expected since the swing frequency is inversely proportional the square root of the hoist cable length of payload. Figures 5.79 and 5.80 shows that the shortest hoist cable length produces larger swing amplitude and frequency of payload responses compared than the others.

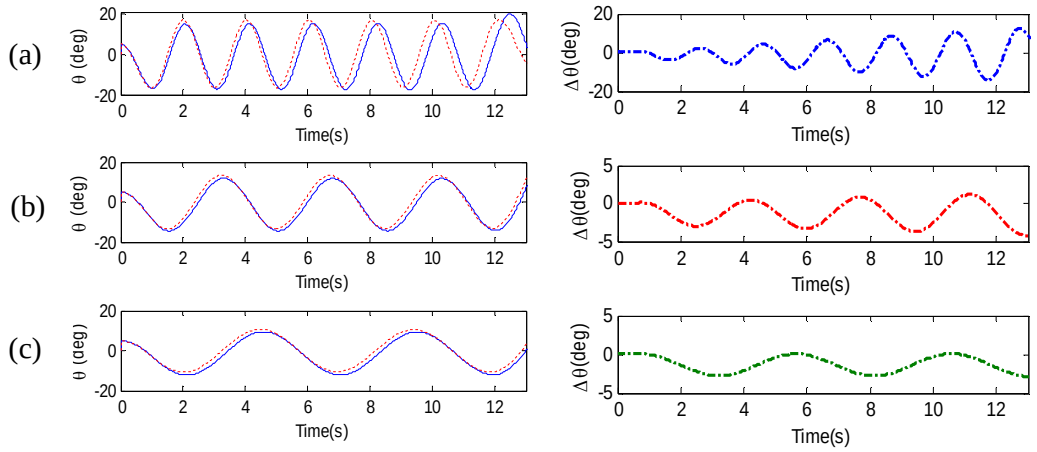

Figure 5.79: Time history of θ and $\Delta\theta$ under case III: (—) flexible model; (- - -) rigid model; (-.-.-) $\Delta\theta$ (a) $\ell = 1\,m$ (b) $\ell = 3\,m$ (c) $\ell = 6\,m$

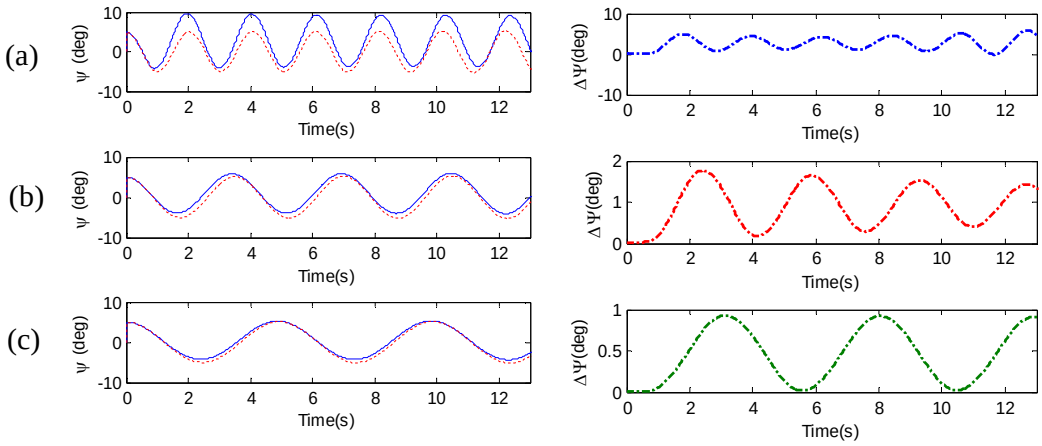

Figure 5.80: Time history of φ and $\Delta\varphi$ under case III: (—) flexible model; (- - -) rigid model; (-.-.-) $\Delta\varphi$ (a) $\ell = 1\,m$ (b) $\ell = 3\,m$ (c) $\ell = 6\,m$

The maximum axial (X), vertical (Y) and lateral (Z) displacements of the central point c_p of the top beam are shown in Figure 5.81. The maximum displacements decrease with the increase of payload cable length. Similar with case I, the shorter cable produces the higher displacement than the others. This is a reasonable result because the shorter cable produces larger the swing angles. The larger swing angles, the larger the external force in the axial (X) force component f_{0x}, the lateral (Y) force component f_{0y} and (Z) force component f_{0z} applied on the crane framework as it can be seen in the right side of Equation (52). This result is also found by Wu [12] in portal frame.

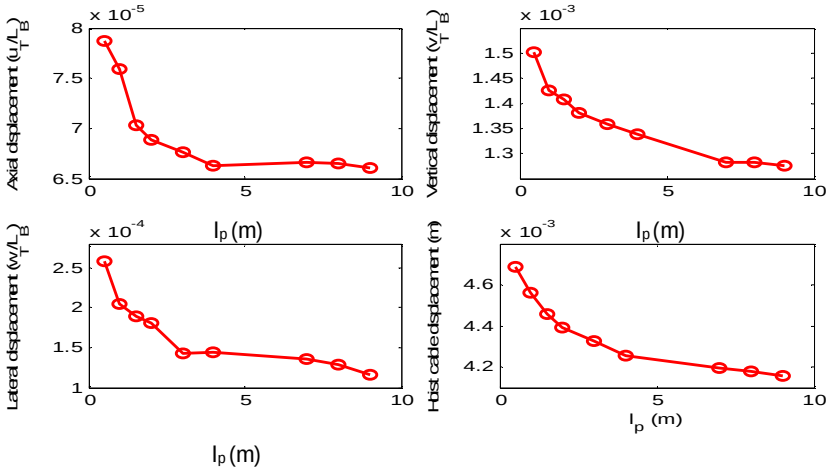

Figure 5.81: Maximum dynamic responses of crane framework under cable length variation for case III

5.6.3.2 *Effect of Payload Mass Variation for case III*

Similar with case I in Section 5.4.4, the combined trolley and payload mass $(m_T + m_P)$ contributes to the dynamics of gantry crane system. Figures 5.82 and 5.83 clearly show the sensitivity of gantry crane system with respect to the payload mass variation. The increase of payload mass has discernable effect on the amplitude and frequency of payload swing angles, where the amplitude and frequency increase with the increase of payload mass.

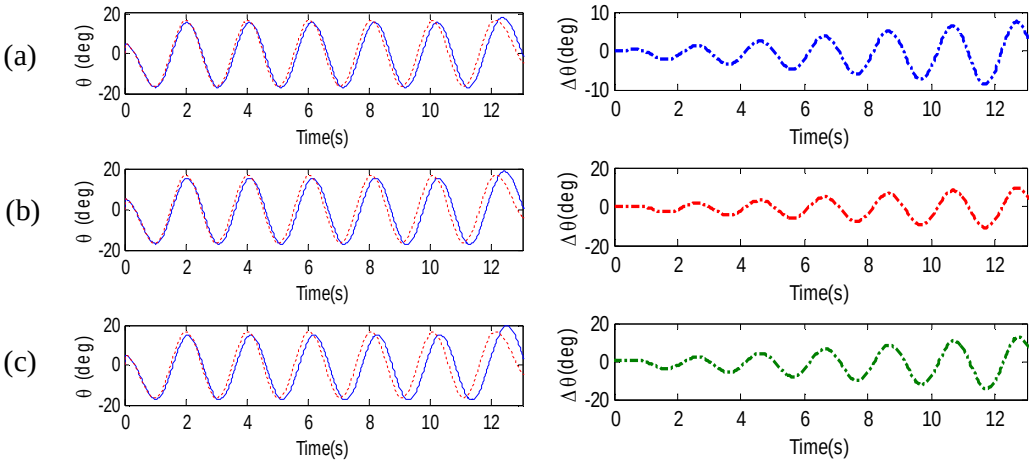

Figure 5.82: Time history of θ and $\Delta\theta$ under case III: (—) flexible model; (- - -) rigid model; (-.-.-) $\Delta\theta$ (a) $m_P = 700\ kg$ (b) $m_P = 900kg$ (c) $m_P = 1200\ kg$

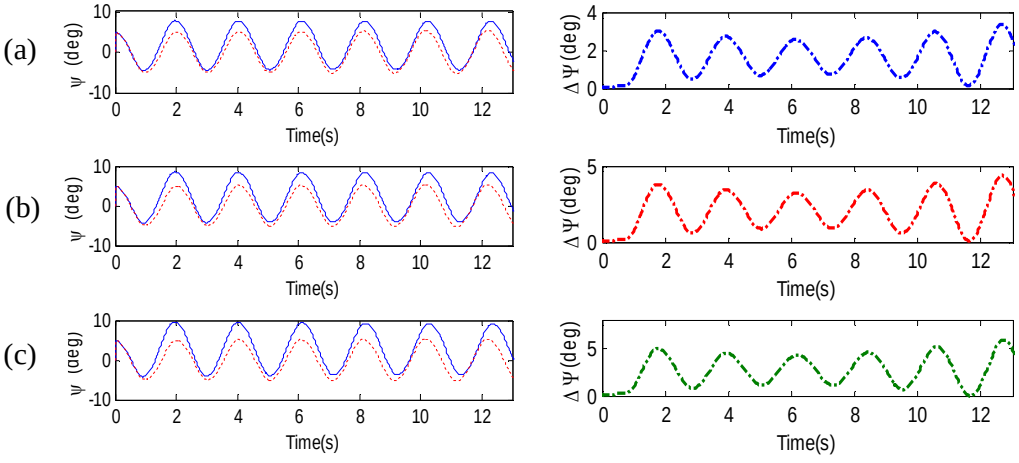

Figure 5.83: Time history of φ and $\Delta\varphi$ for case III: (—) flexible model; (- - -) rigid model; (-.-.-) $\Delta\varphi$ (a) $m_P = 700\ kg$ (b) $m_P = 900kg$ (c) $m_P = 1200\ kg$

Unlike case I, It is found that the frequency has minimum changes in $\Delta\theta$ and $\Delta\varphi$. It must be the contributions of trolley dynamics $\dot{x}_T, \ddot{x}_T$ in Equations (48d)-(48g). Similar result has also been reported by Oguamanam *et al.* [6].

Figure 5.84 shows that heavier payload mass produces larger maximum axial (X), vertical (Y) and lateral (Z) displacements of the central point c_p of the top beam. Similar with case I, The increases are slightly linear for axial, vertical, lateral and hoist cable displacements.

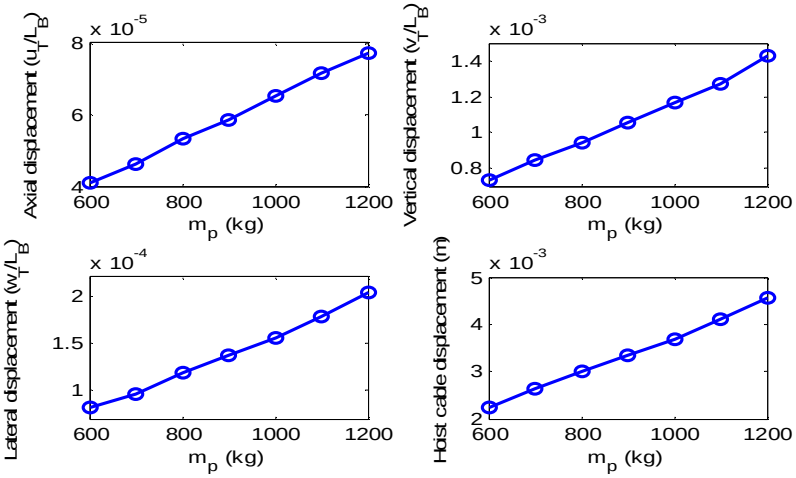

Figure 5.84: Maximum dynamic responses of crane framework under payload mass variation for case III

5.7 Summary

FFT analysis reveals that there are four peak points of frequency of crane framework response. The first peak point is the natural frequency of the payload, while the second peak point is appearance of second harmonic of the natural frequency of the payload. The third peak point corresponds to the natural frequency of hoist cable and the last is the third natural frequency of crane framework. By knowing the frequency content of crane framework response, it can be found out that the dynamic response of crane framework is dominated by the third mode shape which is vertical deformation of the top beam of crane framework.

Numerical simulation results show that the vibration amplitudes, frequencies and phase of the gantry crane system are affected by the flexibility of crane framework

and hoist cable. All the flexible models of gantry crane system have longer periods or lower frequencies compared to the rigid model. The gantry crane system with flexible hoist cable-crane framework produces greater amplitudes in swing angles $\theta, \varphi, \Delta\theta, \Delta\varphi$ and FFT analysis confirms that it has the lowest swing angles frequency compared to the gantry crane system with flexible hoist cable or crane framework only with respect to rigid model.

The parametric studies describe that the variation of parameters of gantry crane system such as structural damping, initial payload swing angle, payload mass, cable length, hoist cable stiffness and crane framework flexibility affect the state variables of gantry crane system, such as θ, φ, δ for dynamics of gantry crane and dynamic responses of crane framework. For dynamics of gantry crane, it is found that the swing angles amplitudes increase with the increase of initial swing angles of payload and payload mass, the decrease of cable length, cable stiffness and cross-sectional dimensions of crane framework. Minimum changes in amplitudes are observed in the variation of structural damping. The decrease of swing angles frequency is found in increasing of structural damping, cable length, hoist cable stiffness and decreasing of payload mass. Minimum changes in frequency are found in increasing of initial swing angles of payload and crane framework flexibility.

Under the increase of structural damping, dynamic displacements of crane framework in the axial (X), vertical (Y) and lateral (Z) direction and hoist cable decay and converge into their corresponding static displacements. The trend of maximum dynamic displacements of the crane framework, measured at the central point c_p of the top beam of crane framework is slightly linear for axial and nonlinear for lateral and vertical under the increase of initial swing angles of payload. Under the increase of the payload mass, the trends are slightly linear for all the displacements. The trends decrease for all the displacements under the increase of the cable stiffness and crane framework flexibility.

If the crane framework is induced by moving loads without the effect of payload swings as case II, some dynamic characteristics can be found. Finding results show that DAF for vertical displacement is about 1.25, 22.3 for axial and very large DAF for lateral displacement for constant velocity, $V = 1$ m/s.

The vibration amplitudes increase by the increase of moving mass magnitudes, where there is no change in vibration frequency at all moving load magnitude range. It is also interesting to note that all the dynamic responses, measured at the central point c_p of the top beam converge into certain displacements which are greater than the corresponding static displacement due to effect of structural damping. The difference between the static and the final dynamic displacement increase by increasing moving mass magnitude. The increase of moving mass speed will increase the vibration amplitude and frequency of all displacements at all velocity histories. Compared to axial and lateral, vertical displacement is slightly induced. These results are also reported by Wu [6].

Particularly for case III, input force as a driving force for trolley motion is performed in order to test the dynamic model. Under bang-bang input force, the accelerations and decelerations phases can be clearly seen in swing angle θ compared to swing angle φ. That is because the horizontal (x) inertia force induced by moving trolley carrying a swinging payload significantly affects the payload swing in planar motion than that in space motion due to input force is applied in the horizontal direction. Further, amplitudes and frequencies of $\Delta\theta$ are about 2 times when trolley moves to 12 m (final position) than 3m and 4m. There is no discernable effect in $\Delta\varphi$ observed. DAF for axial displacements are 1.21 when trolley moves to 3 m, while 1.12 for 6 m. DAF for vertical displacements are almost the same for all trolley position, it is about 1.37, while lateral displacements have very large DAF because the crane framework is more rigid when it is loaded with static load compared to loaded with moving trolley with swinging payload.

When harmonic input force are subjected to gantry crane system, the amplitudes of swing angles increase erratically when the harmonic frequency of input force approaches the natural frequency of payload. The amplitudes of swing angles increase almost 10 times below and 5 times above the harmonic frequency. It is observed that when the harmonic frequency of input force approaches the natural frequency of payload, DAF for axial displacement is about 32.614; while for vertical displacement is about 4.54. Similar with bang-bang input force, lateral displacement produces very large DAF.

The stiffness of hoist cable variation for case III reveal that the frequencies of θ and φ increase with the decrease of the hoist cable stiffness with respect to their rigid model. The amplitudes of $\theta_{flexible}$ increase with the increase of hoist cable stiffness approaching θ_{rigid}, while minimal changes are found in amplitude of $\varphi_{flexible}$. Compared than case I, minimum changes in frequency and greater changes in amplitude of $\Delta\theta$ and $\Delta\varphi$ are observed. That is because the contributions of trolley velocity and acceleration, $\dot{x}_T, \ddot{x}_T$ in the payload dynamics in Equations (48d)-(48g).

The increase of cross-section dimensions of crane framework will make the time history of θ and φ are getting close into the rigid model. Unlike case I, the contributions of trolley velocity and acceleration $\dot{x}_T, \ddot{x}_T$ are dominant for the lowest cross-sectional properties among the others. Similar with case I under cable length variation, a definite change in amplitudes and frequencies are clearly observed. It is shown that the shortest hoist cable length produces larger swing amplitude and frequency of payload responses compared than the others.

It is clearly shown that the sensitivity of gantry crane system with respect to the payload mass variation. The increase of payload mass has discernable effect on the amplitude and frequency of payload swing angles, where the amplitude and frequency increase with the increase of payload mass. Unlike case I, It is found that the frequency has minimum changes in $\Delta\theta$ and $\Delta\varphi$. It must be the contributions of trolley dynamics $\dot{x}_T, \ddot{x}_T$.

Similar with case I, The increase of payload mass make the increases of maximum axial (X), vertical (Y) and lateral (Z) displacements of the central point c_p of the top beam. The trends are slightly linear for axial, vertical, lateral and hoist cable displacements for payload mass. Under the increase of hoist cable stiffness, cross-sectional dimensions of crane framework and hoist cable length, the trends decrease for all the maximum displacements.

All the simulation results show that gantry crane and framework is a coupled dynamic system, where bidirectional dynamic interaction is contributed by the flexibility of the crane framework and hoist cable.

CHAPTER 6

CONTROLLER DESIGN AND SIMULATIONS

6.1 Introduction

This chapter is application of work in Chapter 4 and 5 in control system. Control methods as described in Section 2.5 are utilized in this chapter to suppress its dynamic effect. Controller design and simulations are model-based control where dynamic model in Equations (48d)-(48g) and (52) are taken as plant model. By setting up $\varphi(t) = 0$, the dynamic model and controller are applicable for planar swing only. Control simulations begin by employing ZVDD as open-loop control strategy, while PID and FLC are applied as controller for closed-loop control strategy. These three controllers are used to evaluate each performance to transfer the payload and suppress the swing response of the payload simultaneously, with the flexibility of crane framework and hoist cable are taken into account into the plant model. Control simulations are conducted to show the effect of structural flexibility on controller performance compared to rigid model assumption.

6.2 Controller Design

Those three controllers are chosen as benchmark due to fact that the PID controller represents a well-known model-based controller; ZVDD is input shaper which is well-known as open loop control strategy and fuzzy logic as intelligent control. It is noted that, outputs of flexible gantry crane system as controlled system are trolley position, x_T and velocity $\dot{x}_T$, swing angle θ and swing velocity $\dot{\theta}$.

Elasticity effect of crane framework is measured at the central point c_P of the top beam as shown in Figure 6.57. This measurement point is mounted in that position due to that point produces maximum displacement of crane framework as shown in the previous chapter. All the parameters for crane framework and crane system are identical with Table 5.3 and 5.4, except for the payload mass, $m_P = 200kg$ .The objective of the controller design are to transfer the gantry crane as fast as possible with minimum swing angle of payload. The gantry crane position is transferred for travel distance of 12m, from the left end to the right end of the top beam of crane frame work. All controllers are designed for a motion such that the trolley has maximum acceleration and deceleration of $\pm 1\, m/s^2$. It is noted that the disturbance in every block diagram of controllers is the initial condition of payload swing angle.

6.2.1 Feed-Forward Control

Block diagram of ZVDD shaper is shown in Figure 6.1. The amplitudes and time locations of ZVDD shaper are determined by using Equations (2.31)-(2.32) in Chapter 2. The ZVDD shaper will be convoluted with the command signal of the system to generate shaped input for the system.

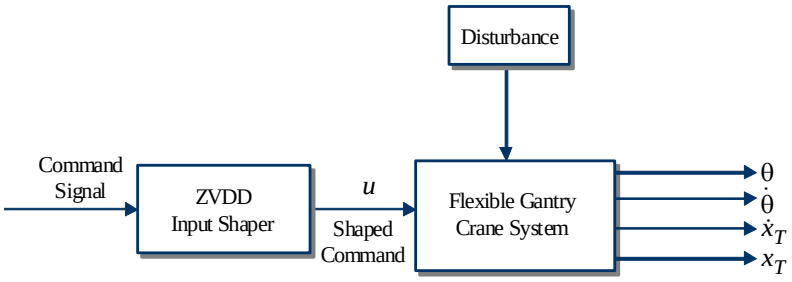

Figure 6.1: ZVDD shaper

This process is illustrated in Figure 6.2. ZVDD shaper's amplitude and time location are as shown in Table 6.1 for cable length $l = 1\, m$, where the linear natural frequency of payload is $f_p = \frac{1}{2\pi}\sqrt{\frac{g}{\ell}\cdot\left(1+\frac{m_P}{m_T}\right)}\left(\approx 1.1147\ Hz\right)$. However, any arbitrary unshaped input force can be used to simulate the performance of the control design.

Table 6.1: ZVDD parameters

Parameters	1	2	3	4
Amplitude	0.1250	0.3750	0.3750	0.1250
Time Location	0	0.5791	1.1582	1.7373

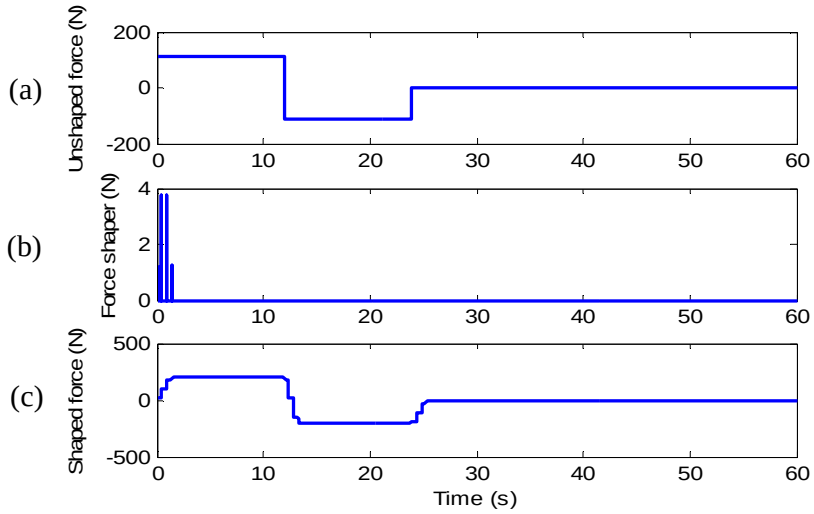

Figure 6.2: Convolution of ZVDD shaper

6.2.2 Feed-Back Control

6.2.2.1 Fuzzy Logic Controller (FLC)

The terms G_1, G_2 and G_3 are gains for two inputs and one output of the fuzzy logic controller used with the normalized universe of discourse for the fuzzy membership functions. Scaling factors G_1, G_2 are chosen to convert the two inputs within the universe of discourse and to activate the rule base effectively, whereas G_3 is selected such that it activates the system to generate the desired output.

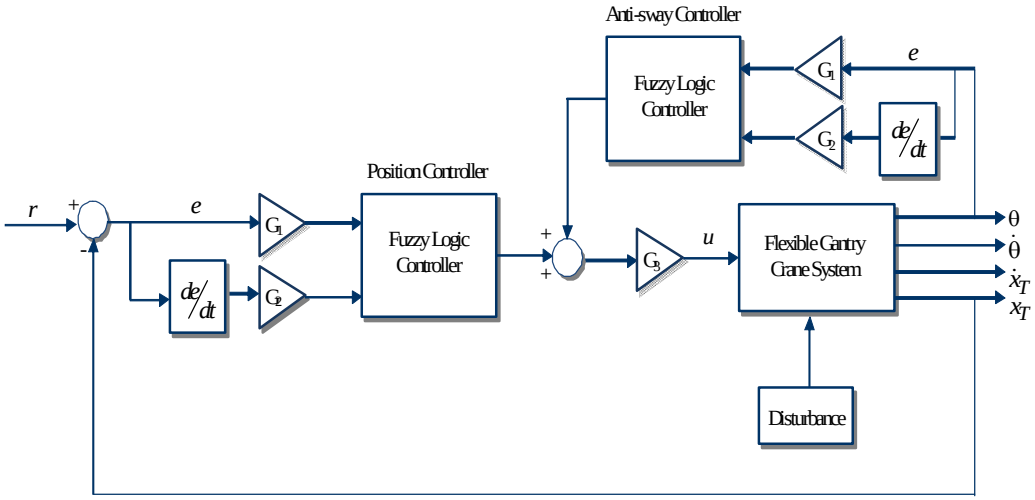

Figure 6.3: PD-type Fuzzy logic control structure

Initially all these gains are chosen based on trial and error, where the values are $G = \{0.9 \quad 0.07 \quad 300\}$. In this thesis, the trapezoidal and triangular membership functions are chosen for the inputs and the output. To construct a rule base, inputs of system, namely the trolley position error and trolley position error derivative, also output for system namely force are partitioned into five fuzzy sets overlapping each other for position control as displayed in Figure 6.4.

- **Trolley position error**

The error of trolley position is defined as the difference between the desired position of trolley and the actual position of the trolley which can be written as follows.

$$e_{x_T}(t) = r(t) - x_T(t) \tag{68}$$

where r is desired position of trolley and x_T is actual position of trolley at time t.

Positive values of error indicate that actual position of trolley is lower than desired position. Conversely, negative values of error indicate that actual position of the trolley is higher than the desired position. Such error variables are mapped into fuzzy sets using trapezoidal and triangular membership functions become five fuzzy sets namely, Negative Big (NB), Negative Small (NS), Zero (Z), Positive Small (PS) and Positive Big (PB) as depicted in Figure 6.4a.

- **Trolley position error derivative**

Fuzzy sets for trolley position error derivative are mapped into five sets also as shown in Figure 6.4b. Derivative error of trolley velocity is defined as a derivative of $e_{\dot{x}}(t)$ with respective to time which can be written as follows.

$$\nabla e_{x_T}(t) = d\left(e_{x_T}(t)\right) \Big/ dt \tag{69}$$

- **Trolley force output**

Fuzzy sets for trolley force $u_{x_T}(t)$ consist of five sets as well as shown in Figure 6.4c.

Similar with position controller, membership functions for anti-sway controller covers swing angle error, swing angle error derivative and input force which are depicted in Figure 6.5.

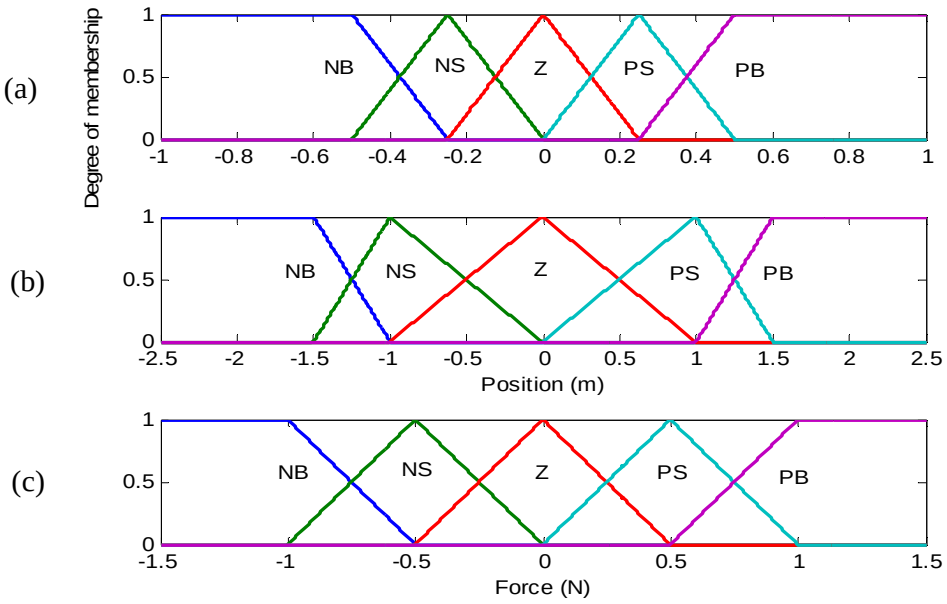

Figure 6.4: Membership functions for position controller
(a) e_{x_T} (b) ∇e_{x_T} (c) u_{x_T}

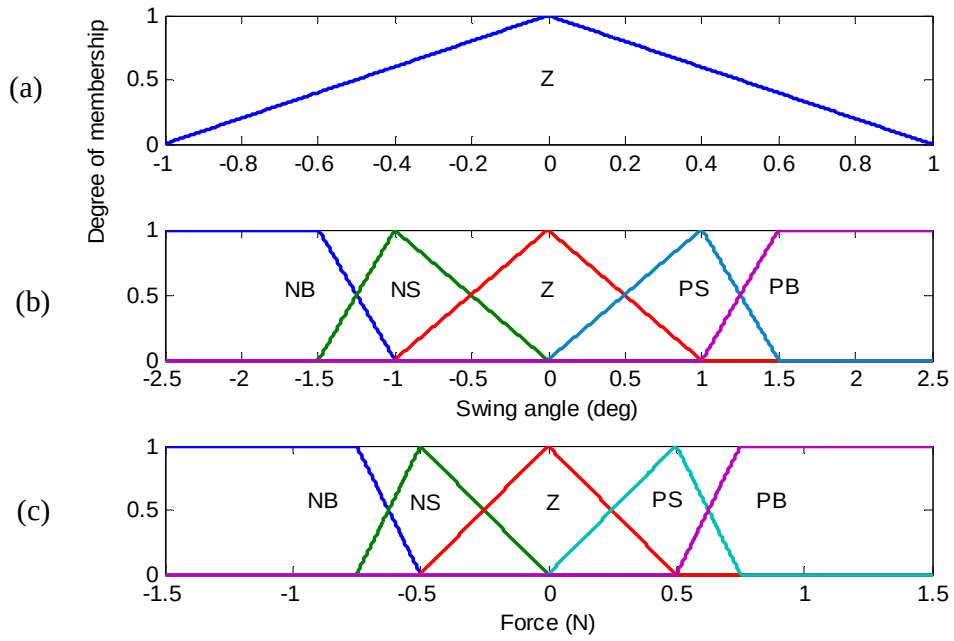

Figure 6.5: Membership functions for anti-sway controller
(b) e_θ (b) ∇e_θ (c) u_θ

- **Fuzzy Inference Engine**

After membership functions of the input and the output variables are determined, fuzzy control rules are developed to connect between input and output variables. In this stage, decision making is conducted based on value of inputs which have been fuzzified. The rule base of FLC is generated according to engineering judgment and experience.

For convenience, these fuzzy rules are displayed in the decision matrices as shown in Table 6.2 and Table 6.3.

Table 6.2: Fuzzy rules for position control

Error rate / Error		∇e_{x_T}				
		NB	NS	Z	PS	PB
e_{x_T}	NB	NB	NB	NB	NB	NB
	NS	NB	NS	NS	PS	PB
	Z	NB	NS	Z	PS	PB
	PS	NB	NS	PS	PS	PB
	PB	NB	NB	PB	PB	PB

Table 6.3: Fuzzy rules for anti-swing control

Swing angle / Swing angle rate		∇e_θ				
		NB	NS	Z	PS	PB
θ	Z	NB	NS	Z	PS	PB

These fuzzy rules are interpreted easily, for example: if e_{x_T} is NS and ∇e_{x_T} is Z, then for this case, fuzzy rules become:

If e_{x_T} is Negative Small and ∇e_{x_T} is Zero, then u_{x_T} is Negative Small

In similar way, the other rules contained in Table 6.3 and Table 6.4 can be interpreted.

Based on the value of e_{x_T} and ∇e_{x_T} in Table 6.3 above, in every time there will be more than one fuzzy rule fired. It is solved by fuzzy set operation as described in Section 2.5.2. As sample, the fuzzy inference system for position control is displayed in Figure 6.6, which is simulated by using fuzzy logic toolbox in Matlab®.

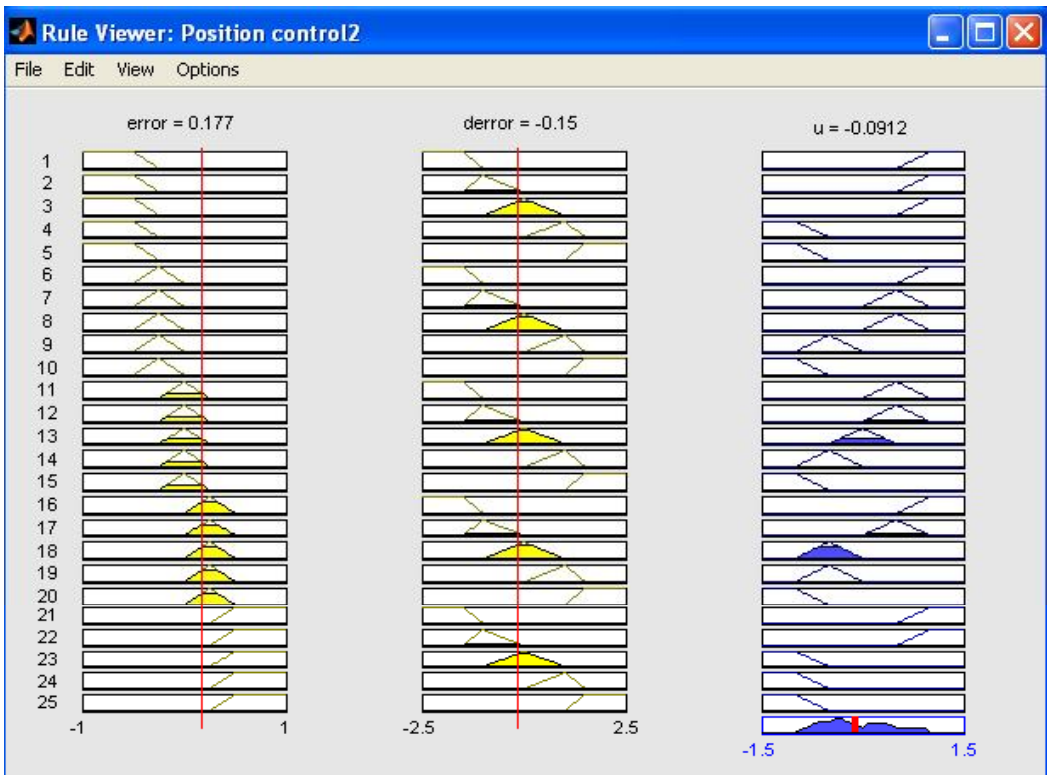

Figure 6.6: Fuzzy inference system simulations

The fuzzy rules are extracted based on underdamped system. Intuitively, the trolley of the crane moves to positive direction and the payload sway on clockwise direction. The force should be applied to negative direction in order to compensate the swing.

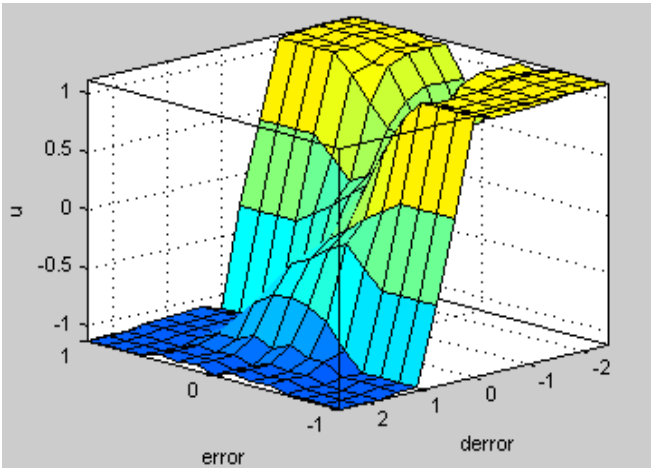

Figure 6.7: Three dimension of fuzzy control action

Meanwhile, if the trolley moves to negative and the payload sway to anti clockwise direction; the forced should be imposed to positive direction to suppress the swing motion. In the case there is no swing, no force should be applied.

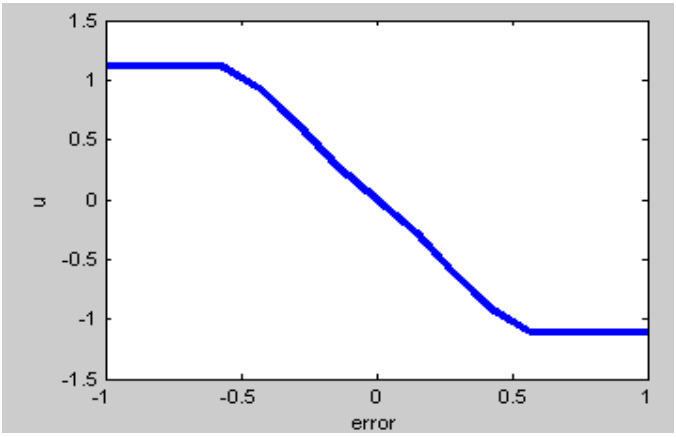

Figure 6.8: Fuzzy control actions with constant ∇e_{x_T}

Three dimension graphic of control action is depicted in Figure 6.7. From the figure, it is seen that controller output is function of error (e_{x_T}) and error derivative (∇e_{x_T})value. The mapping of the function is nonlinear.

As comparison, Figure 6.8 shows control action variation with respect to error (e_{x_T}) value, where error derivative (∇e_{x_T})value is kept constant. From the figure, it can be observed that for small error (e_{x_T}) value, the minimum control action will be received. Vice versa, for large error (e_{x_T}) value, the maximum control action will be gained.

6.2.2.1 PID Based Controller

The structure of PID control is shown in Figure 6.9. It consists of two separate controller, position and anti-swing controller. The output of each controller will be combined, and sent into the plant, as noted by u. Each of this controllers use the same K_P, K_i and K_d of PID, where these gains are obtained by trial and error. Finally, optimal gains of PID controller are displayed in Table 6.4. Scaling factors G_1, G_2, G_3 for each controller are chosen in such a way that it activates the system to generate the desired output. The values of these scaling factors are $G = \{0.8 \quad 0.05 \quad 0.2\}$.

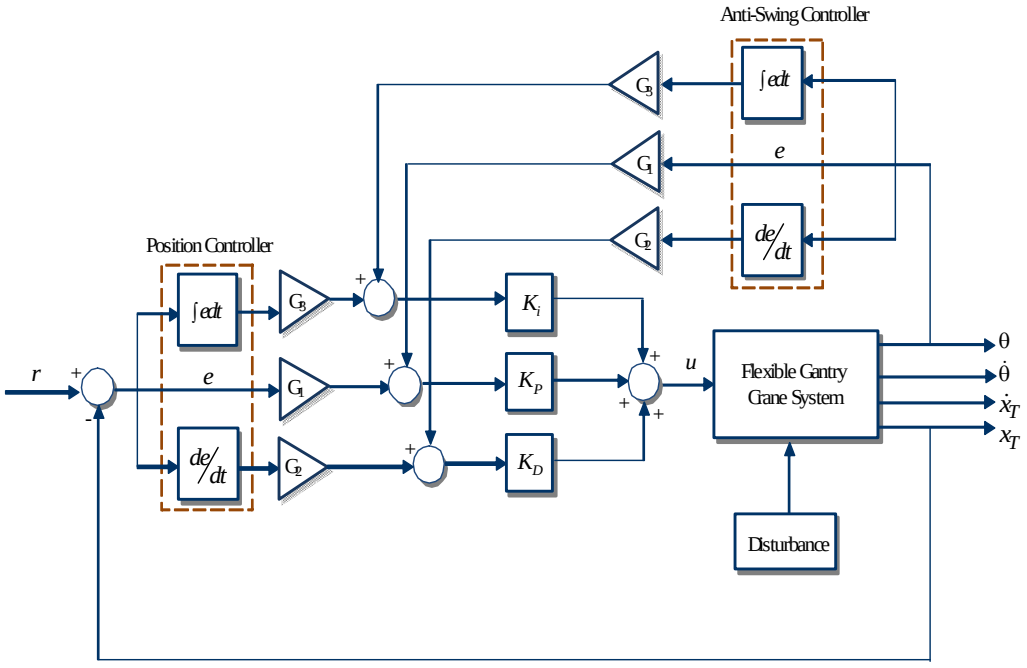

Figure 6.9: PID controller

Table 6.4: PID parameters

Controllers	Gain		
	K_p	K_i	K_d
PID controller (Position control)	320	0.25	0.05
PID controller (Anti-swing)			

6.3 Simulation Results

The graphical results of the trolley position (x_T), swing angles (θ) of payload, trolley velocity $(\dot{x}_T)$ and control force (u) for ZVDD are shown in Figure 6.10, Figure 6.11 for PID, and Figure 6.12 for FLC. Simulation results reveal that all controllers are able to control the gantry crane system with rigid model assumption.

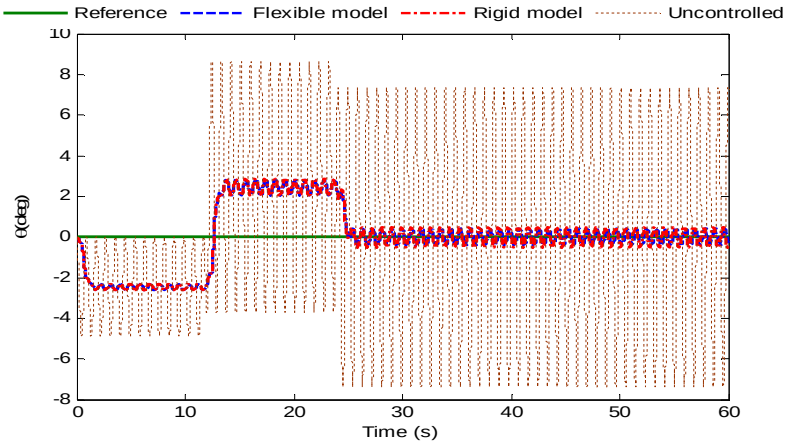

(a)

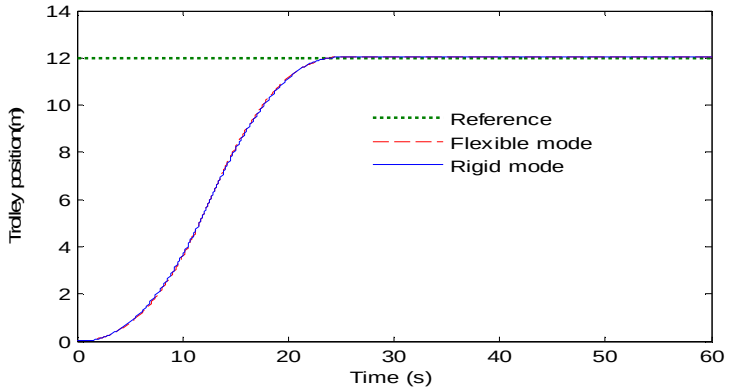

(b)

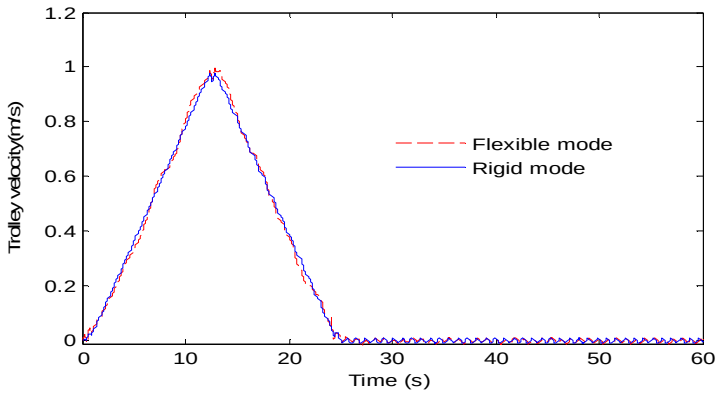

(c)

Figure 6.10: Simulation results with ZVDD; Swing angle (b) trolley position (c) trolley velocity

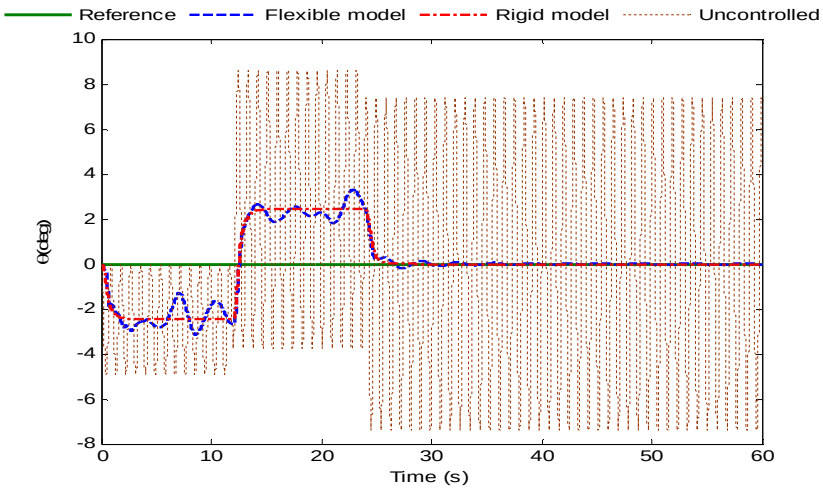

(a)

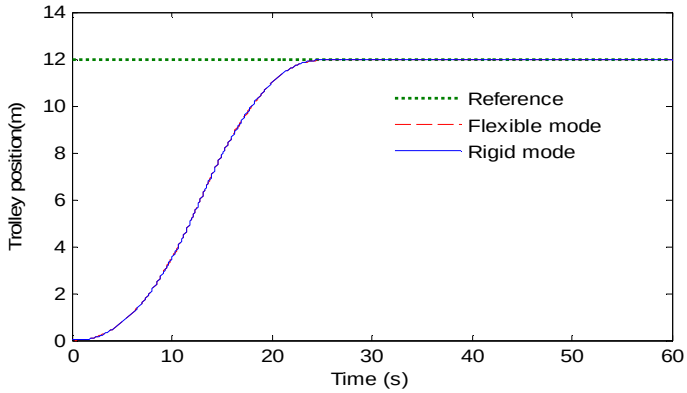

(b)

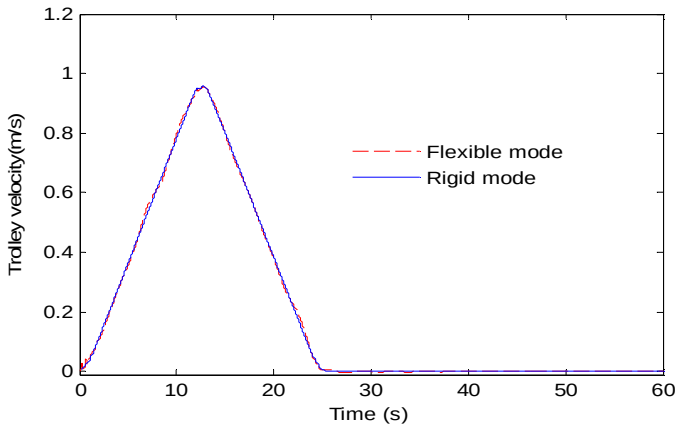

(c)

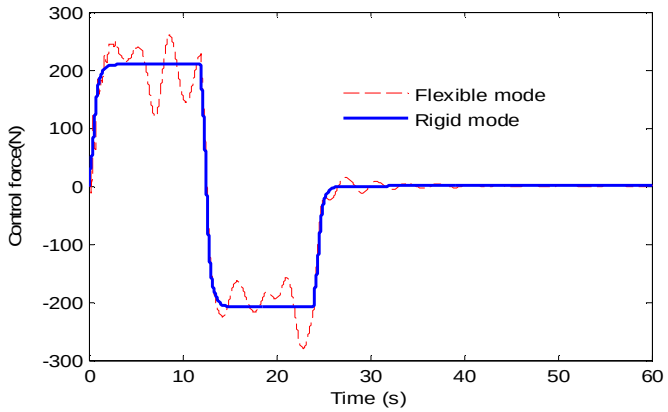

(d)

Figure 6.11: Simulation results with FLC
(a) Swing angle (b) trolley position (c) trolley velocity (d) control force

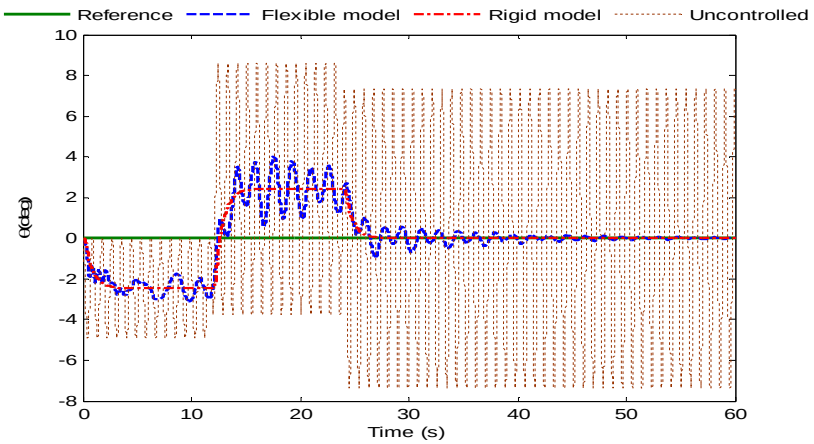

(a)

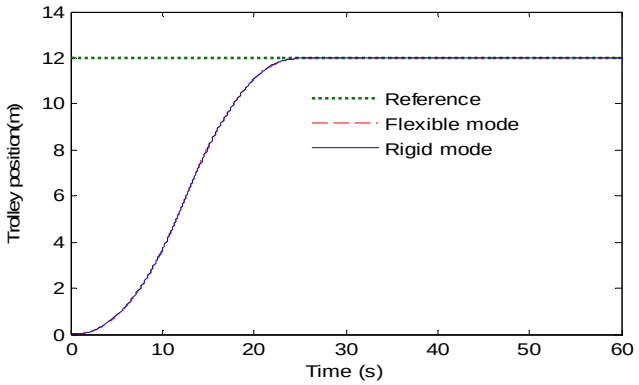

(b)

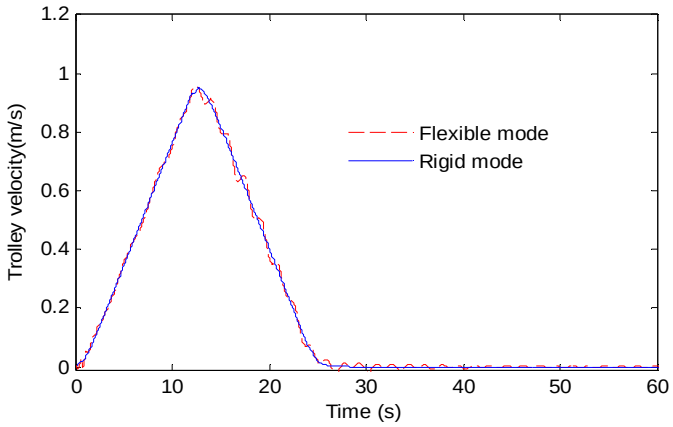

(c)

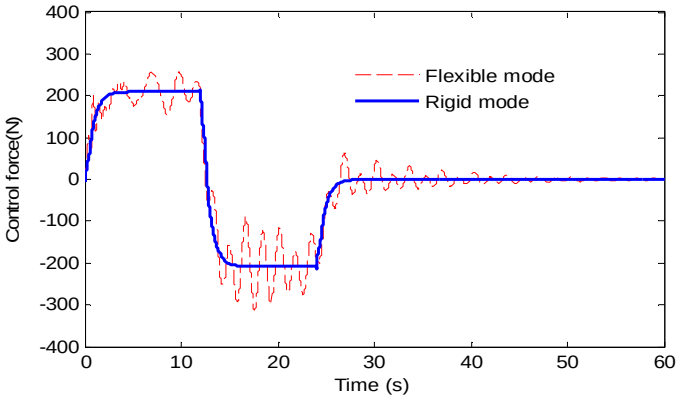

(d)

Figure 6.12: Simulation results with PID controller
Swing angle (b) trolley position (c) trolley velocity (d) control force

In fact, if the flexibility of crane framework and hoist cable is introduced, there are clear overshoots in swing angle, trolley velocity and control force as depicted by all controllers. All the controllers show the degradation of their performances in controlling the flexible gantry crane compared to rigid gantry crane.

A summary of the performance of the controllers by observing Figure 6.13 is given in Table 6.4. It can be seen that there is no overshoot in the trolley position for the three controllers. PID has the highest payload swing and its swing angle magnitude, while ZVDD has the larger steady state error compared to the others. The control simulations reveal that FLC has better performance in controlling the flexible gantry crane. It is strongly presumed that the larger construction of gantry crane, the worse performance of controllers with respect to the rigid model.

Table 6.4: Performance comparison

Comparison	ZVDD	FLC	PID
Swing angle magnitude	Lowest	Lower	Highest
Payload swing	Lowest	Lower	Highest
Trolley position overshoot	No overshoot	No overshoot	No overshoot
Steady state error of swing angle (deg)	0.5^{o}	0.05^{o}	0.1^{o}

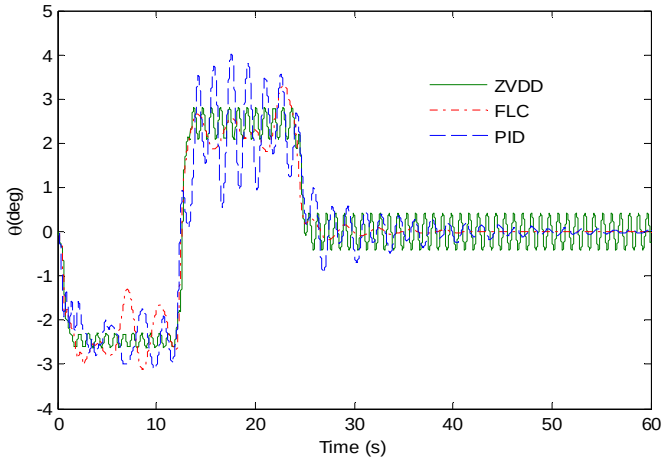

Figure 6.13: Swing angle responses comparison

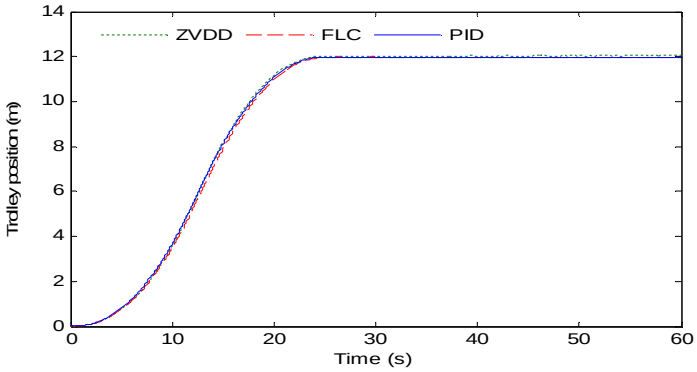

Figure 6.14: Trolley position responses comparison

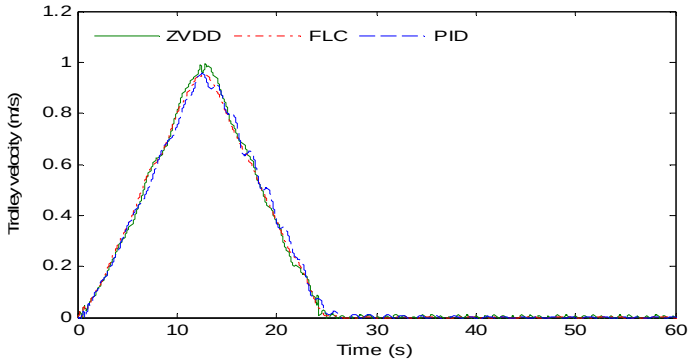

Figure 6.15: Trolley velocity responses comparison

6.4 Summary

The problem of transporting a suspended load with considering the flexibility of crane framework and hoist cable has been addressed and solved by three types of controllers. The simulations show that the swing angle and trolley position of flexible and rigid model of gantry crane can be controlled simultaneously. The performance and the stability are also good, especially for PID and FLC. However, it is only applicable for rigid model. The simulation results confirm that the flexibility of crane framework and hoist cable hardly affect the controller performance. ZVDD, FLC, PID controllers have rough fluctuations in controlling the payload swing and trolley velocity. However, there is no overshoots in controlling the trolley position for the three controllers. Compared to FLC and PID, ZVDD has larger steady state error, it is about 0.1^{o}.

CHAPTER 7

CONCLUSIONS AND RECOMMENDATIONS

7.1 Conclusions

Dynamical model of flexible gantry crane system can be modeled as a system consisting of the elastic spherical pendulum payload which moves along the top beam of flexible crane framework by means of finite element method in conjunction with moving finite element method and Lagrange's equation. The derived equations of motion show that the gantry crane behaves as an elastic spherical pendulum with moving flexible pivot point. The moving pivot point undergoes acceleration in three directions which provided by the flexibility of crane framework and affected by the flexibility of hoist cable.

The derived equations of motion generate three loading cases on gantry crane system, namely swinging payload with stationary trolley as case I, moving trolley with stationary payload (moving load) as case II and moving trolley with swinging payload as case III. As verification, if the crane framework and hoist cable are rigid, the derived equations of motion correctly simplified to nonlinear equations, which exactly fulfill Newton's of motion for classical pendulum system either with fixed pivot point or moving pivot point.

The proposed computational technique, namely combinational Newmark-β and fourth-order Runge-Kutta method can solve the equations of motion and predict the dynamic characteristic of flexible gantry crane system. The simulation results show that the dynamic responses of crane framework and gantry crane are bidirectional interaction, where the state variables of gantry crane such as swing angles, hoist cable and trolley motion affect the dynamics of crane framework and conversely.

Under case I, it is proved that the gantry crane system with flexible hoist cable-crane framework produces greater amplitudes in swing angles $\theta, \varphi, \Delta\theta, \Delta\varphi$ and FFT analysis confirms that it has the lowest swing angles frequency compared to the gantry crane system with flexible hoist cable or crane framework only with respect to rigid model. Moreover, all the flexible models of gantry crane system have longer periods or lower frequencies in the time histories of swing angles of payload with respect to the rigid model for all parametric studies either in case I or case III.

It is clearly seen that the trend of the maximum axial (X), vertical (Y) and lateral (Z) displacements of the central point c_p of the framework increase with the increase of payload mass. The increases are slightly linear for axial, vertical, lateral and hoist cable displacements either case I or case III. Under the increase of hoist cable stiffness, cross-sectional dimensions of crane framework and hoist cable length, the trends decrease for all the maximum displacements for both cases.

Moreover, the control simulations confirm that the flexibility of crane framework and hoist cable significantly affect the controller performances. ZVDD, FLC, PID controller have rough fluctuations in controlling the flexible gantry crane with respect to their performances in controlling the rigid model of gantry crane. However, there is no overshoots in controlling the trolley position for the three controllers. Compared to FLC and PID, ZVDD has larger steady state error, it is about 0.1^{o}.

7.2 Recommendations

This thesis has proven that the combinational direct integration technique can solve the generated equations of motion in order to predict and control the dynamic behavior of flexible gantry crane system. However, further study is required to include the actual hosting mechanism of the crane which is multi-cable, the trolley and payload as distributed mass. Future areas that can be studied are optimization of structural design, modern fatigue life, reliability design and other purposes. The experimental validation is recommended.